

**Medical Faculty of the  
Martin-Luther University Halle-Wittenberg**

**Characterization of age-related changes within the lysine acetylation pattern  
of immune effector cells**

Dissertation obtaining the academic degree  
Doktor rerum medicarum (Dr. rer. medic.)  
In the field of Medical Immunology

by Georgiana Toma,  
born on 11.04.1991 in Buzău, Romania  
Supervisor: Prof., Dr., Seliger Barbara  
Reviewers:

- Apl. Prof. A. Navarrete Santos
- PD C. Kaether, Jena

01.06.2021

07.03.2022



*"Inside every old person is a young person wondering what happened".*

- Terry Pratchett

## Abstract

Over time, the human organism is exposed to an increasing number of pathogens, which reduces the reserve of naïve CD8<sup>+</sup> T cells. The overall result is maladaptive protection against new pathogens and lower vaccine efficacy<sup>1-6</sup>. Therefore, therapies aimed at older individuals are required to take into account the age-dependent effect on efficacy. However, not all therapeutic strategies consider the age of the individual as a factor, especially when treating prevalent conditions such as inflammation and inflammatory diseases. Deacetylase inhibitors (HDACis) have been used to treat a wide range of conditions, from inflammatory diseases to various cancers<sup>7-10</sup>. Therefore, it is imperative to study the interplay between acetylation and aging within T cells.

To this end, for the current exploratory study, CD8<sup>+</sup> T cells were isolated from young and old healthy blood donors and treated with HDACi. The functional effects on activation, secretion, proliferation, and apoptosis were then evaluated through biomolecular approaches. To better understand the intracellular outcome of acetylation, high-throughput transcript analysis and protein expression profiles were also performed, along with the relative protein and transcript expression of proteins participating in the signaling pathways involved in the activation and differentiation of CD8<sup>+</sup> T cells.

A strong correlation was found between HDACi treatment and T cell activation, secretion, and proliferation. While an increase in acetylation does not disturb the apoptosis rate of the cells, it alters the cytoskeleton and signaling proteins enough for the wider, general effect on CD8<sup>+</sup> T cells to be immobilizing. The emerging difference between young and old CD8<sup>+</sup> T cells stems from the underlying differences between the two groups. The activation and secretion of old CD8<sup>+</sup> T cells was much higher, and it was sustained even after HDACi treatment, whereas young CD8<sup>+</sup> T cells underwent an almost complete interruption of their functions.

The present results suggest that the differences between young and old CD8<sup>+</sup> T cells are greater than previously thought and that the efficacy of HDACi treatment is modulated by aging.

Toma, Georgiana: **Characterization of age-related changes within the lysine acetylation pattern of immune effector cells**. Halle, Univ., Med. Fak., Diss., pages – 80, figures – 36, tables – 11, 2021.

## Referat

Im Laufe der Zeit ist der menschliche Organismus mehr Krankheitserregern ausgesetzt. Dadurch verringert sich die Reserve an naiven CD8<sup>+</sup>-T-Zellen. Das Endresultat ist ein fehlangepasster Schutz gegen neue Krankheitserreger und eine geringere Impfstoffwirksamkeit<sup>1-6</sup>. Deshalb müssen Therapien für ältere Menschen den altersabhängigen Effekt auf die Wirksamkeit berücksichtigen. Allerdings berücksichtigen nicht alle Therapiestrategien das Alter der Person als Faktor. Dies ist insbesondere bei der Behandlung verbreiteter Leiden wie Entzündungen und entzündlichen Erkrankungen der Fall. Deacetylase-Inhibitoren (HDACis) wurden zur Behandlung einer Vielzahl an Krankheiten von entzündlichen Erkrankungen bis hin zu verschiedenen Krebsarten eingesetzt<sup>7-10</sup>. Deshalb ist es unabdingbar, das Zusammenspiel zwischen Acetylierung und Alterung innerhalb von T-Zellen zu untersuchen.

Zu diesem Zweck wurden für die vorliegende explorative Studie CD8<sup>+</sup>-T-Zellen von jungen und alten gesunden Blutspendern isoliert und mit HDACi behandelt. Die funktionellen Auswirkungen auf Aktivierung, Sekretion, Proliferation und Apoptose wurden anschließend mittels biomolekularer Vorgehensweisen beurteilt. Um das intrazelluläre Ergebnis der Acetylierung besser zu verstehen, wurden neben der relativen Protein- und Transkriptexpression von Proteinen, die an den Signalwegen beteiligt sind, welche an der Aktivierung und Differenzierung von CD8<sup>+</sup>-T-Zellen mitwirken, auch Hochdurchsatz-Transkriptanalysen und Proteinexpressionsprofile durchgeführt.

Es wurde eine starke Korrelation zwischen der HDACi-Behandlung und der Aktivierung, Sekretion und Proliferation von T-Zellen festgestellt. Während eine Erhöhung der Acetylierung die Apoptoserate der Zellen nicht stört, verändert sie das Cytoskelett und die Signalproteine so weit, dass die breitere, allgemeine Wirkung auf CD8<sup>+</sup>-T-Zellen immobilisierend ausfällt. Der sich abzeichnende Unterschied zwischen jungen und alten CD8<sup>+</sup>-T-Zellen resultiert aus den zugrundeliegenden Unterschieden zwischen den beiden Gruppen. Der Ausgangswert bei der Aktivierung und Sekretion alter CD8<sup>+</sup>-T-Zellen war viel höher und blieb auch nach der HDACi-Behandlung erhalten. Dagegen kam es bei jungen CD8<sup>+</sup>-T-Zellen zu einer fast vollständigen Störung ihrer Funktionen.

Die vorliegenden Ergebnisse legen nahe, dass die Unterschiede zwischen jungen und alten CD8<sup>+</sup>-T-Zellen größer als bislang angenommen sind und dass die Wirksamkeit einer HDACi-Behandlung durch Alterung moduliert wird.

Toma, Georgiana: **Charakterisierung altersbedingter Veränderungen im Lysin-Acetylierungsmuster von Immuneffektorzellen.** Halle, Univ., Med. Fak., Diss., Seiten – 80, Abbildungen – 36, Tabellen – 11, 2021.

# Table of Contents

Abstract .....	I
Referat.....	II
List of abbreviations .....	IV
1. Introduction .....	1
1.1. Adaptive immune cells and aging .....	1
1.1.1. Activation of cytotoxic T cells.....	1
1.1.2. Formation of immunological memory.....	5
1.1.3. Age-related alterations to the function of cytotoxic T cells .....	5
1.2. Protein post-translational modifications .....	6
1.2.1. Classification of deacetylases .....	7
1.2.2. Histone and non-histone protein acetylation.....	8
1.2.3. Deacetylation in aging and anti-aging .....	9
2. Aims and objectives .....	11
3. Methods .....	12
3.1. Materials .....	12
3.1.1. Commercially available reagents, equipment and tools .....	12
3.1.2. Chemical solutions, gels, and recipes .....	16
3.1.3. Biological material .....	17
3.2. Evaluation of the effect of acetylation on CD8 <sup>+</sup> T cell activation in aging .....	18
3.2.1. T cell culture conditions .....	18
3.2.2. Characterization of CD8 <sup>+</sup> T cells by flow cytometry .....	19
3.2.3. Functional analysis of activated CD8 <sup>+</sup> T cells after HDACi treatment .....	20
3.3. Protein and transcript expression profiles of activated CD8 <sup>+</sup> T cell.....	21
3.3.1. Relative protein expression .....	21

3.3.2.	Two-dimensional protein expression profile analysis -----	22
3.3.3.	Identification of proteins expressed differently between young and old CD8 <sup>+</sup> T cells -	24
3.3.4.	Relative and absolute quantification of the gene expression of CD8 <sup>+</sup> T cells -----	26
3.4.	Statistical methods and interpretation of high throughput data .....	30
3.4.1.	RNA sequencing data analysis -----	30
3.4.2.	Network analysis and gene ontology term enrichment -----	31
3.4.3.	Additional statistical methods -----	32
4.	Results .....	33
4.1.	Expression of deacetylases and the acetylome of CD8 <sup>+</sup> T cells.....	33
4.1.1.	Impact of T cell activation on the expression of HDACs-----	33
4.1.2.	Changes within the acetylome in CD8 <sup>+</sup> T cells from young and old donors -----	33
4.1.3.	Impact of HDACi treatment on the expression of HDACs-----	34
4.2.	Identification of differently expressed proteins .....	35
4.2.1.	Expression profiles and identification of modified proteins after HDACi treatment----	35
4.2.2.	Network analysis of identified proteins and GO term enrichment -----	39
4.3.	Effect of HDACi treatment on CD8 <sup>+</sup> T cell function .....	42
4.3.1.	Characterization of CD8 <sup>+</sup> T cells -----	42
4.3.2.	Surface expression of activation markers and proliferation capacity-----	42
4.3.3.	Cytokine secretion patterns during aging-----	43
4.3.4.	Apoptosis rates for the selected age groups -----	45
4.3.5.	Signaling transduction after HDACi treatment -----	46
4.4.	Absolute quantification of transcript expression in activated CD8 <sup>+</sup> T cells without HDACi treatment .....	47
4.4.1.	Functional comparison of the total CD8 <sup>+</sup> T cells and CD8 <sup>+</sup> CD45RA <sup>-</sup> memory T cells----	47
4.4.2.	Data overview and quality control-----	50
4.4.3.	Age-related GO term enrichment-----	52

4.4.4. Group-specific processes and functions-----	56
5. Discussion.....	59
5.1. HDAC expression before and after inhibiting deacetylation.....	59
5.1. Identifying differently acetylated proteins based on 2DE expression profiles .....	60
5.2. Age-dependent distribution of CD8 <sup>+</sup> T cell subpopulations.....	62
5.1. Disruption of CD8 <sup>+</sup> T cell functions and cellular signaling by inhibiting cellular deacetylation 62	
5.2. Transcriptional differences between young and old donors without HDACi .....	65
6. Conclusions and future perspectives .....	69
7. Bibliography .....	71
8. Theses.....	80
9. Supplementary material.....	VIII
Declarations .....	XXIII
Acknowledgements.....	XXIV

## List of abbreviations

2DE	two-dimensional electrophoresis
ABC	ammoniumbicarbonat
Ac-CoA	acetyl-coenzyme A
acetyl-tubulin	acetylated-tubulin
ACN	acetonitril
ACTN4	alpha-actinin-4
AGO1	protein argonaut 1
AKT	protein kinase B
APC	antigen presenting cell
APC	allophyocyanin
APS	ammoniumpersulfat
BCL2	apoptosis regulator
BMI	body mass index
BSA	bovine serum albumin
BV605	briliant violet 605
CCR7	C-C chemokine receptor type 7
CD62L	L-selectin
cDNA	circular DNA
CFSE	carboxyfluorescein succinimidyl ester
CHAPS	3-[(3-Cholamidopropyl)-dimethylammino]-1propansulfonat
CM	central memory
CMV	cytomegalovirus
CNR2	cannabinoid receptor 2
Cq	quantification cycle
DICER1	dicer 1 – ribonuclease type 3
DIGE	difference gel electrophoresis
DMSO	dimethylsulfoxid
DOC	11-deoxycorticosterone
DTT	dithiothreitol
EDTA	ethylen diamin tetraacetic acid
EF2	elongation factor 2
EM	effector memory
Eomes	eomesodermin
ER	endoplasmic reticulum
ERK	extracellular signal regulated kinase
FACS	fluorescence-activated cell-sorting
FCS	fetal calf serum
FCS	forward scatter
FDR	false discovery rate
FITC	fluorescein
FoxO	forkhead box O
GAPDH	glyceraldehyde-3-phosphate dehydrogenase

GM-CSF	granulocyte-macrophage colony-stimulating factor
Gorilla	Gene Ontology enRiChment anaLysis and visualizAtion tool
HAT	acetyltransferase
HCD2	3-hydroxyacyl-CoA dehydrogenase type-2
HDAC	deacetylase
HDACi	deacetylase inhibitor
HIF1A	hypoxia-inducible factor 1 subunit alpha
HLA	human leukocyte antigen
HNRPF	heterogeneous nuclear ribonucleoprotein F
HSP90A	heat shock protein 90 alpha
IF4A1	eukaryotic initiation factor 4A
IFN-γ	interferon-gamma
IL	interleukine
IL-2R	interleukine 2 receptor
IL7R	interleukine 7 receptor
IPG	immobilized pH gradient
IPS	internal protein standard
JAK	Janus kinases
JNK	c-Jun N-terminal kinase
KAT	lysine acetyltransferase
KPYM	pyruvate kinase PKM
LDHB	L-lactate dehydrogenase B chain
mAb	monoclonal antibody
MALDI-TOF MS	matrix-assisted laser-desorption/ionization time-of-flight mass spectrometer
MAPK	mitogen-activated protein kinase
MHC	major histocompatibility complex
miRNA	microRNA
MOWSE	MOlecular Weight SEarch
mTOR	target of rapamacyne
mTORC	mechanistic target of rapamycine complex
NA	not applicable
NAD+	nicotinamide adenine dinucleotide
NAM	nicotinamide
NAT	N-acetyltransferase
NCBI	National Center for Biotechnology Information
NDSB	non-detergent sulfobetaine 256
NEFL	neurofilament light
NF-kB	nuclear factor 'kappa-light-chain-enhancer' of activated B-cells
NOD2	nucleotide-binding oligomerization domain-containing protein 2
NP-40	nonyphenol-40
OXPPOS	oxidative phosphorylation system
p-AKT	phosphorylated-AKT
PBMC	periphereal blood mononuclear cells
PBS	phosphate buffered saline

PCA	principal component analysis
PE	phycoerythrin
PenStrep	penicillin streptomycin
PI	propidium iodide
pI	isoelectric point
PLSL	plastin-2
PTM	posttranslational modification
PTN6	tyrosine-protein phosphatase non-receptor type 6
qPCR	quantitative polymerase chain reaction
RF	regulation factor
RHG39	rho GTPase-activating protein 39
Ripa	radioimmunoprecipitation assay
ROCK2	Rho associated coiled-coil containing protein kinase 2
RT	room temperature
S1PR5	sphingosine-1-phosphate receptor 5
SDHA	succinate dehydrogenase subunit A
SDS	sodium dodecyl sulphate
SDS-PAGE	SDS–polyacrylamide gel electrophoresis
SELL	L-selectin
SFPQ	splicing factor, proline- and glutamine-rich
SIRT	sirtuins
SLFN5	schlafen family member 5
SOD2	superoxide dismutase 2
SSC	side scatter
STAT	signal transducer and activator of transcription proteins
TAE	tris, acetic acid, and EDTA
TBB3	tubulin beta-3 chain
TBB4A	tubulin beta-4A chain
TBP	TATA-binding box protein
TBS-T	tris-buffered saline with tween
TBX21	T-box transcription factor 21
Tc	cytotoxic T cell
TCA	tricarboxylic acid cycle
TCA	trichloroacetic acid
TCR	T cell receptor
TEMED	tetramethylethylenediamin
TEMRA	terminally differentiated effector memory T cells
TFA	trifluoroacetic acid
TNFRSF11	TNF receptor superfamily member 11
TNF- $\alpha$	tumor necrosis factor alpha
Tris	tris(hydroxymethyl)aminomethane hydrochloride
TRUB1	probable tRNA pseudouridine synthase 1
TSA	trichostatin a
VIME	vimentin
WB	western blot

XRCC5  
YI018

x-ray repair cross-complementing protein 5  
uncharacterized FLJ76381

## 1. Introduction

Aging can be defined as a gradual deterioration of the organism's physiological functions as a whole. This is the result of a time-dependent accumulation of cellular and DNA damage<sup>11</sup>. And considering the increase in aging populations all over the world<sup>12</sup>, it would be worthwhile to better understand the biological mechanisms of aging, especially in the context of the adaptive immune system, which forms the immunological memory and contributes to the efficacy of vaccines<sup>1</sup>. The immune system is heavily affected by aging. First, the production of naïve lymphocytes is drastically decreased. Second, functionally impaired memory lymphocytes start to accumulate<sup>13-15</sup>.

Cytotoxic T cells represent one of the main defense mechanisms of the organism against intracellular pathogens such as viruses<sup>16</sup>. The intercellular pathways that lead to the activation of these cells depend on the function of proteins and specific post-translational modifications of proteins (PTMs). When the enzymes regulating PTMs are defective, cellular functions are compromised<sup>17</sup>. Acetylation is a simple chemical modification that has a significant impact on the cellular environment. It operates primarily through the regulation of gene expression by modifying the histones, but also by altering the cytoskeleton and most cellular chaperones.

### 1.1. Adaptive immune cells and aging

The main function of cytotoxic T cells is to kill infected host cells, and they accomplish this by secreting perforin and granzymes, which dissolve the membrane of target cells and degraded the cellular DNA, respectively<sup>18</sup>. When a naïve T cell encounters an antigen-presenting cell (APC), it binds to it by the APC's major histocompatibility complex (MHC) class I molecule, which activates the T cell. This first phase is known as *priming* or *activation* (Figure 1). The cell then enters a massive proliferation phase known as *clonal expansion*. After the infection is cleared, most activated T cells undergo apoptosis or *contraction*, and only some become memory T cells. *Maintenance* is the final stage, whereby memory T cells self-replicate and sustain a stable population over several years<sup>16</sup>.

#### 1.1.1. Activation of cytotoxic T cells

**Co-stimulation of T cells.** Two signals are required for T cells to be activated. The binding between the T cell receptor (TCR) complex and the peptide-MHC complex represents the first activation signal. However, since APCs may present peptides without being activated, this is not sufficient to fully activate the T cells. A second antigen-nonspecific signal is necessary<sup>19</sup>, and it occurs when CD28 from the surface of the T cells recognizes the CD80 proteins from the surface of the APCs<sup>20</sup>. Because the CD80 proteins are presented by

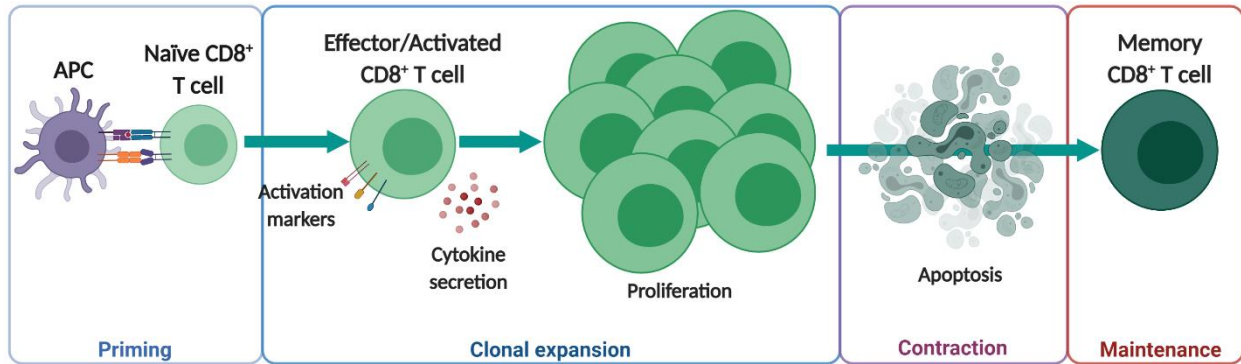


**Figure 1. Activation of T cells after antigen exposure.** Four stages can be identified in the life cycle of T cells: priming or activation, clonal expansion, contraction, and maintenance. The first step is achieved within hours, while the intense proliferation and subsequent apoptosis last several days. Memory CD8+ T cells are formed after an infection is cleared, and these cells can last for years in the human organism. The figure was created with BioRender.com.

the APC only when they are activated, this ensures that the T cells do not mount a response to self-proteins<sup>19</sup>.

However, it has been shown that CD8+ T cells do not require a second signal to respond to certain infections<sup>21</sup>. Furthermore, CD8+ memory T cells have a shorter reaction time because they skip the first step of priming that naïve T cells have to undergo<sup>22,23</sup>. Memory CD8+ T cells can be activated by any host cell that presents the antigen in its MCH class I molecules, not only by specialized APCs<sup>16</sup>. To mimic the *in vivo* activation *in vitro*, T cells must also be stimulated with two artificial signals. Anti-CD3 antibodies were used successfully to simulate the TCR, as CD3 is one of the proteins in the TCR complex. A combination of anti-CD3 and anti-CD28 has been shown to mount a strong response from CD8+ T cells<sup>24,25</sup>.

**Activation markers.** The activation of CD8+ T cells begins a cascade of intracellular events. These events ultimately change the phenotype of the cell and induce massive proliferation as well as increased secretion of cytotoxic factors. Following activation, most CD8+ T cells upregulate certain surface molecules that can be used as markers for activation. These markers include CD69, CD25, and CD71.

The disulfide-linked homodimer CD69 is upregulated very quickly on the cellular membrane of T cells after activation<sup>26</sup>. It can be seen on the surface of T cells as early as 2–3 h after activation. The homodimer peaks at 24 h, after which it starts to decrease in expression, but it is still detectable at 120 h<sup>27</sup>. It has been difficult to identify the concrete function of CD69 in human cells; however, in murine cells, the marker is involved in many inflammatory disorders<sup>28–30</sup>. For CD4+ T cells, it participates indirectly in the development of these cells by influencing the expression of proteins from the JAK-STAT pathway (JAKs: Janus kinases, STATs: signal transducer and activator of transcription proteins)<sup>31</sup>. It has not been shown to have a significant effect on CD8+ T cells.

CD25 is a subunit of the interleukine-2 (IL-2) receptor (IL-2R), and thus it participates in the negative feedback loop in IL-2 secretion. Activated naïve T cells secrete IL-2, which is captured by the IL-2R of the same cells. Following internal activation of STAT5 and induction of B lymphocyte-induced maturation protein-1, the loop is closed by suppressing IL-2 secretion<sup>32</sup>. Although CD25 is mostly regarded as a CD4<sup>+</sup> T cell-related marker as it is expressed on resting CD4<sup>+</sup> regulatory T cells<sup>33</sup>, it has also been observed on resting memory CD8<sup>+</sup> T cells<sup>34,35</sup>. On activated CD8<sup>+</sup> T cells, CD25 expression peaks after 48 h and lasts for about 120 h<sup>27</sup>. CD71 is the transferrin receptor. It plays a role in the iron uptake of the cell and is ubiquitously expressed, especially on proliferating cells<sup>36</sup>. Therefore, it can be used as an indicator for proliferation and subsequently for T cell activation. This marker peaks on CD8<sup>+</sup> T cells at 48 h and maintains a stable expression for 72 h after activation<sup>27</sup>.

***The metabolic shift of activated T cells.*** In their steady-state, T cells rely primarily on the mitochondrial oxidative phosphorylation system (OXPHOS) to generate energy. After TCR activation, the demand for energy and metabolic intermediaries increases. The higher influx of nutrients, namely amino acids, and the consequent energy generated act as activators for the cellular mechanistic target of the rapamycin (mTOR) pathway<sup>37</sup>. The proteins in this pathway form two complexes, mTORC1 and mTORC2, the second of which participates in the further activation of T cells downstream from the TCR<sup>38</sup>. Simultaneously, a metabolic shift occurs from OXPHOS to anaerobic glycolysis<sup>39,40</sup>, because the latter is quicker than the former, although it is less efficient<sup>41</sup>. This shift happens despite the continual oxygen availability<sup>42</sup>. In addition, the activated T cells increase the expression of receptors for glucose and other nutrients on their membranes, which compensates for the overall inefficiency of glycolysis. With aging, however, nutrient-sensing of resting and activated T cells is disrupted<sup>43</sup> due to mitochondrial defects and dysregulations in the signaling pathways.

***Signaling proteins.*** There are numerous proteins involved in the signaling cascade of the TCR. One notable class of proteins is the serine-threonine kinases<sup>44</sup>. Within this class, protein kinase B (AKT) plays a major role in many cellular processes, including proliferation, apoptosis, and glucose metabolism. All these processes are increased in T cells after TCR activation and CD28 co-stimulation. Thus, AKT is essential for the transition of memory T cells<sup>45</sup> to glycolysis, and although the underlying mechanisms differ, AKT is also necessary for naïve T cell activation<sup>46</sup>. One other important role of AKT is the phosphorylation of forkhead box O (FoxO) proteins (Figure 2). After TCR activation and CD28 co-stimulation, AKT is phosphorylated either by mTORC2 or by other proteins<sup>38</sup>, which activate it and enable it to reach the nucleus, where the FoxO proteins are located in quiescent naïve T cells. FoxO proteins are transcription factors that are more active in naïve T cells, where they promote the expression of molecules such as L-selectin (CD62L) and C-

C chemokine receptor type 7 (CCR7). After they are phosphorylated, FoxO proteins exit the nucleus and form a complex with the 14-3-3 proteins, and their transcription activity is thereby blocked<sup>44,47</sup>.

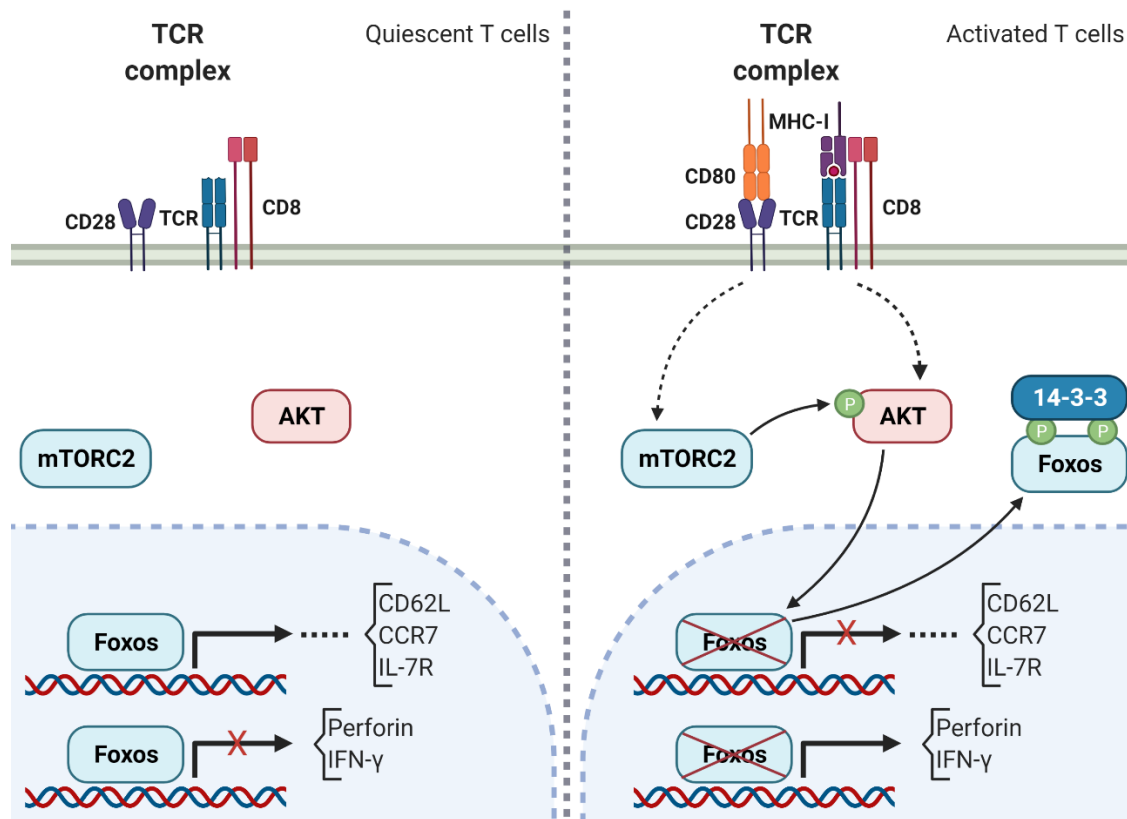


**Figure 2. Simplified TCR signaling pathway.** Within quiescent T cells, the FoxO family of proteins blocks the transcription of inflammatory and cytotoxic factors. After TCR stimulation and CD28 co-stimulation, AKT relocates to the nucleus and phosphorylates the FoxO proteins, which then move into the cytosol and bind to the 14-3-3 proteins. This allows the transcription of pro-inflammatory and cytotoxic factors and blocks the transcription of naïve-related molecules such as CD62L. The figure was created with BioRender.com.

**Polarization.** Similar to CD4<sup>+</sup> T cells, CD8<sup>+</sup> T cells can be polarized into type 1 (Tc1) or type 2 (Tc2)<sup>48</sup>. These two subdivisions can arise depending on the cytokines present in their environment and can propagate the corresponding type of immune response<sup>49–51</sup>. Thus, Tc2 are created by type 2 cytokines, such as IL-5, IL-13, and IL-9, and are mostly present in diseases triggered by type 2 cytokines, such as severe eosinophilic asthma<sup>52,53</sup> or rheumatoid arthritis<sup>54</sup>. Correspondingly, Tc1 cells are generated in the type 1 condition with IFN- $\gamma$  and IL-12 (Figure 3). These cells respond better in immunotherapies when type 1 cytokines are required<sup>55</sup>, including in allergology<sup>56</sup>. However, it has recently been shown that human CD8<sup>+</sup> naïve T cells preferentially respond to type 1 conditions<sup>57</sup>.

**Secretion patterns.** Since the main role of cytotoxic T cells is to kill infected host cells, they secrete large amounts of perforin and granzymes, the former disrupting the membrane of the target cell and the latter entering the cell and disrupting the cellular genome<sup>16</sup>. Naïve CD8<sup>+</sup> T cells mostly secrete IL-2, which is

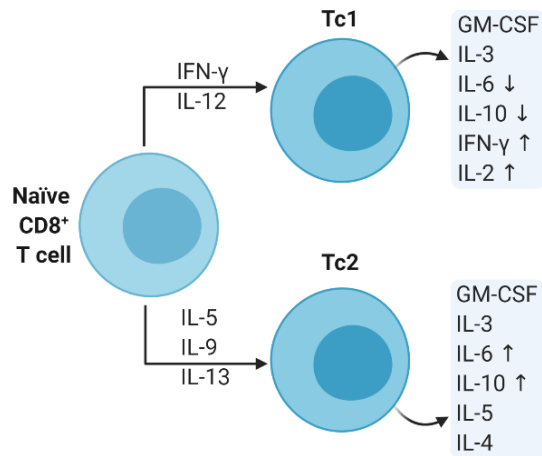


**Figure 3. Polarization and secretion patterns of CD8<sup>+</sup> T cells.** As a consequence of the microenvironment, CD8<sup>+</sup> T cells can be polarized into cytotoxic type 1 (Tc1) or 2 (Tc2) cells. The figure was created with BioRender.com.

needed for their survival. It has been hypothesized that effector CD8<sup>+</sup> T cells may have a wide secretion spectrum containing IL-2, IL-3, IL-4, IL-5, IL-6, IL-10, granulocyte-macrophage colony-stimulating factor (GM-CSF), interferon-gamma (IFN-γ), lymphotoxin, and tumor necrosis factor-alpha (TNF-α). If the CD8<sup>+</sup> T cells are restricted by their polarization, then the cells have a specific pattern of secretion: for Tc1 – IFN-γ, IL-2, and low levels of IL-6 and IL-10, and for Tc2 – IL-4, IL-5, and high levels of IL-6 and IL-10<sup>58</sup>. Both Tc1 and Tc2 secrete GM-CSF and IL-3, albeit in small amounts<sup>48</sup>. The eventual polarization and secretion pattern of CD8<sup>+</sup> T cells is decided by the APC and environmental conditions.

### 1.1.2. Formation of immunological memory

**The Lanzavecchia model.** After an infection clears and the immune response subsides, several types of memory T cells remain in circulation in a resting state. The Lanzavecchia model<sup>59</sup> describes four main subpopulations of both CD8<sup>+</sup> and CD4<sup>+</sup> T cells. The model uses two specific surface markers to distinguish between the subpopulations: CD45RA and CCR7. The CD45 surface marker belongs to the tyrosine phosphatase family. It has several isoforms, most notably CD45RA, which is expressed by naïve T cells and some memory cells<sup>60,61</sup>. The CCR7 molecule is a surface marker involved in homing the T cells back to secondary lymphatic organs<sup>16,59</sup>. Based on these two surface markers, the Lanzavecchia model classifies the CD8<sup>+</sup> T cell population into the following groups: naïve cells (CD45RA<sup>+</sup> CCR7<sup>+</sup>), central memory (CM; CD45RA<sup>-</sup> CCR7<sup>+</sup>), effector memory (EM; CD45RA<sup>-</sup> CCR7<sup>-</sup>), and terminally differentiated effector memory T cells re-expressing CD45RA (TEMRA; CD45RA<sup>+</sup> CCR7<sup>-</sup>). The main difference between CM and EM CD8<sup>+</sup> T cells is their surface expression of CCR7, which determines their localization. CM T cells can relocate to the lymph nodes using this surface marker. Another difference is that EM T cells have a more rapid response and produce larger amounts of perforin<sup>62</sup>.

### 1.1.3. Age-related alterations to the function of cytotoxic T cells

**Cellular senescence.** The Hayflick limit represents the number of times that a cell can replicate before its telomeres are too damaged and the cell undergoes growth arrest<sup>63</sup>. It is clear that growth arrest is induced

not only by damage to the telomeres but also DNA damage in general, among other factors<sup>64</sup>. Although senescence is known to be very complex, its main feature is growth arrest.

Growth is a key feature of T cells, which are required to undergo extensive and successive bursts of proliferation that need to end abruptly<sup>16</sup>. This leads to a senescence-like population of T cells, TEMRA, which accumulates with age. The functional characterization of TEMRA cells is not clear at this point. However, they have lower rates of proliferation, are prone to becoming apoptotic, and possess greater cytotoxicity<sup>65</sup>. In recent years, high levels of circulating CD8<sup>+</sup> TEMRA subsets have become an indicator for kidney transplant rejection<sup>66,67</sup>.

Cellular senescence can be regulated by PTMs, especially by acetylation. Sirtuins, a class of deacetylases, have an adverse role in senescence, as they are decreased in senescent cells<sup>68</sup>. In particular, SIRT2 serves as a cellular senescence marker<sup>69</sup>, and the activity and overexpression of Sirtuins either induce autophagy<sup>70</sup> or significantly reduce the probability of senescence phenotypes<sup>71,72</sup>.

**Stem cell exhaustion.** The continuous replenishing of the T cell compartment depends initially on the thymus<sup>73</sup>. However, the thymus starts to regress after the first year of life and continues to do so at an approximate rate of 3% per year until middle age, and some remnants of it are retained throughout life<sup>74</sup>. The naïve T cell compartment depends entirely on the thymus, and the involution of it greatly restricts the capacity of the naïve population to respond to infections in aged individuals<sup>2-6</sup>. Deacetylases are vital to the proper functioning of stem cells. A reduction in their activity, or even a knock-out of some deacetylases, is detrimental to the pluripotency of stem cells<sup>75,76</sup>.

**Inflammaging by CD8<sup>+</sup> T cells.** During the aging process, there is a shift in the predominant T cell population from naïve to memory. There are multiple types of memory cells with complex functions<sup>77</sup>. The shift in the predominant type of T cells is one cause for the increase of pro-inflammatory factors such as IL-6, TNF- $\alpha$ , and IFN- $\gamma$  in older individuals<sup>78-80</sup>. While IL-2 may also increase in old age, some studies have found no change in the circulatory amounts<sup>80,81</sup>. The increase in pro-inflammatory factors corresponds with the decrease in anti-inflammatory cytokines, although IL-4 and IL-10 have been shown to fluctuate in older populations<sup>81,82</sup>. The direct source of these circulating factors may be the increased number of memory T cells. For example, TEMRA cells, which accumulate over time, have been shown to secrete more pro-inflammatory factors<sup>83</sup>.

### 1.2. Protein post-translational modifications

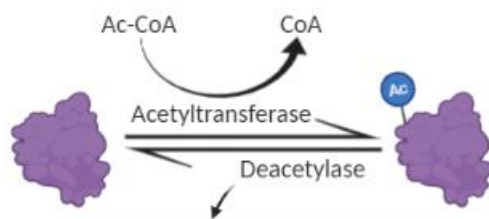
PTMs can occur from the moment the proteins are synthesized by ribosomes<sup>84</sup>. The purpose of these modifications varies from initiating signaling cascades<sup>85</sup> to structural organization<sup>86</sup>, or as a response to

cellular stress<sup>87</sup>. Thus, the proteome does not correspond one-to-one with the genome. While one gene can theoretically be translated into one protein, that protein can be modified in many ways, which extends its purpose. It has been estimated that the proteome is between 10 to 100 times more complex than the genome, in part due to PTMs<sup>88</sup>. However, some have argued that it may not be possible to find the upper limit to the complexity of the proteome, due to the number of factors that contribute to it<sup>89</sup>.

PTMs can range from small inorganic molecules such as nitric oxide groups to very complex organic groups such as polysialylation. Acetylation and phosphorylation are both small modifications, and they have been the most commonly observed PTMs in experiments<sup>90</sup>. However, phosphorylation has been the most studied modification<sup>91</sup>. Although histone acetylation has been known to be a major player in the cellular landscape since the 1960s<sup>92-94</sup>, acetylation as a PTM has not been heavily studied until recently.

### 1.2.1. Classification of deacetylases

**Acetylation.** This mostly enzymatic reaction regulates many cellular processes, including DNA repair,



Class I	HDAC1 HDAC2	HDAC3 HDAC8	Zn <sup>2+</sup>
Class IIa	HDAC4 HDAC5	HDAC7 HDAC9	Zn <sup>2+</sup>
Class IIb	HDAC6 HDAC10		Zn <sup>2+</sup>
Class III	SIRT1 SIRT2 SIRT3 SIRT4	SIRT5 SIRT6 SIRT7	NAD <sup>+</sup>
Class IV	HDAC11		Zn <sup>2+</sup>

**Figure 4. Representation of the enzymatic reaction of acetylation.** Two types of enzymes participate in acetylation: (1) acetyltransferases, which add the acetyl group on proteins and use acetyl-Coenzyme A (Ac-CoA) as an acetyl donor, and (2) deacetylases, which perform the reverse reaction. Deacetylases are divided into two families based on whether Zinc or NAD<sup>+</sup> is used as the co-factor, and the families are further divided into four classes. The figure was created with BioRender.com.

mRNA stability, protein-protein interaction, and protein localization<sup>95,96</sup>. In the mitochondria, acetylation can be non-enzymatic, due to the basic pH and high levels of acetyl-coenzyme A<sup>97</sup> (Ac-CoA). Specifically, in T cells, the TCR signal strength is strongly associated with the levels of Ac-CoA, which eventually regulate the lysine acetylation levels. This correlation is the result of TCR-mediated phosphorylation of a key citrate synthase by AKT in the metabolism of Ac-CoA<sup>98</sup>. In the other organelles and the cytoplasm, acetylation is a reversible enzymatic reaction controlled by two types of enzymes. Acetyltransferases add the acetyl group, and deacetylases remove it (Figure 4). As these enzymes were first found to target histones, they are known as histone acetyltransferases (HATs) and histone deacetylases (HDACs). Unlike HDACs, HATs have a more complex classification, because some of these enzymes represent protein complexes with very broad functions. HATs can be roughly divided into three major families, one of which is the p300/CREB-binding protein complex<sup>99</sup>.

**Deacetylases.** HDACs are the *erasers* of acetylation, and the classification of these enzymes is based on the co-factors used. The first family represents the Zn<sup>+</sup>-dependent “classical” HDACs, while the second family is nicotinamide adenine dinucleotide (NAD)<sup>+</sup>-dependent and its members are called sirtuins<sup>91,100</sup> (SIRT). The numbering of the HDACs (1–11) and SIRTs (1–7) is simply in the order in which they were discovered. Class I HDACs mostly target histones, although they also have other substrates. Meanwhile, class III enzymes (sirtuins) have been shown to perform other catalytic functions besides deacetylase activities: some sirtuins function as hydrolases<sup>101</sup>, adenine dinucleotide-ribosyltransferases,<sup>102</sup> or demalonylases, and desuccinylases<sup>103</sup>.

### 1.2.2. Histone and non-histone protein acetylation

**Epigenetic changes.** Non-genomic information can be stored in the chromatin structure, gene networks, and PTMs of the histone proteins<sup>104</sup>. This information is passed down from parent to offspring in the same way as genomic information,<sup>105</sup> and it can be modified by aging. Methylation and acetylation are two PTMs that have a significant effect on the chromatin structure by influencing the conformation of the histones and the location of the transcription factors<sup>95,106</sup>. Both PTMs also have a major impact on the whole cellular environment, as they have been linked to increased inflammation initiated by macrophages<sup>107</sup>. In addition, faulty PTM regulation results in the accumulation of misfolded proteins and protein aggregates. Several age-related disorders, such as cardiovascular and neurodegenerative diseases<sup>108–110</sup>, have been shown to result from the accumulation of misfolded proteins.

**Histone acetylation.** Histones are basic proteins;<sup>111</sup> therefore, a PTM such as acetylation, which introduces a negative charge, can induce a strong modification to the higher organization of these proteins. The presence of the acetyl group on the histones enables differentiation between euchromatin and heterochromatin<sup>112</sup>. The acetylation sites on histones are highly conserved, with 3.6 residues in between them, in a similar fashion to the  $\alpha$ -helix structure<sup>113</sup>. Since acetylation influences the flexibility of the chromatin, its effects on specific gene expression has been heavily studied<sup>114–116</sup>.

**Non-histone protein acetylation.** About 20 years after cellular acetylation was discovered, several non-histone proteins were shown to be acetylated<sup>91</sup>. Amongst the first were the high mobility group proteins in 1979<sup>117</sup> and  $\alpha$ -tubulin in 1983<sup>118,119</sup>. In 2007, it was shown that acetylation occurs in the lumen of the endoplasmic reticulum (ER) and the Golgi apparatus as well as in the nucleus<sup>120</sup>. Later, acetylation in the ER was shown to be a key component in the regulation of proteostasis<sup>121,122</sup>.

One of the most important cellular components which are altered by acetylation is the cytoskeleton. In the case of T cells, the shape of the cytoskeleton changes not only during an infection due to T cell activation, but also when the cell moves to the infection site. The cytoskeleton organizes the immune

synapse when necessary, and acetylation regulates the organization of tubulin<sup>123</sup>. Acetylation also stabilizes the tubulin microtubules<sup>124</sup> and affects the mobility of cells by modifying actin and cortactin<sup>125,126</sup>.

**Regulation of cellular metabolism.** Since acetylation has such a wide range of targets, it has an extensive effect on the metabolism of the cell<sup>127</sup>. First, acetylation indirectly controls the transcription of genes. Second, it directly modifies the characteristics of key proteins. The function and localization of glyceraldehyde-3-phosphate dehydrogenase<sup>128,129</sup> (GAPDH) and several proteins involved in the tricarboxylic acid cycle<sup>130</sup> (TCA) are regulated by acetylation. As T cells undergo a metabolic shift during activation, GAPDH and the TCA cycle proteins increase their activities, and a disturbance at this stage ultimately affects the activation of T cells (Figure 5).

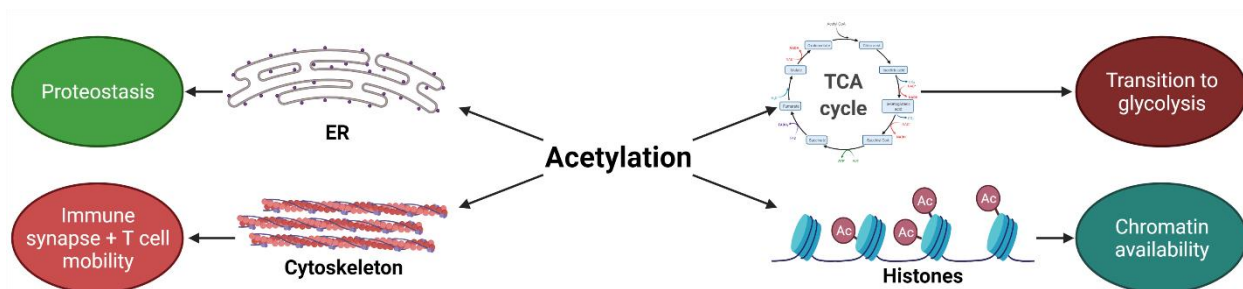


**Figure 5. Cellular functions of acetylation.** A small number of the roles acetylation plays in the cell are presented. Acetylation influences chromatin availability by changing the overall charge of the histones, proteostasis by modifying the pH of the ER, the mobility of the cells by altering the cytoskeleton, and the transition of T cells to glycolysis by modifying the proteins involved in the TCA cycle. The figure was created with BioRender.com.

### 1.2.3. Deacetylation in aging and anti-aging

**HDACs in CD8<sup>+</sup> T cells.** Acetylation plays an important role in the functioning of CD8<sup>+</sup> T cells. Class I HDACs are involved in the maturation of T cells. Specifically, HDAC3 prevents MHC-II-restricted thymocytes from maturing into CD8<sup>+</sup> T cells<sup>131,132</sup>, and HDAC4 controls several transcription factors such as NF- $\kappa$ B<sup>133,134</sup>, which are essential to T cell functions, although an HDAC4 knock-down does not seem to affect the functioning or development of CD8<sup>+</sup> T cells<sup>135</sup>. HDAC11 is a known negative regulator of immune functions.<sup>136</sup> In T cells, its knock-down increases effector functions by increasing the expression of eomesodermin<sup>137</sup> (Eomes).

**Sirtuins.** Deacetylases have been proven to be essential to proper cellular functions. Some sirtuins, such as SIRT1, SIRT3, and SIRT6, have been correlated with aging. The link between SIRT1 and aging has been established by numerous studies. The expression of this sirtuin decreases in aged murine tissues<sup>138,139</sup>, with a sharp decline in the central neuronal and hepatic tissues<sup>140</sup>. Decreased expression of SIRT1 in mice

leads to rapid aging and several disease phenotypes<sup>141,142</sup>. The anti-aging effect of SIRT1 consists in its function as an anti-inflammatory regulator. Along with melatonin, it influences the circadian rhythm and antagonizes inflammaging<sup>143</sup>.

Unlike the other sirtuins, SIRT3 promotes longevity. Studies on centenarians have shown that SIRT3 is strongly expressed in the peripheral blood mononuclear cells (PBMC) of long-lived individuals. It has also been shown to increase with caloric restriction, a dietary method that promotes longevity<sup>144,145</sup>. *In vitro* and *in vivo* models with decreased expression of SIRT3 have shown increased amounts of reactive oxygen species<sup>146</sup>, which leads inevitably to greater DNA damage. SIRT1 and SIRT6 can be linked to longevity only hypothetically because they protect against metabolic disease – an age-related illness<sup>147</sup> and increased double-strand DNA break repair<sup>148</sup>. In addition, the over-expression of SIRT6 extends the life span of male mice<sup>149</sup>. Mice with a SIRT6 knock-down show an accelerated aging phenotype and die at a young age. For these mice, the CD4<sup>+</sup> and CD8<sup>+</sup> T cell populations also drop very rapidly<sup>150</sup>. Despite all this, there is evidence that sirtuins promote tumor growth through the same processes previously discussed<sup>151,152</sup>.

**Deacetylase inhibitors.** HDACs have increased expression in cancers,<sup>153,154</sup> and molecules that inhibit these enzymes have been tested for their anti-cancerous and anti-inflammatory properties<sup>7–10</sup>.

Trichostatin A<sup>155</sup> (TSA) is used as a pan-HDAC inhibitor against Zn<sup>+</sup>-dependent HDACs and has been shown to reduce proliferation and interfere in the differentiation of several cell types<sup>156–158</sup>; it is currently being tested in several clinical trials<sup>159</sup>. Because TSA acts as a general inhibitor of deacetylation, it can influence the expression of histones and the chromatin structure<sup>160,161</sup>, which leads to a different gene expression. EX-527<sup>162</sup> is a small molecule that inhibits sirtuins through an NAD<sup>+</sup>-dependent mechanism<sup>163</sup>. This molecule has been shown to aid in neurogenesis by inhibiting SIRT1,<sup>164</sup> and it has a protective effect against lung injury and diabetic nephropathy in mice<sup>165,166</sup>. However, so far, no clinical trials have been conducted with EX-527 in humans, and only one study that started in 2020 has been documented<sup>167</sup>.

Nicotinamide (NAM) is derived from vitamin B3. This molecule exists physiologically in human cells and is quickly transformed into NAD<sup>+</sup>, a highly important co-factor in cellular metabolism<sup>168</sup>. NAD<sup>+</sup> is essential for the activity of sirtuins, and the molecule in itself plays a controversial role, as it can act as either an inhibitor or an activator of sirtuins<sup>169,170</sup>. This molecule is involved in several key cellular processes<sup>168</sup>. It has also been shown to decrease with aging, which is determined by CD38, a membrane-bound hydrolase that breaks down NAD<sup>+</sup><sup>171</sup>. A decline in NAD<sup>+</sup> has been associated with several diseases such as diabetes, Alzheimer's, atherosclerosis, and even depression<sup>172</sup>. However, NAM on its own is primarily used as an oral supplement for vitamin B3 deficiencies<sup>173</sup>.

## 2. Aims and objectives

Aging is a general physiological process that affects all aspects of life. Recently, PTMs have emerged as key regulators of cellular processes. However, the overlapping effects of aging and PMTs have not been widely studied, especially in the context of the adaptive immune system. Therefore, the current thesis aims to investigate the role of acetylation at the cellular level of aging CD8<sup>+</sup> T cells.

To this end, CD8<sup>+</sup> T cells were magnetically sorted from young and old healthy blood donors, with the following objectives:

1. The relative expression of HDACs was analyzed both at a transcript level and a protein level both after only activating the CD8<sup>+</sup> T cells and after activating and treating them with HDACi.
2. Two-dimensional gel electrophoresis and precise fluorescent staining were used to analyze the proteome of CD8<sup>+</sup> T cells from young and old donors, and the expression profiles were compared between the two age groups.
3. Proteins that showed a different expression after HDACi treatment were identified using mass spectrometry, then the protein-protein interaction network and functional enrichment analysis were done using a search tool for the retrieval of interacting genes online tool.
4. The function of CD8<sup>+</sup> T cells from both age groups was analyzed after stimulation with or without HDACi treatment by measuring and comparing the surface expression of activation markers, the secretion of cytokine and pro-inflammatory factors, the proliferation capacity, and the apoptosis rate.
5. The transcriptome of activated CD8<sup>+</sup> T cells from young and old donors was determined with RNA sequencing and the pathways affected by aging were identified with gene ontology enrichment tools.

### 3. Methods

#### 3.1. Materials

##### 3.1.1. Commercially available reagents, equipment and tools

*Table 1. Reagents and equipment.*

Materials	Distributor
	Reagents
100 bp DNA Ladder	Thermo Fisher Scientific, Waltham, MA, USA
11-deoxycorticosterone (DOC)	Sigma-Aldrich Chemie GmbH, Taufkirchen bei Munchen, Germany
2XRNA Loading Dye	Thermo Fisher Scientific
3-[(3-Cholamidopropyl)-dimethylammino]-1propansulfonat (CHAPS)	AppliChem GmbH, Darmstadt, Germany
Acetone	Sigma-Aldrich GmbH
Acetonitrile (ACN)	AppliChem GmbH
Acrylamide	Sigma-Aldrich GmbH
Agarose	BioLine GmbH, Luckenwalde, Germany
Agarose with a low melting point	SERVA Electrophoresis GmbH, Heidelberg, Germany
Ammonium sulfate (NH <sub>4</sub> ) <sub>2</sub> SO <sub>4</sub>	AppliChem GmbH
Ammonium bicarbonate (ABC)	AppliChem GmbH
Ammonium persulfate (APS)	AppliChem GmbH
Ampuwa water	Fresenius Kabi GmbH, Bad Homburg, Germany
Anti-CD28, clone REA1047	BD Biosciences
Anti-CD3, clone OKT3	Thermo Fisher Scientific
Benzonase	Novagen, San Diego, CA, USA
Bicoll 1.077 g/ml	Biochrom, Berlin, Germany
Bovine Serum Albumin (BSA)	Sigma-Aldrich GmbH
Bromphenol-blue	AppliChem GmbH
Calbiochem A non-detergent sulfobetaine (NDSB 256)	AppliChem GmbH
Calcium chloride - CaCl <sub>2</sub>	Sigma-Aldrich GmbH
Coomassie-Brilliant-Blue G-250	AppliChem GmbH
Deacetylation inhibition (HDACi) cocktail	SantaCruz, Dallas, TX, USA
Dimethyl sulfoxide (DMSO)	Carl Roth GmbH + Co KG, Karlsruhe, Germany
Disodium hydrogen phosphate - Na <sub>2</sub> HPO <sub>4</sub>	AppliChem GmbH
Dithiothreitol (DTT)	AppliChem GmbH
Dulbecco`s Phosphate Buffered Saline (PBS)	Sigma-Aldrich GmbH
Dulbecco's Modified Eagle Medium for cell culture	Gibco® by Life Technologies, Karlsruhe, Germany
Ethanol absolute	Sigma-Aldrich GmbH
Ethylene diamine tetra-acetic acid (EDTA)	Sigma-Aldrich GmbH
Fetal Calf Serum (FCS)	PAN Biotech, Aidenbach, Germany
Glycerol	AppliChem GmbH
Glycine	AppliChem GmbH
Hydrochloric acid - HCl	AppliChem GmbH
IL-2 Recombinant Human Protein	ThermoFisher
Immobilized DryStrip Cover Fluid	GE Healthcare, Buckinghamshire, UK
Immobilized DryStrip pH 3-10 NL, 18cm	GE Healthcare
Iodamicine	AppliChem GmbH

L-Glutamine	Lonza, Verviers, Belgium
L-Lysine	AppliChem GmbH
Low Molecular Weight SDS-PAGE Marker Kit	GE Healthcare
Lumi-Light Western-Blotting Substrate	Roche Diagnostics, Mannheim, Germany
Matrix for MALDI-TOF mass spectrometry (α-Cyano-4-hydroxy-cinnamic acid)	Bruker Daltonics Inc, Bremen, Germany
Methanol	Carl Roth GmbH
Non-detergent sulfobetaine 256 (NDSB)	Sigma-Aldrich GmbH
Nonylphenol-40 (NP-40)	Sigma-Aldrich GmbH
Ortho-Phosphoric acid - orto-H <sub>3</sub> PO <sub>4</sub>	Merck Milipore, Darmstadt, Germany
PageRuler™ Prestained Protein Ladder, 10 to 180 kDa	Thermo Fisher Scientific
Penicillin/Streptomycin Mix (PenStrep)	PAA Laboratories GmbH, Pasching, Austria
Peptide Calibration Standard II	Bruker Daltonics
Pharmalytes pH 3-10	GE Healthcare
Phosphatase inhibitor cocktail 2	Sigma-Aldrich
Phosphatase inhibitor cocktail 3	Sigma-Aldrich
Plus One DryStrip Cover Fluid	GE Healthcare
Polysorbate 20 (Tween 20)	AppliChem GmbH
Ponceau S	AppliChem GmbH
Potassium Chloride - KCl	AppliChem GmbH
Potassium phosphate monobasic - KH <sub>2</sub> PO <sub>4</sub>	AppliChem GmbH
Propidium Iodine	Sigma-Aldrich GmbH
Protease Inhibitor Cocktail II	Merck Milipore
SERVA Lightning SciDye Set	SERVA Electrophoresis GmbH
SignalFire ECL Reagent	Cell Signaling Tech.
Sodium chloride - NaCl	AppliChem GmbH
Sodium dodecyl sulphate (SDS)	AppliChem GmbH
Sodium thiosulfate (Na <sub>2</sub> S <sub>2</sub> O <sub>3</sub> )	AppliChem GmbH
Tetraacetythylenediamine (TEMED)	AppliChem GmbH
Thiourea	AppliChem GmbH
Trichloroacetic acid (TCA)	AppliChem GmbH
Trifluoro acetic acid (TFA)	AppliChem GmbH
Tris(hydroxymethyl)aminomethane hydrochloride (Tris) Ultrapure	AppliChem GmbH
Trypsin	Promega
Urea	AppliChem GmbH
X-Vivo™ 15 medium	Lonza
β-Mercaptoethanol	AppliChem GmbH
<b>Kits</b>	
2 X SYBR Green qPCR Master Mix	Promega, Madison, WI, USA
Annexin V-FITC - apoptosis kit	Miltenyi, Bergisch Gladbach, Germany
Carboxyfluorescein succinimidyl ester (CFSE)	-
CellTrace™ Cell Proliferation Kit	Thermo Fisher Scientific
CD8 <sup>+</sup> Memory T cell Isolation kit, human	Miltenyi
CD8 <sup>+</sup> microbeads, human	Miltenyi
CD8 <sup>+</sup> CD45RA <sup>+</sup> Effector T Cell Isolation Kit, human	Miltenyi
Effector CD45RA <sup>+</sup> CD8 <sup>+</sup> kit	Miltenyi
GoTaq G2 Flexi DNA Polymerase	Promega
Memory CD8 <sup>+</sup> kit	Miltenyi
MultiSort kit	Miltenyi
RevertAid First Strand cDNA synthesis kit	Thermo Fisher Scientific

Machines	
BD LSR Fortessa flow cytometer	BD Biosciences
Bio-5000plus	Microtek, Hsinchu, Taiwan
CFX Connect Real-Time System	Bio-Rad, Hercules, CA, USA
CO <sub>2</sub> Incubator	Thermo Fisher Scientific
Cold centrifuge	Thermo Fisher Scientific
DigestPro MSi	INTAVIS Bioanalytical Instruments AG, Cologne, Germany
E-Box VX5	Vilber, Collégien, France
ETTAN IPGphor IEF Isoelectric Focusing Unit	Amersham Pharmacia Biotech, San Francisco, CA, USA
FLA-5100 fluorescent image analyzer	FujiFilm, Tokyo, Japan
FujiFilm LAS-300	FujiFilm
Hoefler EPS 2A200 Electrophoresis Power Supply	Marshall Scientific, Hampton, NH, USA
Infinite 200 PRO Microplate Reader	Tecan Group Ltd., Mannedorf, Switzerland
MACS Midi magnet	Miltenyi
MACS Mini magnet	Miltenyi
MACS Multi Stand	Miltenyi
Matrix-assisted laser-desorption/ionization time-of-flight (MALDI-TOF) mass spectrometer	Bruker Daltonics Inc
Mini-PROTEAN(R) Tetra System	Bio-Rad
MTP 384 target plate ground steel	Bruker Daltonics Inc
NanoQuant Plate™	Atlantic Lab Equipment, Beverly, MA, USA
PowerPac Basic power source	Bio-Rad
Spot picker GelPal	Genetix, Munchen, Germany
Strip holder	GE Healthcare
SubCell GT chamber	Bio-Rad
Tecan M200 Plate Reader	Atlantic Lab Equipment
Trans-Blot Cell chamber	Bio-Rad
Transsonic 460	Elma Schmidbauer GmbH, Singen, Germany
Plasticware	
12 well plate	Sarstedt, Nümbrecht, Germany
24 well plate	Sarstedt
50 ml Leucosep™ Tubes	Greiner Bio-One GmbH, Kremsmünster, Austria
70 µm pre-separation filters	Miltenyi
75x12mm tube	Sarstedt
96 well collect plate	INTAVIS
96 well reaction plate	INTAVIS
Immobilized pH Gradient strip 3-10 pH	GE Healthcare
LS columns	Miltenyi
MS columns	Miltenyi
Nitrocellulose membrane	GE Healthcare
NucleoSpin RNA isolation kit	Machery-Nagel, Düren, Germany
Pasteur pipette	Sigma-Aldrich GmbH
Zip Tips	Merck Milipore
Software	
2D Delta software	DECODON, Greifswald, Germany
BD FACS Diva software	BD Biosciences
Biological database Network	<a href="https://biodbnet-abcc.ncifcrf.gov/db/db2dbRes.php">https://biodbnet-abcc.ncifcrf.gov/db/db2dbRes.php</a>
Bio-Rad CFX Maestro software	Bio-Rad
BioRender	<a href="https://biorender.com/">https://biorender.com/</a>
Biotools 3.2	Bruker Daltonics Inc

CFX Maestro	Bio-Rad
FCAP Array	BD Biosciences
FCS Express 6 Plus Research Edition	DeNovo Software, San Diego, CA, USA
FlexAnalysis	Bruker Daltonics Inc
FlexControl Ultraflex Tof/Tof	Bruker Daltonics Inc
Gene Ontology enRichment analysis and visualizAtion tool (GORilla)	<a href="http://cbl-gorilla.cs.technion.ac.il/">http://cbl-gorilla.cs.technion.ac.il/</a>
GraphPad Prism 9	personal license
Image Studio™ Lite	LI-COR Biotechnology, NE, USA
MASCOT search engine	Matrix Science, Durham, NC, USA
National Center for Biotechnology Information (NCBI) Reference Sequence Database	<a href="https://www.ncbi.nlm.nih.gov/refseq/">https://www.ncbi.nlm.nih.gov/refseq/</a>
Primer Blast	<a href="https://www.ncbi.nlm.nih.gov/tools/primer-blast/">https://www.ncbi.nlm.nih.gov/tools/primer-blast/</a>
ScanWizard Bio	Microteck
String – search tool for the retrieval of interacting genes	<a href="https://string-db.org/">https://string-db.org/</a>
The R project for Statistical Computing	<a href="https://www.r-project.org/">https://www.r-project.org/</a>
Venny 2.1.0	<a href="https://bioinfogp.cnb.csic.es/tools/venny/">https://bioinfogp.cnb.csic.es/tools/venny/</a>
UniProt	<a href="https://www.uniprot.org/">https://www.uniprot.org/</a>

**Table 2. Flow cytometry antibodies.** For each antibody the fluorophore, clone and dilution are given below.

Name	Fluorophore	Clone	Dilution	Distributor	Purpose
Anti-CD3	FITC	Sk7	1:70	BD Biosciences	Subset
Anti-CD8	BV605	SK1	1:140	BD Biosciences	identification
Anti-CCR7	PE	3D12	1:35	BD Biosciences	Naive/memory
Anti-CD45RA	APC	REA1047	1:470	Miltenyi	discrimination
Anti-CD25	PE	M-A251	1:70	BD Bioscience	Activation markers
Anti-CD69	FITC	FN50	1:70	BD Bioscience	
Anti-CD71	APC	CY1G4	1:235	Biolegend, San Diego, CA, USA	

**Table 3. Western blot antibodies.**

Antibody	Dilution	Source	Distributor	
Primary antibodies				
Acetylated lysine	1:500	Rabbit	Cell Signaling Tech., Danvers, MA, USA	
HDAC11 (D5I8E)	1:1000	Rabbit		
HDAC3 (7G6C5)	1:1000	Mouse		
HDAC4 (D15C3)	1:1000	Rabbit		
Tubulin	1:1000	Mouse		
acetyl-Tubulin	1:1000	Rabbit		
AKT	1:1000	Rabbit		
phospho-AKT	1:1000	Rabbit		
14-3-3 zeta/delta	1:1000	Rabbit		
HSP90	1:1000	Rabbit		
Secondary antibodies				
Anti-mouse horseradish peroxidase-conjugated IgG	1:1000	Horse		
Anti-rabbit HRP-conjugated IgG	1:1000	Goat		

### 3.1.2. Chemical solutions, gels, and recipes

The solvent for all the buffers was double-distilled water, unless stated otherwise. A substance followed by “/HCl pH x” indicates that the pH level was adjusted with HCl (AppliChem GmbH, Darmstadt, Germany).

*Buffers:*

**T cell culture medium:** X-Vivo™ 15 (Lonza) with 1% (v/v) L-glutamine (Lonza, Verviers, Belgium), 1% (v/v) penicillin/streptomycin mixture (Sigma-Aldrich Chemie GmbH, Taufkirchen bei Munchen, Germany).

**Phosphate-buffered saline (PBS), pH 7.4:** 70 mM NaCl (AppliChem GmbH), 1.5 mM KCl (AppliChem GmbH), 750 nM KH<sub>2</sub>PO<sub>4</sub> (Sigma-Aldrich GmbH), 400 nM Na<sub>2</sub>HPO<sub>4</sub> (Sigma-Aldrich GmbH).

**Fluorescence-activated cell-sorting (FACS) buffer:** PBS with 2mM ethylenediaminetetraacetic acid (EDTA; Sigma-Aldrich GmbH), 0.5% (v/v) fetal calf serum (FCS; PAN Biotech, Aidenbach, Germany).

**Tris, acetic acid, and EDTA (TAE) buffer:** 40 mM tris(hydroxymethyl)aminomethane hydrochloride (Tris; AppliChem GmbH), 20 mM acetic acid (Carl Roth GmbH + Co KG, Karlsruhe, Germany), 1 mM EDTA (Sigma-Aldrich GmbH).

**Radioimmunoprecipitation assay (Ripa) buffer, pH 8:** 50 mM Tris (AppliChem GmbH), 150 mM NaCl (AppliChem GmbH), 0.1% (m/v) sodium dodecyl sulphate (SDS; AppliChem GmbH), 0.5% (m/v) 11-deoxycorticosterone (DOC; Sigma-Aldrich GmbH), 1% (v/v) nonylphenol-40 (NP-40; Sigma-Aldrich GmbH).

**Western blot (WB) running buffer:** 0.25 M Tris UltraPure (AppliChem GmbH), 2 M glycine (AppliChem GmbH), 0.1% (m/v) SDS (AppliChem GmbH).

**Ponceau S buffer:** 3% (v/v) trichloroacetic acid (AppliChem GmbH), 2% (m/v) Ponceau S (AppliChem GmbH).

**WB transfer buffer:** 0.25 M Tris UltraPure (AppliChem GmbH), 2 M glycine (AppliChem GmbH), 20% (v/v) methanol (Carl Roth).

**Tris-buffered saline with Tween (TBS-T) buffer, pH 7.6:** 20 mM Tris UltraPure (AppliChem GmbH), 140 mM NaCl (AppliChem GmbH), 1% (v/v) Polysorbate 20 (Tween 20; AppliChem GmbH).

**Minimal labeling buffer, pH 8.5:** 9.5 M Urea (AppliChem GmbH), 4% (m/v) 3-[(3-cholamidopropyl)-dimethylammonio]-1-propanesulfonate (CHAPS; AppliChem GmbH), 1% (m/v) dithiothreitol (DTT; AppliChem GmbH), 0.5% (v/v) Pharmalytes (AppliChem GmbH).

**2x Rabilloud buffer:** 7 M urea (AppliChem GmbH), 2 M thiourea (AppliChem GmbH), 30 mM Tris UltraPure (AppliChem GmbH), 4% (m/v) CHAPS (AppliChem GmbH), 2% (m/v) DTT (AppliChem GmbH), 1% (v/v) pH 3–10 ampholytes (AppliChem GmbH), traces of bromophenol blue (AppliChem GmbH).

**Rabilloud buffer:** 7 M urea (AppliChem GmbH), 2 M thiourea (AppliChem GmbH), 4% (m/v) CHAPS (AppliChem GmbH), 1% (m/v) DTT (AppliChem GmbH), 0.2 M Calbiochem A non-detergent sulfobetaine

(NDSB 256; AppliChem GmbH), 0.5% (v/v) pH 3–10 ampholyte (AppliChem GmbH), traces of bromophenol blue (AppliChem GmbH).

**Equilibration buffer:** 6 M urea (AppliChem GmbH), 2% (m/v) SDS (AppliChem GmbH), 50 mM Tris/HCl pH 8.8 (AppliChem GmbH), 30% (v/v) glycerol (AppliChem GmbH).

**Equilibration buffer 1:** equilibration buffer with 1.5% (m/v) DTT (AppliChem GmbH).

**Equilibration buffer 2:** equilibration buffer with 4.8% (m/v) iodamicine (AppliChem GmbH).

**SDS–polyacrylamide gel electrophoresis (SDS-PAGE) running buffer for two-dimensional electrophoresis (2DE) gels:** 25 mM Tris (AppliChem GmbH), 192 mM glycine (AppliChem GmbH), 0.1% (m/v) SDS (AppliChem GmbH).

**Fixation buffer:** 40% (v/v) ethanol absolute (Sigma-Aldrich GmbH), 10% (v/v) acetic acid (Carl Roth GmbH).

**Coomassie staining solution:** 23.1% (v/v) orto- $\text{H}_3\text{PO}_4$  (Carl Roth GmbH), 10% (m/v)  $(\text{NH}_4)_2\text{SO}_4$  (AppliChem GmbH), 20% (v/v) methanol (AppliChem GmbH), 0.1% (m/v) Coomassie Brilliant Blue G-250 (AppliChem GmbH).

*Gels:*

**WB running gel (10%):** 4.8 ml double-distilled water, 2.5 ml acrylamide (Sigma-Aldrich), 2.5 ml 1.5M Tris, pH 8.8 (AppliChem GmbH), 0.1 ml 10% (m/v) SDS (AppliChem GmbH), 0.1 ml 10% (m/v) ammonium persulfate (APS; AppliChem GmbH), 4  $\mu\text{l}$  tetramethylethylenediamine (TEMED; AppliChem GmbH).

**WB stacking gel (5%):** 2.4 ml double distilled water, 0.5 ml acrylamide (Sigma-Aldrich), 1 ml 1.5M Tris pH 6.8 (AppliChem GmbH), 0.04 ml 10% (m/v) SDS (AppliChem GmbH), 0.04 ml 10% (m/v) ammonium persulfate (APS; AppliChem GmbH), 6  $\mu\text{l}$  TEMED (AppliChem GmbH).

**2DE gel:** 43.3 ml acrylamide (Sigma-Aldrich), 50 ml 1M Tris pH 8.8 (AppliChem GmbH), 5.3 ml glycerol (AppliChem GmbH), 0.6 ml 1M  $\text{Na}_2\text{S}_2\text{O}_3$  (AppliChem GmbH), 32.6 ml double-distilled water, 1.3 ml 10% (m/v) APS (AppliChem GmbH), 66.6  $\mu\text{l}$  TEMED (AppliChem GmbH).

### 3.1.3. Biological material

**Donors' characteristics.** Two distinct age groups of healthy blood donors were established as either young (<30 years old), or old (>60 years old). Balanced numbers of donors from both age groups were used for each experiment. The donors were classified based on age only unless stated otherwise. Buffy coats from the donors were obtained from the blood bank<sup>174</sup> of the University Hospital in Halle (Saale) with the donors' consent

**PBMC isolation.** The PBMCs were separated using the density gradient method with Biocoll 1.077 g/ml (Biochrom, Berlin, Germany). In a 50-ml Leucosep Falcon tube (Greiner Bio-One GmbH, Kremsmünster, Austria), 15 ml Biocoll was added. The tube was centrifuged at 1,000 g for one minute to allow the solution

to pass through the filter. A 1:1 mixture of buffy coat and PBS (Sigma-Aldrich GmbH) was then added over the filter of the Leucosep tube. The tube was centrifuged at 1,000 g for 10 min at the lowest setting for acceleration and no deceleration. The density of the Bicolll and the centrifugation step separated the white blood cells above the interphase between the Bicolll and plasma, forming a white ring. The white blood cells were collected with a Pasteur pipette (Sigma-Aldrich GmbH) and washed once with PBS. All the collected PBMCs were frozen in FCS (PAN Biotech) with 10% dimethyl sulfoxide (Carl Roth + Co KG) and stored in a freezer at  $-150^{\circ}\text{C}$ .

**Isolation of CD8<sup>+</sup> T cells.** The CD8<sup>+</sup> T cells were magnetically sorted using CD8<sup>+</sup> beads (Miltenyi, Bergisch Gladbach, Germany) according to the manufacturer's protocol, and the PBMCs were filtered using 70- $\mu\text{m}$  pre-separation filters (Miltenyi) before starting the sorting protocol. The CD8<sup>+</sup> CD45RA<sup>-</sup> memory T cells were sorted in two steps. The first step was a magnetic positive purification of the total CD8<sup>+</sup> T cell population using a MultiSort Kit (Miltenyi) according to the manufacturer's protocol. The MultiSort CD8<sup>+</sup> beads were removed using the MultiSort Release Reagent from the kit, and the cell suspension was washed once with FACS buffer. The second step split the CD8<sup>+</sup> T cell population into the specific subpopulation required. The CD8<sup>+</sup> CD45RA<sup>-</sup> memory T cells were sorted by applying the Memory CD8<sup>+</sup> Kit (Miltenyi) following the manufacturer's protocol, but the last step of the protocol, which implied a CD8<sup>+</sup>-positive selection with microbeads, was omitted.

## 3.2. Evaluation of the effect of acetylation on CD8<sup>+</sup> T cell activation in aging

### 3.2.1. T cell culture conditions

**Activation of CD8<sup>+</sup> T cells.** The T cell culture medium was used to culture the cells. The purified CD8<sup>+</sup> T cells were seeded at a density of  $10^6$  cells/ml in a 12- or 24-well plate (Sarstedt, Nümbrecht, Germany). To activate the CD8<sup>+</sup> T cells, two monoclonal antibodies (mAb) were used: 2.5  $\mu\text{g}/\text{ml}$  anti-CD3, clone OKT3 (Thermo Fisher Scientific, Waltham, MA, USA) and 1  $\mu\text{g}/\text{ml}$  anti-CD28, clone REA1047 (BD Biosciences, San Jose, CA, USA). The anti-CD3 mAb was plated for at least 16 hours before each assay at  $4^{\circ}\text{C}$  in sterile PBS. After the CD8<sup>+</sup> T cells were sorted, the PBS was removed from the plate with the anti-CD3 mAb, and one-fourth of the final volume of the empty T cell culture medium was added over the plate and left at room temperature (RT) for at least 10 min. Half of the final volume of the T cell culture medium containing the final amount of CD8<sup>+</sup> T cells was subsequently added, as was the last quarter of the final volume of the T cell culture medium containing the anti-CD28 mAb (Figure 6). From this point onward, the term "activated" or "+activation" refers to the cells that received the aforementioned anti-CD3 and anti-CD28 mAbs, while "non-activated" or "-activation" indicates the cells that did not receive the activating mAbs.

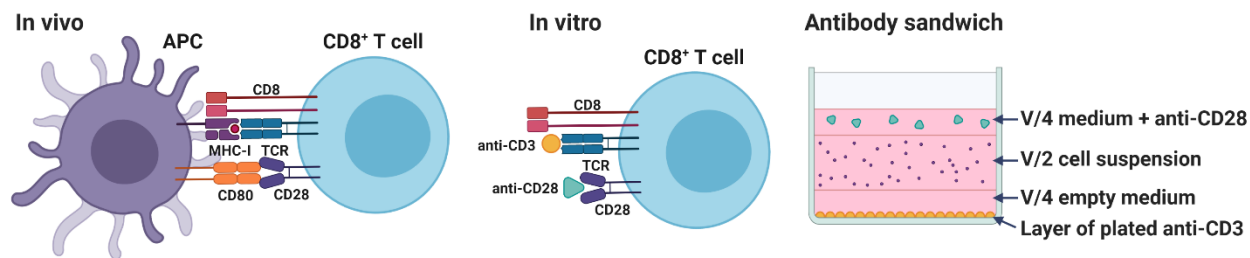


**Figure 6. In vitro T cell activation.** To mirror the in vivo activation of T cells, anti-CD3 and anti-CD28 mAb were used. The anti-CD3 mAb was plated overnight in the culture dish. The final volume of medium ( $V$ ) was divided into 3 parts and was added in steps so that the cells would be trapped between the plated anti-CD3 mAb and the soluble anti-CD28 mAb. The figure was created with BioRender.com.

**Deacetylase inhibitor treatment.** After receiving activating mAbs anti-CD3 and anti-CD28, the CD8<sup>+</sup> T cells were treated with or without a deacetylase inhibitor cocktail (HDACi; Santa Cruz, Dallas, TX, USA) with a 1:250 dilution to a final concentration of 160 nM TSA, 4  $\mu$ M Ex-527, and 1.6 mM NAM. The term “HDACi-treated” or “+HDACi” henceforth refers to the cells that received the HDACi treatment, while the term “HDACi-untreated” or “-HDACi” indicates the cells that did not receive the HDACi treatment. The culture time of each assay is indicated in the respective subchapter. All calculations and assays were done by comparing the CD8<sup>+</sup> T cells that were activated and HDACi-untreated to those that were activated and treated with HDACi unless stated otherwise.

### 3.2.2. Characterization of CD8<sup>+</sup> T cells by flow cytometry

**CD8<sup>+</sup> T cell subpopulation discrimination.** Approximately  $10^5$  thawed PBMCs were pelleted, resuspended in FACS buffer, and stained with CD3 fluorescein (FITC; BD Biosciences), CD8 Brilliant Violet 605 (BV605; BD Biosciences), CD45RA allophycocyanin (APC; Miltenyi), and CCR7 phycoerythrin (PE; BD Biosciences; Table 2) for 10 min in the dark and on ice before being washed once with FACS buffer. Live/dead exclusion was performed using 2  $\mu$ l of a 50- $\mu$ g/ml propidium iodine solution (PI; Sigma-Aldrich GmbH) per 75 x 12-mm tube (Sarstedt). The gating strategy for obtaining living cells is the same for all flow cytometric assays, with the exception of apoptosis measurements. The first gate of forward scatter (FSC) versus side scatter (SSC) was used to discriminate the lymphocytes from the monocytes. The second gate set on PE and PerCP-Cy5.5 distinguished between live and dead cells; the double-negative cells in this gate were the living ones. The third gate was used for doublet exclusion by plotting the FSC area against its width. A population with roughly the same width can be identified as single cells.

Once the live single lymphocytes were determined, these cells could be further separated based on their surface markers. The next gate was set on FITC versus Qdot 605 (same as BV605), which allowed for the evaluation of CD3 and CD8, respectively. The double-positive cells were further gated for APC versus PE, representing CD45RA versus CCR7, respectively. The final discrimination was obtained using a quadrant

gate that separated the CD8<sup>+</sup> T cells according to the following taxonomy: naïve – CD45RA<sup>+</sup>CCR7<sup>+</sup>, central memory (CM) – CD45RA<sup>-</sup>CCR7<sup>+</sup>, effector memory (EM) – CD45RA<sup>-</sup>CCR7<sup>-</sup>, and terminally differentiated EM T cells re-expressing CD45RA (TEMRA) – CD45RA<sup>+</sup>CCR7<sup>-59,175</sup>. To assess the efficiency of each sorting method, approximately 10<sup>5</sup> of the sorted CD8<sup>+</sup> T cells were stained with CD3 FITC and CD8 BV605, and the number of double-positive cells was determined. Only preparations with a purity of CD3<sup>+</sup>CD8<sup>+</sup> T cells >95% were used. For the memory subpopulation, only preparations with a purity of CD3<sup>+</sup> CD8<sup>+</sup> CD45RA<sup>-</sup> T cells >95% were used. All flow cytometric data were acquired using a BD LSRFortessa flow cytometer with the BD FACSDiva software (both from BD Biosciences).

### 3.2.3. Functional analysis of activated CD8<sup>+</sup> T cells after HDACi treatment

**Activation markers.** To assess the activation levels<sup>27</sup>, CD8<sup>+</sup> T cells were magnetically activated and cultured for 2 days with or without HDACi treatment, as described earlier. After the 2 days, approximately 10<sup>5</sup> cells were pelleted, resuspended in FACS buffer, and stained with CD69 FITC, CD25 PE (both from BD Biosciences), and CD71 APC-H7 (Biolegend, San Diego, CA, USA; Table 2) for 10 min in the dark and on ice before being washed once more with FACS buffer. The percentage of cells expressing each activation surface marker was determined by gating the positive cells in the histogram of each fluorophore after the live single lymphocytes were assessed using the aforementioned procedures.

**Cytokine secretion.** The CD8<sup>+</sup> T cells were magnetically sorted, activated, and kept in culture for 2 days with or without HDACi treatment, as described previously. After the 2 days, the cell suspension was centrifuged at 300 g and 4°C for 5 min. The supernatant was used to determine the concentration of cytokines, using BD Cytometric Bead Array Flex Sets (BD Bioscience) containing interferon-gamma (IFN- $\gamma$ ), tumor necrosis factor-alpha (TNF- $\alpha$ ), IL-3, IL-4, IL-5, IL-6, IL-10, granulocyte-macrophage colony-stimulating factor (GM-CSF), granzyme A, and granzyme B, according to the manufacturer's specifications. Standard solutions of known concentrations of each soluble protein were provided by the distributor, and a standard curve for each protein could be established. The acquisition settings and gating strategy were optimized as indicated by the manufacturer's protocol. The acquired data were analyzed using the FCAP Array software (BD Biosciences), and the results are presented in pg/ml or ng/ml.

**Proliferation capacity.** The CD8<sup>+</sup> T cells were magnetically sorted, activated, and cultured with or without HDACi treatment, as previously described, for five days. After this incubation period, 3 x 10<sup>6</sup> CD8<sup>+</sup> T cells were stained with a CellTrace™ Carboxyfluorescein Succinimidyl Ester (CFSE) Cell Proliferation Kit (Thermo Fisher Scientific) to a final concentration of 10  $\mu$ M, as described in the literature<sup>176</sup>. The cells were stained for 15 min in the dark at RT and washed once with FACS buffer. The data were acquired immediately. The average number of divisions for each cell was evaluated with the standard specifications for proliferation

assays provided by FCS Express 6 Plus Research Edition (DeNovo Software, San Diego, CA, USA), and presented as proliferation indexes that indicate the average number of divisions undergone by the cells.

**Apoptosis rate.** To determine the rate at which T cells become apoptotic after receiving HDACi treatment, CD8<sup>+</sup> T cells were magnetically sorted, activated, and cultured for 2, 5, and 10 days with or without HDACi treatment, following the aforementioned procedures. The cells incubated for 10 days had a medium change on day 5. Approximately 10<sup>5</sup> CD8<sup>+</sup> T cells were stained using an Annexin V FITC Kit (Mlitenyi), according to the manufacturer's protocol and the data were acquired immediately. For this assay, the gating strategy was as follows: the first gate was FSC versus SSC, to separate the cells from any potential debris; the second gate was the FSC area versus FSC width, which removed doublets; and the last gate was for the double staining of annexin V (FITC) and PI (PE). The cells were defined as alive (Annexin<sup>-</sup> PI<sup>-</sup>), debris (Annexin<sup>-</sup> PI<sup>+</sup>), dead (Annexin<sup>+</sup> PI<sup>+</sup>), or apoptotic (Annexin<sup>+</sup> PI<sup>-</sup>).

### 3.3. Protein and transcript expression profiles of activated CD8<sup>+</sup> T cell

#### 3.3.1. Relative protein expression

To determine the effect of activation on the relative protein expression of HDACs, non-activated CD8<sup>+</sup> T cells were compared to activated ones, and the results were described as "activation." To determine the effect of activation and HDACi treatment on the relative protein expression of the HDACs, HDACi-untreated activated CD8<sup>+</sup> T cells were compared with HDACi-treated activated CD8<sup>+</sup> T cells, and the results were described as "activation and HDACi treatment." The CD8<sup>+</sup> T cells were magnetically sorted, activated, and treated as previously described. The cells were cultured for 2 days and then pelleted and washed once with ice-cold PBS. The cell pellet was lysed using RIPA buffer supplemented with 1:1,000 Benzonase (Novagen, San Diego, CA, USA), 1:100 Protease Inhibitor Cocktail II (Merck Milipore, Darmstadt, Germany), 1:100 Phosphatase Cocktail 1, 1:100 Phosphatase Cocktail 2 (both from Sigma-Aldrich GmbH), and 1:40 HDACi cocktail (Santa Cruz). The cell lysate was incubated on ice for 40 min and then centrifuged at 13,000 g for 30 min at 4°C, and the clear cell lysate was placed into a clean tube. The total protein content of the lysates was measured using the Bradford method, as previously described<sup>177</sup>. A total of 20 µg total protein per sample was separated in a 10% SDS-PAGE gel at 50 V for 30 min, and at 100 V for 1.5 to 2 hours, using WB running buffer. Afterward, the proteins were transferred to a nitrocellulose membrane (GE Healthcare, Uppsala, Sweden) using a tank blotting system (Trans-Blot Cell Chamber, Bio-Rad) filled with cold WB transfer buffer at 100 V for 75 min and placed in an ice-water bath. Subsequently, the membranes were incubated for 1 h in 5% (m/v) bovine serum albumin (Sigma-Aldrich GmbH) in TBS-T and then washed with TBS-T three times for 10 min each. The membranes were incubated overnight at 4°C with the primary

antibodies (Table 3; Cell Signaling Technologies, Danvers, MA, USA) and washed again with TBS-T three times for 10 min each. The membranes were then incubated for 1 h with the secondary antibody (anti-rabbit or anti-mouse horseradish peroxidase-conjugated, Cell Signaling Technologies) and washed again with TBS-T three times for 10 min each. The substrate used for HDAC4 was Lumi-Light Western-Blotting Substrate (Roche Diagnostics, Mannheim, Germany), while that for HDAC3 and HDAC11 was SignalFire ECL Reagent (Cell Signaling Technologies). The chemiluminescence signals were recorded with a FujiFilm LAS-300 Fluorescent Image Analyzer (FujiFilm, Tokyo, Japan). The protein fold change was determined using Image Studio™ Lite (LI-COR Biotechnology, NE, USA) and normalized to the Ponceau staining of each membrane. The data were presented as a ratio between the signal of the “activated” or “activated and HDACi-treated” CD8<sup>+</sup> T cells and that of the “non-activated” or “activated and HDACi-untreated” cells. Values >1 represented an increase in expression for the “activated” or “activated and treated” samples relative to the “non-activated” or “activated and untreated” samples, while values <1 indicated a relative decrease.

### 3.3.2. Two-dimensional protein expression profile analysis

**Protein preparation for two-dimensional gels.** The CD8<sup>+</sup> T cells were magnetically sorted, activated, treated or not with HDACi, and cultured for 2 days, as previously described. After the 2 days, the cells were pelleted and washed once with ice-cold PBS. Minimal labeling buffer with an 8.5 pH was added over the pellets; then, the samples were sonicated three times for 5 min each at a frequency of five pulses per second with a Transsonic 460 (Elma Schmidbauer GmbH, Singen, Germany). The cell lysates were centrifuged at 11,000 g and 15°C for 90 min. The soluble proteins were transferred to a new tube, and the protein content was measured as previously described<sup>178</sup>. For the analytical two-dimensional (2D) gels, an internal protein standard (IPS) was established as an equal mixture of all the HDACi-untreated and -treated preparations from each donor, and a total of 10 µg IPS was used on each gel. For the preparative gels, four pools were established: HDACi-untreated – young, HDACi-untreated – old, HDACi-treated – young, and HDACi-treated – old. The cell lysates from 10 donors were mixed for each pool.

**Difference gel electrophoresis labeling.** The cell lysates were labeled with difference gel electrophoresis (DIGE) dyes (SERVA Lighting SciDye Set, Serva, Heidelberg, Germany), according to the manufacturer’s protocol. A total of 10 µg of each HDACi-untreated preparation was labeled with Lightning Dye Sci5, and 10 µg of each HDACi-treated preparation was labeled with Lightning Dye Sci3. The IPS was labeled with Lightning Dye Sci2. Afterward, 1 µl of 10 mM L-lysine (AppliChem) was added as a blocking reagent for the excess dye, and the samples were kept on ice and in the dark for another 10 min. The volume of each sample was doubled with the addition of 2x Rabilloud buffer, and the samples were kept for another 5–

10 min on ice in the dark. At this point, a mixture of all the samples was achieved while keeping the specific fluorescence labels intact. Therefore, the HDACi-untreated and -treated samples from each donor and an equivalent volume of the IPS were placed in one tube and labeled with the donor's code. Each tube was then brought to a final volume of 350  $\mu$ l by adding Rabilloud buffer.

**First dimension.** For the first dimension, the proteins were separated based on their isoelectric point (pI). To accomplish this, the final volume of the tube corresponding to each donor was placed in a strip holder (GE Healthcare), on top of which an immobilized pH gradient (IPG) strip of pH 3–10 (GE Healthcare) was placed facing downwards, such that the matrix holding the pH gradient was immersed in the protein solution. The strips were left at RT without any current running through them for a 2-h period of rehydration as the first step of the isoelectric focusing. Afterwards, 350  $\mu$ l of Plus One DryStrip Cover Fluid (GE Healthcare) was placed on top of each strip; this ensured that no humidity was lost during the overnight isoelectric focusing using the ETTAN IPGphor IEF Isoelectric Focusing Unit (Amersham Pharmacia Biotech, San Francisco, CA, USA). The protocol covers a total of 20 h. The first step is 10 h at 30 V, then each step is one hour with increasing voltage: 500 V, 1000 V, 5000 V, and finally 8000 V. A total of 48,000 V/h must be applied to the IPG strip. If the isoelectric focusing process resulted in less than 48,000 V/h, a brief additional focusing step was added to reach the targeted total V/h. Each strip was equilibrated with 15 ml each of equilibration buffers 1 and 2 consecutively for 15 min each. The strips were then placed in SDS-PAGE running buffer for at least 5 min.

**Second dimension.** The second dimension represented an SDS-PAGE gel, in which the proteins migrated according to their molecular weight. Specific 13% T/2.5% C gels were prepared a day ahead to ensure complete polymerization. For the overlay, a solution of 1% agarose with a low melting point (SERVA) in SDS-PAGE running buffer with traces of bromophenol was pipetted, and the strip was placed in this solution. To track the molecular weight distribution of the proteins, a Low Molecular Weight SDS-PAGE Marker Kit (GE Healthcare) was used and prepared as per the manufacturer's protocol. The proteins were run at 20 V for 5 h and then overnight at 100 and 120 V for the last 3–4 h. The gels were then washed once with double-distilled water before being immersed in fixation buffer for 45 min at RT in the dark. The gels were then washed with double-distilled water at least four times for 1 h each. The spots were visualized using a Fujifilm FLA-5100 Fluorescent Image Analyzer (FujiFilm, Tokyo, Japan); appropriate lasers and filters were used for each fluorescence pattern, based on the manufacturer's guidelines.

**Expression profiles.** The 2Delta software (DECODON, Greifswald, Germany) was used to analyze the resulting expression profiles. The protein expression profiles were determined by comparing the fluorescence profile of the HDACi-treated to that of the -untreated preparation from the same age group.

An age-dependent regulation factor (RF) was calculated for each age group using the following formula:  $RF_{young/old} = \frac{\text{mean normalized spot intensity of HDACi-treated}}{\text{mean normalized spot intensity of HDACi-untreated}}$ . This RF ratio determines whether the proteins change their expression after HDACi treatment, and it was calculated per spot. A ratio below 0.66 indicates a biologically significant decrease in the expression of the spot following HDACi treatment, while a value higher than 1.5 indicates a biologically significant increase.

To analyze any potential differences in the constitutive expression of the identified proteins between young and old, additional sample-dependent RF factors were calculated according to the following formula:  $RF_X = \frac{\text{mean normalized spot intensity of } X\text{-young}}{\text{mean normalized spot intensity of } X\text{-old}}$ , where X is either the HDACi-untreated or the -treated preparation. All the RFs were calculated using all five biological replicants.

**2D Preparative gels.** From each of the four pools of 10 donors established earlier, a total of 250 µg of protein was used per gel for each age group (Figure 7). The protein solution was brought to a final volume of 350 µl by adding Rabilloud buffer. The aforementioned loading methods and isoelectric focusing protocol were used. The subsequent steps were the same as those described in the previous section, with the distinction that the gels were not fixed immediately after running but washed once with double-distilled water and then stained with Coomassie staining solution overnight in a Dodeca™ Gel Stainer (Bio-Rad). The gels were scanned using the Bio-5000 Plus (Microtek, Hsinchu, Taiwan). The resulting staining pattern was matched to the corresponding fluorescence profile of the analytical gels of the individual donors, and the spots of interest were chosen for further identification.

### 3.3.3. Identification of proteins expressed differently between young and old CD8<sup>+</sup> T cells

**Preparation of proteins for mass spectrometry.** The relevant spots were extracted from the 2D preparative gels using GelPal Genetix and placed in 96-well elution plates (INTAVIS Bioanalytical Instruments AG, Cologne, Germany); then, the gel pieces were de-stained and digested using DigestPro MSi (INTAVIS), via the protocol described in Table 4.A. The final peptide solutions were placed in 96-well collection plates (INTAVIS). Before spotting the samples, the matrix for the matrix-assisted laser-desorption/ionization time-of-flight mass spectrometer (MALDI-TOF MS; Bruker Daltonics Inc, Bremen, Germany) was prepared by adding 0.02–0.03 g of matrix to a solution of 50% acetonitrile (AppliChem GmbH) and 0.1% TFA (AppliChem GmbH) in Ampuwa water (Fresenius Kabi GmbH). The digested samples were spotted on an MTP 384 ground steel target plate (Bruker) using the same DigestPro MSi (INTAVIS) and ZipTips (Merck Millipore) in the protocol described in Table 4.B. After all sample spots were dried on the plate, a 1:1 mixture of the matrix solution and Peptide Calibration Standard II for mass spectrometry

(Bruker) was prepared. Subsequently, 1  $\mu$ l of this final solution was spotted next to the samples on the MTP plate.

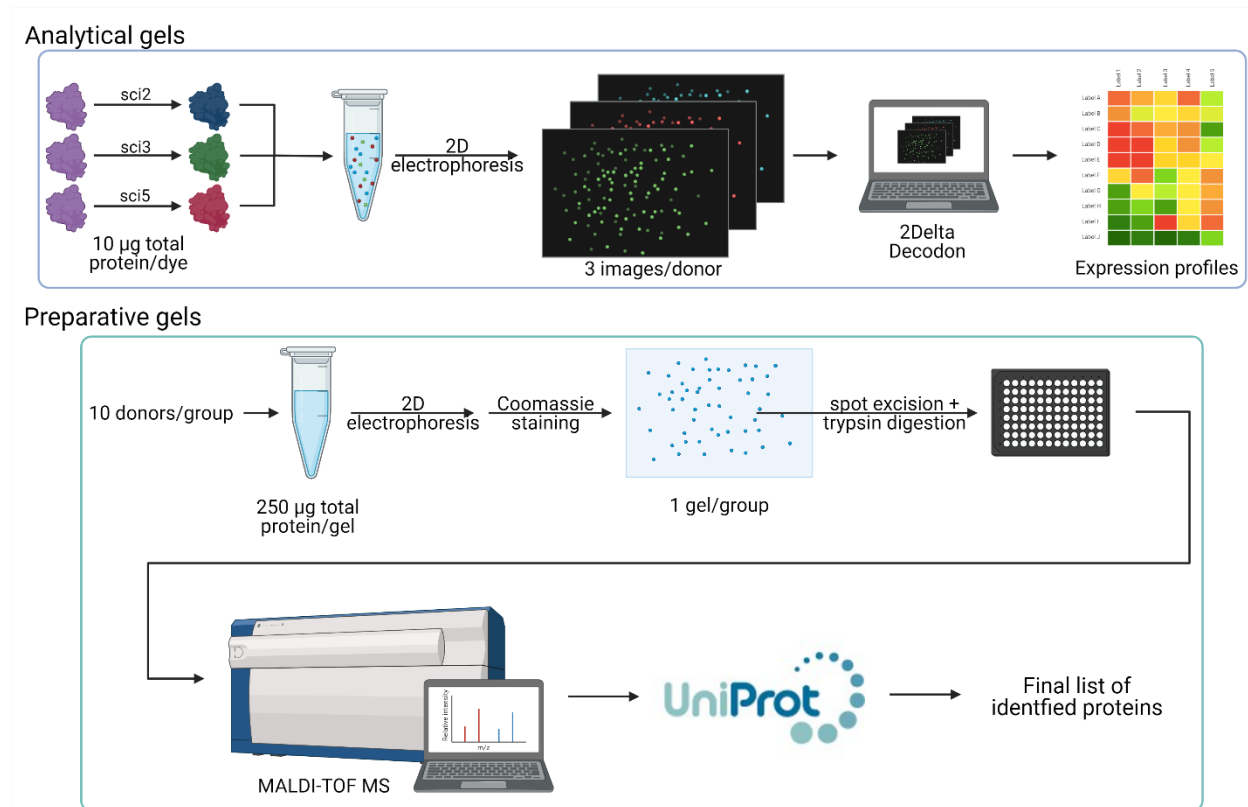


**Figure 7. Different processing methods for analytical and preparative gels.** Five biological replicates were used for the analytical gels. For each donor, 10  $\mu$ g of total protein from the control sample were stained with sci5, 10  $\mu$ g of total protein from the HA sample with sci3, and 10  $\mu$ g of an equal mixture of HDACi-untreated and -treated samples was stained with sci2. The expression profiles were obtained with the 2Delta Decodon software. For the preparative gels, 250  $\mu$ g of total protein was used per gel from a pool of 10 donors. The gels were stained with Coomassie blue, and the relevant spots were excised and analyzed with MALDI-TOF MS. The UniProt database was used to finally identify the proteins. The figure was created with BioRender.com.

**Identification of protein through mass spectrometry.** The protein crystals were analyzed using the MALDI-TOF MS UltrafleXtreme™ (Bruker) with the FlexControl Ultraflex ToF/ToF software (Bruker), via the peptide mass fingerprinting method in the range of 700–3,500 Da. All samples were first calibrated with Peptide Calibration Standard II (Bruker). The background peaks were identified and eliminated using the FlexAnalysis software (Bruker). The identified peptide masses were compared with the theoretical peptide masses from the Matrix/Mascot database (Bruker) using the Biotools 3.2 software (Bruker). The molecular weight search (MOWSE) score<sup>179,180</sup> was then calculated by the software for each protein found. The MASCOT-MOWSE score represents a probability-based calculation that considers the possible peptides resulting from trypsin digestion. The score takes into account if certain amino-acid sequences represent specific domains for certain proteins, based on information from the Swiss-Prot database, UniProt. The

higher the score, the lower the probability that the identified protein is a random event. A score above 56 indicates a significant identification. The protein sequence coverage is calculated as a percentage of the matched peptides out of the full protein sequence. The sequence coverage does not function as a cut-off for protein identification.

**Table 4. Sample processing for MS. (A). De-staining of spots and in-gel digestion. (B). Sample spotting on the MTP 384 ground steel target plate one by one. Notes: \*Step was repeated as many times as indicated; \*\*samples went through the loop one at a time; \*\*\*first volume was taken up by the needle, and the second volume was evacuated through the needle. ABC = ammonium bicarbonate, ACN = acetonitrile, TFA = trifluoroacetic acid.**

A. De-staining of spots and in-gel digestion					
Step	Process	Time (h)	Temperature	Buffer	Volume (μl)
1	Incubation x2*	0:10	RT	50% ABC/ACN	60
2	Incubation	0:10	RT	50 mM ABC	60
3	Incubation x2*	0:10	RT	25 mM ABC	60
4	Incubation x2*	0:10	RT	100% ACN	60
5	Waiting	0:10	RT	-	0
6	Incubation/waiting	3:00	37°C	Trypsin	15
7	Waiting	3:00	37°C	Water	10
8		-	RT	1% TFA	10
9	Incubation	0:20	RT	25 mM ABC	20
10	Incubation	0:20	RT	100% ACN	20
11	Waiting	0:10	RT	-	0

B. Sample spotting on MTP plate with ZipTips			
Loop**	Process	Buffer	Volume (μl)
1	Tip washing	0.1% TFA; 100% ACN	20; 20
2	Tip loading	Sample	50
3	Target elution	100% ACN; Matrix 50% ACN	20; 1
4	Acetone wash	Acetone	10
5	Needle washing	0.1% TFA	25; 250***

### 3.3.4. Relative and absolute quantification of the gene expression of CD8<sup>+</sup> T cells

**RNA isolation and quality control.** For all assays that used RNA, the total RNA was isolated from the cells in the same manner. The cells were pelleted and washed once with ice-cold PBS. The cell pellet was immediately treated with the lysis buffer from a NucleoSpin RNA Isolation Kit (Macherey-Nagel, Düren, Germany) supplemented with β-mercaptoethanol (AppliChem GmbH), as indicated by the kit manual, and stored in a freezer at -80°C or used right away for RNA isolation. The total RNA was then isolated from the cell lysate with the NucleoSpin RNA Isolation Kit according to the company's specifications. The RNA concentration was measured using the Infinite 200 PRO Microplate Reader (Tecan Group Ltd., Mannedorf, Switzerland) and NanoQuant Plate™ (Atlantic Lab Equipment, Beverly, MA, USA), with Ampuwa water (Fresenius Kabi, GmbH, Bad Homburg, Germany) as the blank, and determined through spectrometric measurements of the absorbance at 260 nm. The purity of the total RNA was initially determined by analyzing the ratio of the absorbances at 260 and 280 nm. Only samples for which this ratio had a value

<2 were used. For additional quality controls, the 28S and 18S ribosomal units were separated by agarose electrophoresis. Subsequently, 2.5 µl of each sample was mixed with 2.5 µl 2XRNA Loading Dye (Thermo Fisher), and the mixture was heated to 70°C for 5 minutes. The mixtures were cooled on ice for 1 min and then briefly centrifuged. The total of 5 µl was then loaded onto 1% (m/v) agarose gel and separated at 40 V for 1 h. The two ribosomal bands were visualized under ultraviolet light with the E-Box VX5 (Vilber, Collégien, France).

**Relative gene expression.** To analyze the effect of activation on HDAC gene expression, the relative gene expression was determined using the real-time or quantitative polymerase chain reaction (qPCR) method. For this method, the calculations compared non-activated CD8<sup>+</sup> T cells to activated ones, and the results were described in terms of “activation.” To determine the effect of HDACi concurrent with activation, CD8<sup>+</sup> T cells were activated and cultured with or without HDACi treatment, and calculations were obtained for both types; the results were described as “activation and HDACi treatment.” The CD8<sup>+</sup> T cells were magnetically sorted and cultured for 2 days at a time with activating antibodies and HDACi treatment as indicated. After this incubation period, the total RNA was isolated as previously described, and complementary DNA (cDNA) was synthesized using 500 ng of total RNA per sample with a RevertAid First Strand cDNA Synthesis Kit (Thermo Fisher Scientific). Simple PCRs to check RNA integrity or test primers were performed using Taq polymerase (Promega, Madison, WI, USA), according to the manufacturer’s protocol. The PCR products were run on 1% (m/v) agarose gel (BioLine GmbH, Luckenwalde, Germany) in TAE buffer with the 100 bp DNA Ladder (Invitrogen). The qPCR reactions were established in a final volume of 15 µl using 2X SYBR Green qPCR Master Mix (Promega), and the cDNA was diluted by a ratio of 1:4 before use. The primers (Table 5) were prepared to a concentration of 10 µM, of which 0.75 µl was used per reaction. The reactions were run using the CFX Connect Real-Time System and Bio-Rad CFX Maestro software (both from Bio-Rad, Hercules, CA, USA) with a two-step program (Figure 8). The primers were

Temperature (°C)	Time (min)
95	10:00
95	0:30
55-60	0:30
72	0:30
95	0:10
65	0:05
0.5 gradient	----

**Figure 8. qPCR reaction conditions.** The annealing temperatures differed according to the individual primers. The figure was created with BioRender.com.

obtained from publications or designed in-house using Primer-BLAST<sup>181</sup> with transcript sequences from the Reference Sequence Database<sup>182</sup> of the National Center for Biotechnology Information. The primers were designed to span an exon-exon junction and so that the primer pair would be separated by at least one intron on the corresponding genomic DNA. The primers were chosen to have a minimum size of 18 bp and a maximum size of 21 bp, with guanine-cytosine content values between 40 and 80. These settings were adjusted when necessary.

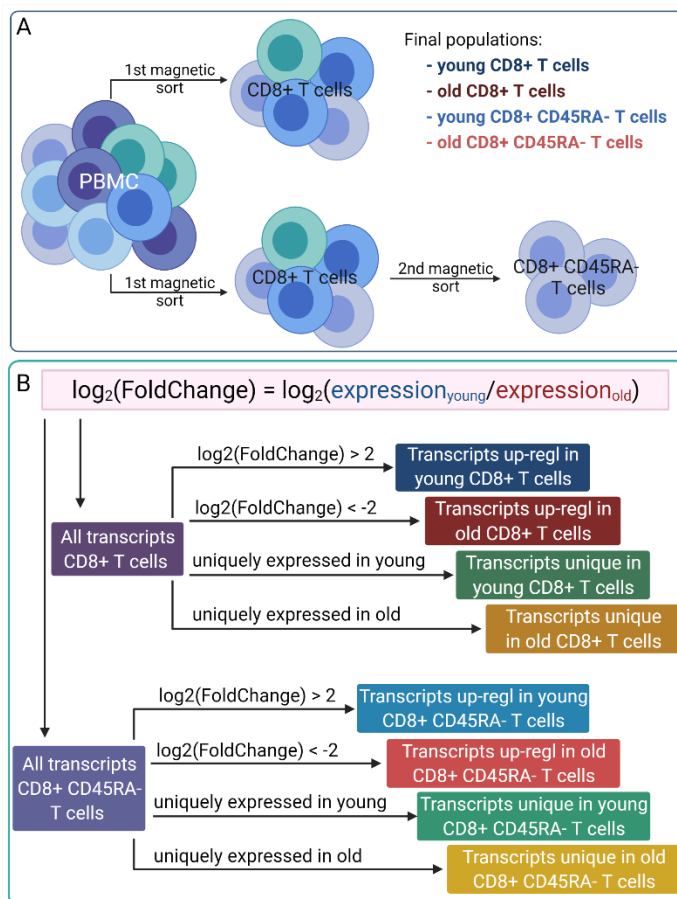
The qPCR data were presented as  $\Delta\Delta Cq$  (fold change) and calculated using TATA-binding box protein (TBP) and succinate dehydrogenase subunit A (SDHA) as housekeepers, according to the following formula<sup>183</sup>:  $\Delta\Delta Cq = (Cq_{HK} - Cq_{GOI})_{treated} - (Cq_{HK} - Cq_{GOI})_{untreated}$ , where  $Cq_{HK}$  is the mean of the quantification cycle (Cq) values of the housekeepers for a donor, and  $Cq_{GOI}$  is the Cq value of the gene of interest in the indicated condition. “Treated” and “untreated” in the formula refer to either: (1) “activated” and “non-activated,” respectively, for the determination of the effect of “activation” on HDAC gene expression, or (2) “activated and HDACi-untreated” and “activated and HDACi-treated,” respectively, for the determination of the effect of “activation and HDACi treatment.”

Table 5. **Primers for qPCR analysis.** All primers were ordered from Integrated DNA Technologies (Coralville, Iowa, USA) and dissolved in Ampuwa water to a final concentration of 10 mM (Fw = forward; Rw = reverse).

Gene	Transcript	Primer	Sequence 5'→3'	Product length	Annealing temperature
<i>SIRT1</i>	NM_012238.5	Fw Rw	GGCGCTTGATGGTAATCAGT CTTGGACTCTGGCATGTCCC	148	60
<i>SIRT3</i>	NM_001370314.1	Fw Rw	GCTTCCTCTAGTGACACTGTTAG TGCAGAAGTAGCAGTTCAGTG	135	58
<i>SIRT6</i>	NM_001321058.2	Fw Rw	CATCCTAGACTGGGAGGA CAGGTTGACGATGACCAG	172	56
<i>HDAC1</i> <sup>184</sup>	NM_004964.3	Fw Rw	GGAAATCTATCGCCCTCACA AACAGGCCATCGAATACTGG	168	58
<i>HDAC2</i> <sup>184</sup>	NM_001527.4	Fw Rw	TAAATCCAAGGACAACAGTGG GGTGAGACTGTCAAATTCAGG	89	58
<i>HDAC3</i> <sup>184</sup>	NM_003883.4	Fw Rw	TAGACAAGGACTGAGATTGCC GTGTTAGGGAGCCAGAGCC	120	58
<i>HDAC4</i> <sup>184</sup>	XM_024453257.1	Fw Rw	GGTTTATTCTGATTGAGAAGTGG ATTGTAAACCACAGTGCTCGC	146	58
<i>HDAC11</i> <sup>185</sup>	NM_001330636.2	Fw Rw	CAATGGGCATGAGCGAGAC TGTGGCGTTGTAGACATCC	68	60
<i>p300</i>	NM_001362843.2	Fw Rw	GGAAGTGCTGGCAACTTACTG CCATAAGGATTGGGGTTGTTC	125	58
<i>Granzyme B</i> <sup>186</sup>	NM_001346011.2	Fw Rw	TGGGGGACCCAGAGATTAATA TTTCGTCCATAGGAGACAATGC	100	58
<i>Granzyme A</i> <sup>187</sup>	NM_006144.4	Fw Rw	TTTCTGGCATCCTCTCTCTCA GGGTCATAGCATGGATAGGG	305	58
<i>TNF-α</i>	NM_000594.4	Fw Rw	GCTGCACTTTGGAGTGATCG TATCTCTCAGCTCCACGCCA	215	56
<i>IFN γ</i>	NM_000619.3	Fw Rw	GCTCTGCATCGTTTTGGGTT ATTGCAGGCAGGACAACCAT	488	56
<i>IL-10</i> <sup>188</sup>	NM_000572.3	Fw Rw	CTGTGAAAACAAGAGCAAGGC GAAGCTTCTGTTGGCTCCC	500	58
<i>IL-6</i>	NM_000600.5	Fw Rw	TTCGGTCCAGTTGCCTTCTC TCACCAGGCAAGTCTCCTCA	316	56
<i>IL-5</i>	NM_000879.3	Fw Rw	AGCCAATGAGACTCTGAGGAT AGGCCTGACTCTTTCTTGCC	359	56
<i>IL-4</i>	NM_000589.4	Fw	TCTTTGCTGCCTCCAAGAACA	235	56

		Rw	TCCAACGTA		
		Fw	CTTTGCCTTTGCTGGACTTC		
<i>IL-3</i>	NM_000588.4	Rw	AGAGAACGAGCTGGACGTTG	335	56
		Fw	TTCAAGTTGTGGGGGTGGAC		
<i>Sell</i>	NM_000655.5	Rw	GCTGGCAAGAAGCTGTGTAAC	433	58
		Fw	TCAACAGGTGCTCTGAGTGG		
<i>CNR2</i>	NM_001841.3	Rw	CGGGTGAGCAGAGCTTTGTA	597	58
		Fw	CCTTACGAGCTTGAGGGCTT		
<i>SLFN5</i>	NM_001330183.2	Rw	TGCTGAAACTGGAAAGTAGCG	406	58
		Fw	CCTGCTAAGCAACCCACTGA		
<i>S1PR5</i>	NM_001166215.2	Rw	TCTCTAGCACGATGAAGGCG	260	58
		Fw	CACGATGTAGCTTACCGCCA		
<i>IL7R</i>	NM_002185.5	Rw	ATAGGATCCATCTCCCCTGAGC	230	58
		Fw	TCCAGGATAACGGAGGCTGG		
<i>BCL2</i>	NM_000633.2	Rw	GATGGTGATCCGGCCAACAA	554	58
		Fw	CCACCTGTTGTGGTCCAAGT		
<i>TBX21</i>	NM_013351.2	Rw	GGAGACAATCATCTGGGTCA	353	58
		Fw	CTGGCCCATAGTGATCTTTGC		
<i>TBP</i>	NM_003194.5	Rw	TCAATTCCTTGGGTTATCTTCACA	73	58
		Fw	TGGGAACAAGAGGGCATCTG		
<i>SDHA</i>	NM_004168.4	Rw	CCACCACTGCATCAAATTCATG	86	58
		Fw	GAGAAGGCTGGGGCTCATTG		
<i>GAPDH</i>	NM_001357943.2	Rw	GGACTGTGGTCATGAGTCCTTC	220	58
		Fw	CGCGCTGTAAGAAGCAACAA		
<i>Tubulin</i>	NM_006009.4	Rw	TCTCCTCCCCAATGGTCTT	207	58
		Fw	TGGTCTGTCTTCTCATGTT		
<i>AKT</i>	NM_005163.2	Rw	TTGTCCACTCCTCCCGCT	600	58
		Fw	CGGGGACCGATTACCCAT		
<i>HIF1</i>	NM_001530.4	Rw	GTGCAGTGAATACCTTCCA	600	58
		Fw	TGAACTGGGGGAGGATTGTG		
<i>Bcl2</i>	NM_000633.3	Rw	TTCACCTGTGGCCAGATAGG	297	58
		Fw	CGGGACAAGAGAAAAGAGGGA		
<i>NF-kB</i>	NM_001077494.3	Rw	ATCGGAAGCCTCTCTGCTTA	372	58
		Fw	CGTTTCTGAGAAGCAGGGCA		
<i>HS90A</i>	NM_001017963.3	Rw	CGAACGTCTCAACCTCTCC	285	60
		Fw	TGTATGGAGCAGCAAGACTGA		
<i>HS90B</i>	NM_003299.3	Rw	ATACACGGCGCACATAGAGC	410	60
		Fw	TCCTAGCACCCACTCGAGAA		
<i>IF4A1</i>	NM_001204510.2	Rw	CAGGGGTACCCACGATGATG	165	60
		Fw	AGCATAGACTGCATCCGAGC		
<i>XRCC5</i>	NM_021141.4	Rw	TCCCATAATCCACGACCT	315	60
		Fw	TGTGTTCCCTGATCACTCGT		
<i>EF2</i>	NM_013302.5	Rw	CACTGTGTTTTGGTGCCCTG	357	58
		Fw	ACCAGTACTACCAAGGACAGC		
<i>PLSL</i>	NM_002298.5	Rw	TTGGGATGACATGCCGACAA	495	60
		Fw	CTACATGGATCCACGGGAAAG		
<i>SFPQ</i>	NM_005066.3	Rw	GGGCCTTCGTA	600	58
			CTTCTCTC		

**High throughput transcript data.** The total CD8<sup>+</sup> T cells and CD8<sup>+</sup> CD45RA<sup>-</sup> memory T cells were magnetically sorted and activated as previously described but without HDACi treatment (Figure 9.A). The cells were cultured for 2 days; the total RNA was then isolated, as previously described, with the same NucleoSpin RNA Kit (Macherey-Nagel). For this analysis, the total CD8<sup>+</sup> T cells and CD8<sup>+</sup> CD45RA<sup>-</sup> memory T cells were not treated with HDACi. Quality control checks were performed according to the



mentioned procedures before continuing with any samples. An equal number of female and male donors were sampled for each age group. These samples were sent to and processed by Novogene (Beijing, China) in 2 batches for RNA sequencing. The platform used was HiSeq-PE150.

**Figure 9. Overview of the workflow. (A).** Final populations used for RNA sequencing. The total CD8<sup>+</sup> T cells were magnetically sorted from the PBMC directly, and for the CD8<sup>+</sup>CD45RA<sup>-</sup> memory T cells, the total CD8<sup>+</sup> T cells were sorted first, then the memory T cells were isolated from the total CD8<sup>+</sup> T cells. **(B).** The final lists of transcripts used for GO term enrichment. The transcripts up-regulated in either young or old donors were determined based on the  $\log_2(\text{FoldChange})$  value. Two additional list were sorted for each cell population, based on the absence of expression for one of the age groups. Up-regl = up-regulated. The figure was created with Biorender.

### 3.4. Statistical methods and interpretation of high throughput data

#### 3.4.1. RNA sequencing data analysis

The bioinformatic analysis of the RNA sequencing data was done by Ioana Lemnian from the Human Genetics Institute, Martin-Luther University, Halle-Wittenberg, using the R software<sup>189</sup>. The R package tximport<sup>190</sup> was used to import the estimated read counts and summarize the transcript abundances, and the DESeq2 package<sup>191</sup> was used to calculate the differentially expressed transcripts. Low-abundance transcripts with fewer than a total of 10 reads in all the samples were removed from the analysis. For each gene, DESeq2 fit a generalized linear model indicating the overall level of gene expression and returning

the value of  $\log_2(\text{FoldChange})$  between old and young. A negative value represents an increase in older donors, while a positive one indicates an increase in younger donors. To analyze the quality of the method, Pearson's correlation, as well as the principal component analysis (PCA), was calculated. To assess the significance of the differential gene expression, DESeq2 used the Wald test. Then the  $p$  values were adjusted for multiple testing using the Benjamini–Hochberg correction.

From all the transcripts found, those with a  $\log_2(\text{FoldChange})$  value under  $-2$  were labeled as *up-regulated in old*, those with the value over  $+2$  *up-regulated in young*, and those that were expressed only in one group were labeled as *unique in young or old* (Figure 9.B). Further analyses were done only with the *up-regulated* or *unique* lists of transcripts.

#### 3.4.2. Network analysis and gene ontology term enrichment

Successfully identified target candidates were analyzed for network interaction using a search tool for the retrieval of interacting genes (STRING) online tool<sup>192,193</sup> with a threshold for confidence of 0.7. The STRING online tool performed gene ontology (GO) term enrichment on the input data as well. The resulting GO terms were filtered for repetitions (e.g., “cytoplasm” and “cytoplasmic part”), redundancies (e.g., “leukocyte activation,” “leukocyte-mediated immunity,” and “leukocyte activation involved in immune response”), and irrelevant terms (e.g., “myelin sheath”). The strength and false discovery rate (FDR) of each GO term were calculated. The strength was calculated as  $\log_{10} = \frac{\text{observed}}{\text{expected}}$ , where the “observed” represent the number of proteins in the input annotated with a certain term, and “expected” denotes the number of proteins expected to be annotated with the same term in a random network of equal size as the input. This equation describes the size of the enrichment effect. The FDR is a  $p$  value corrected for multiple testing using the Benjamini-Hochberg method, and it describes the significance level of the enrichment. The conclusions were based on the terms, which had an FDR smaller than 0.05 and four or more proteins found within the network.

For the high throughput transcript expression data, GO term enrichment was performed using the gene ontology enrichment analysis and visualization tool (GORilla)<sup>194</sup>. This tool presents only GO terms with a  $p$  value under 0.05, however, it also calculated the FDR. For this analysis, the *up-regulated* or *unique* transcripts were separated between young and old based on the  $\log_2(\text{FoldChange})$  value and the final lists of transcripts were used separately. The *up-regulated in young* and *old* lists were sorted by adjusted  $p$  value from lowest to highest and the *unique in young* and *old* were sorted according to the normalized mean of the counts for all preparations from highest to lowest. The “one ranked list” setting for the GORilla search was used for all lists. The search was performed between July and August 2020, and the retrieved

GO terms were curated for redundancies and unrelated results. Venn diagrams of the overlap between different datasets were calculated with Venny 2.1.0<sup>195</sup>. To create the word clouds, the R package textmining<sup>196</sup> was used to load the data, then the packages SnowballC<sup>197</sup> and wordcloud<sup>198</sup> were used to clean the text and execute the final image.

### 3.4.3. Additional statistical methods

The Shapiro-Wilk test was used to ascertain the normality of the distribution of the data. In general, the Mann–Whitney statistical test was used for all data unless stated otherwise. Both tests were calculated with GraphPad Prism 9. All *p* values less than 0.05 were marked with \*, less than 0.01 with \*\*, less than 0.001 with \*\*\*, and less than 0.0001 with \*\*\*\*.

## 4. Results

### 4.1. Expression of deacetylases and the acetylome of CD8<sup>+</sup> T cells

#### 4.1.1. Impact of T cell activation on the expression of HDACs

The CD8<sup>+</sup> T cells were isolated and activated or not for 2 days. The effect of activation on the fold change in the gene and protein expression of selected deacetylases was determined using qPCR and WB, respectively (Figure 10). The calculations were done relative to the non-activated CD8<sup>+</sup> T cells.

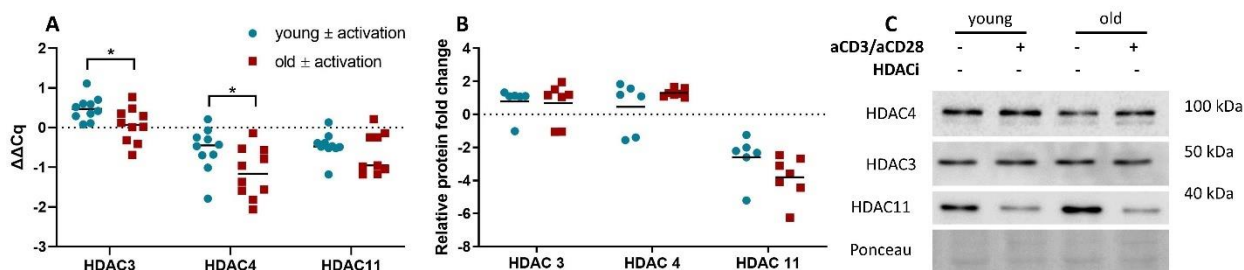


**Figure 10. Gene and protein fold change of selected HDACs after 48h.** (A). The fold change in the gene expression of HDACs after T cell activation was measured with qPCR and calculated between the non-activated and the activated CD8<sup>+</sup> T cells. Housekeepers were TBP and SDHA.  $N = 10$ ,  $* = p < 0.05$ . (B). The relative protein expression of HDACs was measured with WB and calculated between the non-activated and the activated CD8<sup>+</sup> T cells.  $N$  young = 6,  $N$  old = 7. (C). Representative blots for B. All WB data were normalized to the total protein staining with Ponceau S.

A significant difference was observed for HDAC3 and HDAC4 gene expression between the two age groups, with the CD8<sup>+</sup> T cells from old donors presenting a lower expression than the young. HDAC11 gene expression did not present a similar difference between the groups. However, neither presented a gene expression that could be considered biologically significant. The relative protein expression did not reflect entirely the gene expression. The gene expression of SIRT1, 3 and 6 was analyzed as well and no significant biological difference was identified between the age groups (data not shown). This biological similarity between the age groups for the expression of deacetylases was the basis of the HDACi treatment of activated CD8<sup>+</sup> T cells.

#### 4.1.2. Changes within the acetylome in CD8<sup>+</sup> T cells from young and old donors

A treatment with HDACi was established to study the effect of acetylation on CD8<sup>+</sup> T cell functions. This would allow the indirect study of the effects of acetylation. First, the treatment itself had to be validated. The activated CD8<sup>+</sup> T cells were cultured with or without HDACi for 2 days, as previously described. For the relative acetylation profiles, a WB membrane was blotted with a pan-acetylated-lysine antibody. Following the treatment, the acetylation increase was dispersed throughout the cell lysate (Figure 11.A).

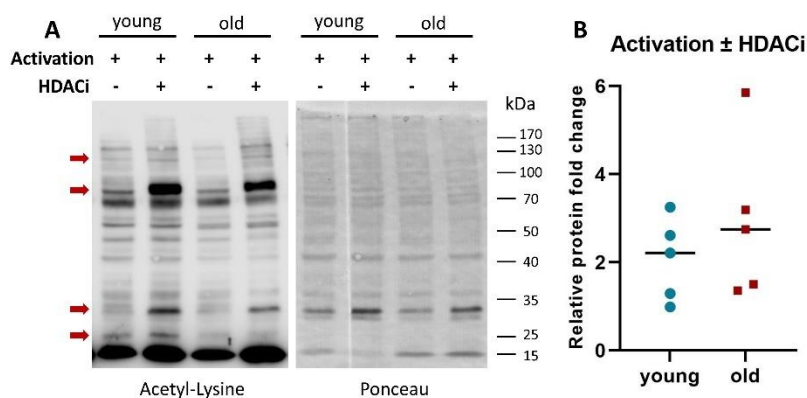


**Figure 11. Acetylation profiles.**  $CD8^+$  T cells were cultured for 48h with the indicated stimulation. (A). An example of the acetylation profiles is shown. Four rows of bands are highlighted to represent the changes occurring after HDACi treatment. (B). The relative protein fold change was calculated as a ratio of the untreated- to treated-HDACi activated  $CD8^+$  T cells. Results were normalized to Ponceau S.  $N = 5$ .

Most bands showed an increase in the signal after HDACi treatment, although some appeared to be unmodified. Overall, there was an increase in the signal for both age groups. There was no clear difference between the younger and older donors (Figure 11.B), although one outlier in the older group exhibited a sixfold increase. These relative acetylation profiles show that the treatment and concentration chosen increase the overall amount of cellular acetylation.

#### 4.1.3. Impact of HDACi treatment on the expression of HDACs

To evaluate how the HDACi treatment affected the expression of the selected HDAC,  $CD8^+$  T cells were treated or not with HDACi for 48h as previously described. The effect of the pan-HDAC inhibition on the fold change in the gene and protein expression of selected HDACs was determined using qPCR and WB, respectively (Figure 12). The calculations were done relative to the activated, but HDACi-untreated  $CD8^+$  T cells. The relative gene expression of HDAC3 and HDAC4 was significantly different between the age groups after only activation, however, the HDACi treatment reduced the significance. Additionally, the gene expression of these two enzymes was not biologically significant, while their protein expression was

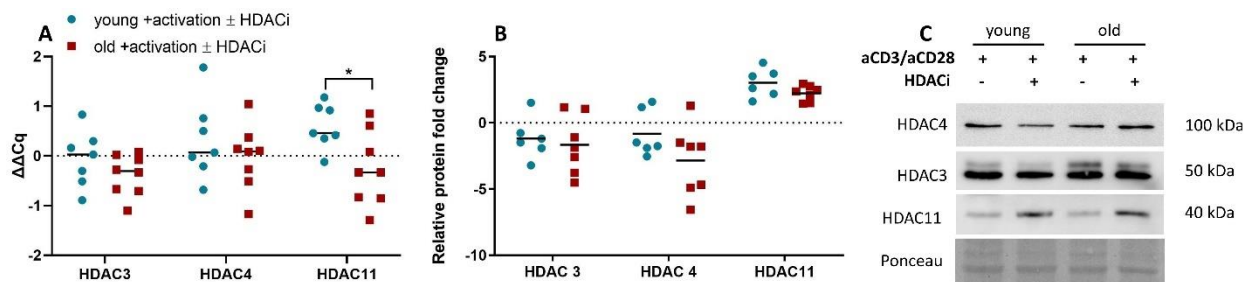


**Figure 12. Gene and protein fold change of selected HDACs after 2 days.** (A). The effect of HDACi treatment on HDAC gene expression during T cell activation was measured with qPCR and calculated between the untreated and the HDACi-treated activated  $CD8^+$  T cells. Housekeepers were TBP and SDHA.  $N$  young = 7,  $N$  old = 8. \* =  $p$  value < 0.05. (B). The relative protein expression of HDACs was measured with WB and calculated between the untreated and the HDACi-treated activated  $CD8^+$  T cells.  $N$  young = 6,  $N$  old = 7. (C). Representative blots for B. All WB data were normalized to the total protein staining with Ponceau S.

decreased almost fivefold. In comparison to the previous findings, the two enzymes do not show a major change in expression pattern.

The expression pattern of HDAC11 is similar between the gene and protein expressions; at the transcript level, HDAC11 expression presented a significant difference between the age group, which was not seen in the protein expression. Overall, activation of CD8<sup>+</sup> T cells induces a decrease in the expression of HDAC11, and T cell activation together with HDACi treatment induces an increase in expression.

## 4.2. Identification of differently expressed proteins

### 4.2.1. Expression profiles and identification of modified proteins after HDACi treatment

To analyze in-depth the proteome of CD8<sup>+</sup> T cells from young and old donors, 2D expression profiles were obtained with DIGE dyes. To this end, CD8<sup>+</sup> T cells were activated and treated or not with HDACi, as previously described. The overview of the data is based on age-dependent RF calculations. The total number of detected spots was 1,503 for the young donors and 1,484 for the old donors (Figure 13). Out of this total, more than 600 spots had an increased expression for the former and less than 600 for the latter. For both age groups, the number of spots with decreased expression was 10 times lower; the old donors had 68 spots and the young 43. While the younger donors had a higher number of spots with increased expression, their older counterparts had more spots with decreased expression. Additionally, the young donors had more statistically significant spots. The number of modified but non-significant spots was 327 for the younger donors and 459 for the older donors. This suggests an increased variability within the CD8<sup>+</sup> T cells from old donors.

Spots that were significantly modified in at least one of the age groups were chosen for MALDI-TOF identification. Multiple spots were identified (Table 6). For further analysis only identified proteins with a MASCOT-MOWSE score above 56 were used and presented. The spot number indicates if multiple proteins were identified on the same spot.

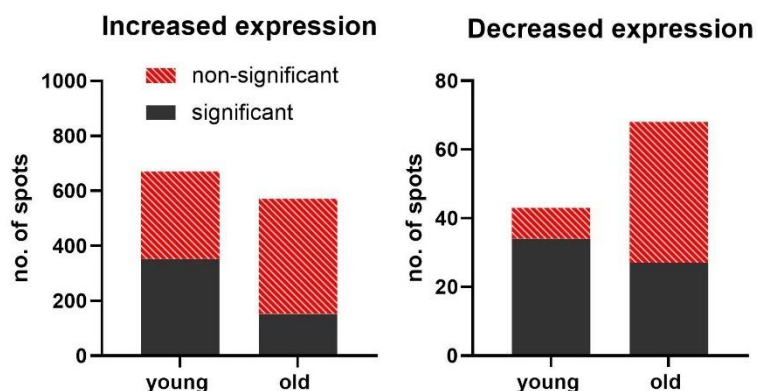


*Figure 13. Expression profiles of modified proteins from CD8<sup>+</sup> T cells of young and old donors after 48h of HDACi treatment. The total number of 2DE modified spots was calculated based on the age-dependent RFs. The statistical significance was calculated with a t test, and the significantly modified spots have a p value below 0.05.*

**Table 6. MALDI-TOF identified proteins and heatmap of their RFs.** A complete list of the identified proteins is presented below. For each protein, the UniProt Accession, UniProt entry name, molecular mass in kDa, MASCOT-MOWSE score, number of peptides that were matched to the protein sequence, protein sequence coverage calculated as a percentage, calculated pI value, and RF are shown. The RFs were calculated based on the 5 biological replicates for each age group using both age-dependent and sample-dependent methods. Yellow represents the highest value and green the lowest. Values below 0.66 represent a decrease in protein expression after HDACi treatment and those over 1.5 represent an increase. The t test was used to calculate the statistical significance. \* = p value < 0.05; \*\* = p value < 0.01; \*\*\* = p value < 0.001; \*\*\*\* = p value < 0.0001.

Spot no.	UniProt Accession	UniProt entry name	Description	Mass (kDa)	Score	Matched peptides	Sequence coverage (%)	Calculated pI	RF young	RF old
1	P63104	1433Z	14-3-3 protein zeta/delta	27.90	96	17	48	4.7	4.82****	3.17**
2	P14618	KPYM	Pyruvate kinase PKM	58.47	120	16	40	8.0	0.64**	0.62
3	P60842	IF4A1	Eukaryotic initiation factor 4A-I	46.35	109	20	44	5.3	0.56**	0.61*
4	P11142	HSP7C	Heat shock cognate 71 kDa protein	71.08	211	32	50	5.4	0.53***	0.52****
5	P23246	SFPQ	Splicing factor, proline- and glutamine-rich	76.22	61	15	23	9.5	1.57**	1.91
6	P13010	XRCC5	X-ray repair cross-complementing protein 5	83.22	180	30	33	5.6	2.09**	1.67
7	P11142	HSP7C	Heat shock cognate 71 kDa protein	71.08	211	32	50	5.4	0.52****	0.53***
8	P07900	HS90A	Heat shock protein HSP 90-alpha	85.01	56	15	21	4.9	0.47*	0.42**
9	Q8NFD4	YI018	Uncharacterized protein FLJ76381	17.10	62	5	30	11.1	0.51***	0.46**
10	P29350	PTN6	Tyrosine-protein phosphatase non-receptor type 6	67.92	78	15	27	7.7	0.62**	0.50**
	P14866	HNRPL	Heterogeneous nuclear ribonucleoprotein L	64.72	66	16	27	8.5		
11	P08238	HS90B	Heat shock protein HSP 90-beta	83.55	205	34	38	5.0	0.42***	0.53***
	P07900	HS90A	Heat shock protein HSP 90-alpha	85.01	122	27	34	4.9		
12	P60842	IF4A1	Eukaryotic initiation factor 4A-I	46.35	117	23	40	5.3	0.56	0.01**
	Q14240	IF4A2	Eukaryotic initiation factor 4A-II	46.60	86	19	38	5.3		
13	P60709	ACTB	Actin, cytoplasmic 1	42.05	183	21	47	5.3	0.46****	0.42*
	P63261	ACTG	Actin, cytoplasmic 2	42.11	183	21	47	5.3		

	P63267	ACTH	Actin, gamma-enteric smooth muscle	42.25	87	13	28	5.3		
	P62736	ACTA	Actin, aortic smooth muscle	42.38	87	13	28	5.2		
	P68032	ACTC	Actin, alpha cardiac muscle 1	42.33	87	14	31	5.2		
	P68133	ACTS	Actin, alpha skeletal muscle	42.37	86	14	31	5.2		
14	P13639	EF2	Elongation factor 2	96.25	95	21	24	6.4		0.57**
15	Q8WWH5	TRUB1	Probable tRNA pseudouridine synthase 1	37.52	56	8	28	8.4		2.02**
16	P13796	PLSL	Plastin-2	70.81	233	33	48	5.3	0.52	
17	Q99714	HCD2	3-hydroxyacyl-CoA dehydrogenase type-2	27.13	71	9	48	7.7	1.72***	
18	O43707	ACTN4	Alpha-actinin-4	105.25	97	21	22	5.3	1.54*	
19	Q9C0H5	RHG39	Rho GTPase-activating protein 39	122.24	65	14	13	7.3	0.65**	
20	P52597	HNRPF	Heterogeneous nuclear ribonucleoprotein F	45.99	129	17	47	5.4	0.58****	
21	P08670	VIME	Vimentin	53.68	123	24	35	5.1	0.62****	
22	P07437	TBB5	Tubulin beta chain	50.10	185	27	48	4.8	0.64**	
	Q13885	TBB2A	Tubulin beta-2A chain	50.27	133	22	37	4.8		
	Q9BVA1	TBB2B	Tubulin beta-2B chain	50.38	133	22	37	4.8		
	P68371	TBB4B	Tubulin beta-4B chain	50.26	144	24	42	4.8		
	P04350	TBB4A	Tubulin beta-4A chain	50.01	119	22	38	4.8		
	Q13509	TBB3	Tubulin beta-3 chain	50.86	107	20	30	4.8		
									RF HDACi-untreated	RF HDACi-treated
23	P07195	LDHB	L-lactate dehydrogenase B chain	36.9	169	22	54	5.71	0.64*	1.74*
24	P07237	PDIA1	Protein disulfide-isomerase	57.48	64	11	25	4.76		0.64

Heat shock protein 90-alpha (HSP90A) was identified in two distinct spots, one by itself and one with HSP90B. Several isomers of actin were identified in two different spots, including four muscle isomers. This does not represent an impurity; however, these isomers were not included in further analysis. Multiple tubulin chains were identified on the same spot, and all these different chains have very high MASCOT-MOWSE scores and high sequence coverages. Similarly, two isomers of eukaryotic initiation factor 4A (IF4A1 and IF4A2) were identified in one spot, and both had very high scores and coverages. The RFs are presented as a heatmap (Table 6), where yellow represents the highest value and green the lowest. Values below 0.66 represent a decrease in protein expression following HDACi treatment, while those over 1.5 represent an increase. The RFs present a similar general trend in both age groups. Even so, both actin and tubulin were significantly decreased in young donors, while the decrease was not significant in their older counterparts. Tubulin did not have a biologically significant RF for the old donors. 14-3-3  $\zeta/\delta$  protein was found to have the highest expression out of all the proteins identified for both age groups, but this is only partially confirmed by our WB data (Figure 14). Although they decreased in both groups, pyruvate kinase PKM (KPYM), IF4A1, and IF4A2 were only significantly altered in the younger donors. Moreover, splicing factor, proline- and glutamine-rich (SFPQ) and X-ray repair cross-complementing protein 5 (XRCC5) increased in both age groups, but they were significant only in the young donors.

Some of the identified proteins were biologically significant only in one age group and these can be divided into two clusters based on their RFs, which were modified in either young or old donors. The cluster

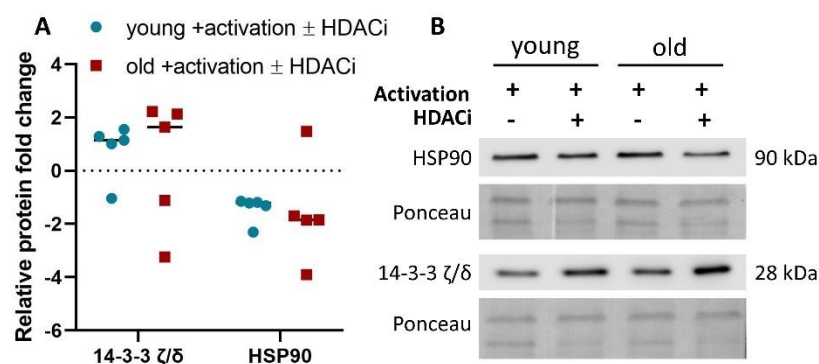


**Figure 14. Relative protein expression of 14-3-3  $\zeta/\delta$  protein and HSP90.** (A). Relative protein expression of 14-3-3  $\zeta/\delta$  protein and HSP90. CD8<sup>+</sup> T cells were stimulated as indicated for 48h. The relative protein expression was normalized to the Ponceau total protein staining and then calculated as a ratio of HDACi-treated to HDACi-untreated samples. N= 5. (B). Representative blots and Ponceau staining for both proteins. The proteins were analyzed on separate membranes; therefore, each blot has a Ponceau stain as a loading control.

modified only in old donors had only two proteins: elongation factor 2 (EF2), which decreased, and probable tRNA pseudouridine synthase 1 (TRUB1), which increased after HDACi treatment. The cluster for younger donors was larger and contained plastin-2 (PLSL), rho GTPase-activating protein 39 (RHG39), heterogeneous nuclear ribonucleoprotein F (HNRPF), vimentin (VIME), and the tubulin

chains, all of which decreased, as well as 3-hydroxyacyl-CoA dehydrogenase type-2 (HCD2) and alpha-actinin-4 (ACTN4), which increased.

The sample-dependent RFs were similarly calculated to the age-dependent RFs, whereby values higher than 1.5 represent an increase in the younger donors, and those below 0.66 represent an increase in the older donors. Only two proteins were found to be differently expressed according to this method. L-lactate dehydrogenase B chain (LDHB) was found to be differently expressed between the HDACi-untreated CD8<sup>+</sup> T cells of the groups, with an increase in the old donors. It also had a high RF (HDACi-treated), which indicates an increase in the young donors after HDACi treatment. Protein disulfide-isomerase is the other protein with a low RF (HDACi-treated), but it is not statistically significant.

The relative expression of 14-3-3  $\zeta/\delta$  protein, as analyzed with WB, did not present the same increase as the expression profiles (Figure 14). The CD8<sup>+</sup> T cells from young donors showed a more homogenous expression than their older counterparts, but neither group saw an increase greater than twofold. HSP90 presented a decreased expression; while it is not significant, it nonetheless correlates with the results from the expression profiles.

#### 4.2.2. Network analysis of identified proteins and GO term enrichment

All the identified proteins were analyzed by STRING functional enrichment, and a network of interactions was observed between several of the input proteins, with a protein-protein interaction enrichment  $p$  value of  $10^{-13}$  (Figure 15.A). One protein, uncharacterized FLJ76381 (YI018), was not recognized by the STRING software and was therefore excluded from further analysis. Several other proteins were not part of the network, as they did not interact with the other proteins from the network, but they were used in the GO term enrichment. These proteins are RHG39, tubulin beta-3 chain, VIME, tyrosine-protein phosphatase non-receptor type 6, XRCC5, PLSL, HCD2, and TRUB1. In the network, three clusters were formed, two of which centered around tubulin and actin, respectively. 14-3-3  $\zeta/\delta$  protein was linked to the actin cluster. The third cluster consisted of heat shock proteins as well as IF4A1, IF4A2, EF2, and SFPO. LDHB and KPYM were separate from the rest of the network.

The protein-protein interaction analysis was followed by a GO term enrichment, which drew data from several databases. All the proteins from the input were considered for the enrichment, except for YI018; redundant (e.g., “immune effector process” and “immune system process”) and unrelated (e.g., “axon extension”) terms were excluded. A total of 404 terms were identified (Figure 15.B), distributed among 6 categories, with Biological Process and Reactome pathways being the categories with the most terms. The distribution of the GO terms can be better visualized as an XY plot between the observed gene count and the  $-\log_{10}(FDR)$  value (Figure 16).

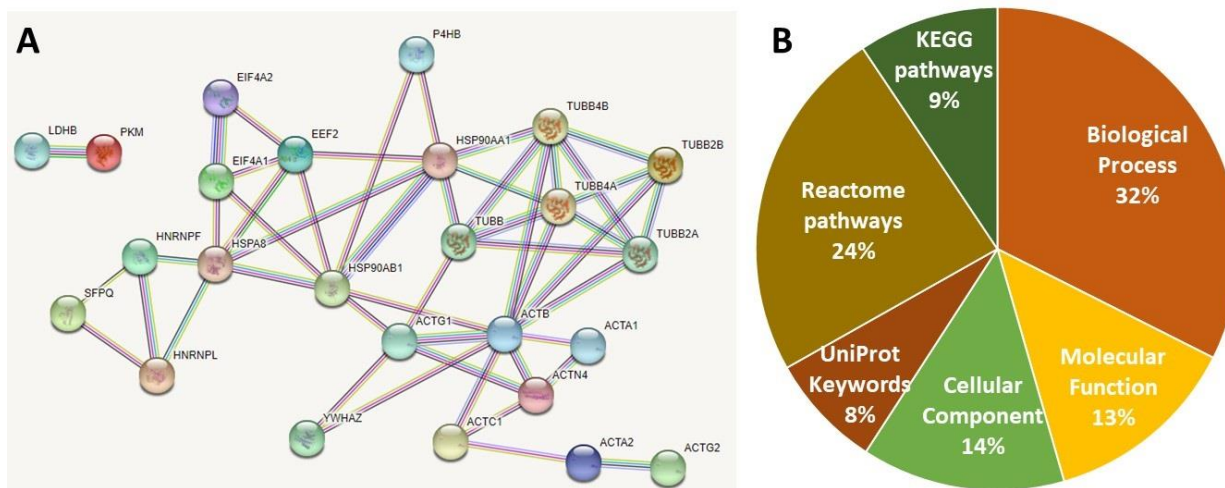


**Figure 15. Network of interactions and GO terms retrieved for the identified proteins. (A).** STRING network of the identified proteins. The option used was “multiple proteins” with a threshold for confidence of 0.7. The edges show the strength of the functional and physical connection between the nodes. **(B).** Overview of GO terms retrieved for the identified proteins. The terms were automatically divided into several categories. The proportion of each category is calculated relative to the total number of terms returned (404).

The biological process with the lowest FDR is “cytoskeletal organization,” while the molecular functions with the lowest FDRs are “structural constituent of the cytoskeleton” and “nucleotide binding.” The Reactome pathway that describes the most proteins from the input and has the lowest FDR is “immune system.” Although the KEGG pathway with the lowest FDR is “pathogenic *Escherichia coli* infection,” it describes a type of immune response. Multiple terms related to immunity and T cells were found. Several terms within the KEGG and Reactome pathways are associated with the immune response (e.g., “influenza A”) or describe the immune system (e.g., “adaptive immune system”).

UniProt keywords mostly describe protein modifications or general functions. The keyword with the lowest FDR was “acetylation,” which describes 29 of the proteins from the input. The proteins that were not described by this keyword are EIF4A2, tubulin beta-4A chain (TBB4A), tubulin beta-3 chain (TBB3), and tyrosine-protein phosphatase non-receptor type 6 (PTN6). This result can be considered as a validation for the HDACi treatment used.

The GO terms of the KEGG pathways described few proteins from the network, but they had low FDRs. For the Reactome pathways, “immune system” had the lowest FDR and represented the highest number of proteins from the network, compared to other terms in this category. Most of the proteins were located in the cytoplasm (Figure 16. F) and were divided between the secretory granule lumen and the intracellular organelles, with the cytoskeleton overlapping with all other compartments. The highest percentage of proteins (39.4%) was shared between the secretory granule lumen and the cytoskeleton, and the second highest (21.2%) was found solely in the cytoplasm.

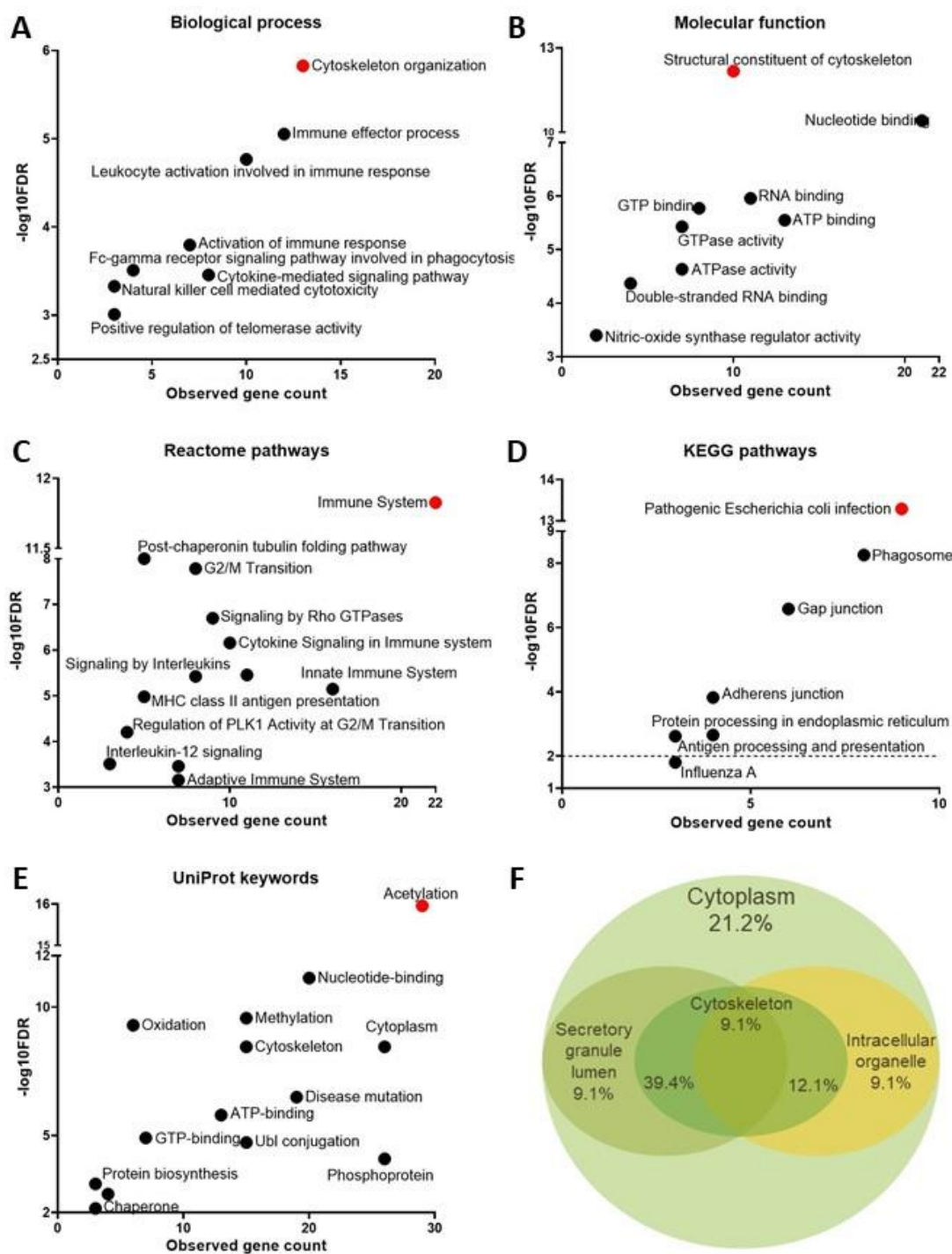
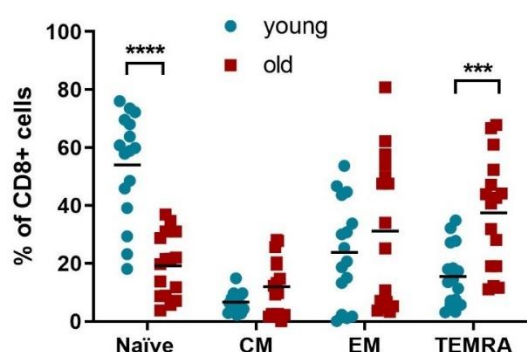


Figure 16. **Visual representation of the top GO terms retrieved for the identified proteins.** The categories of GO terms are as follows: (A) Biological process, (B) Molecular function, (C) Reactome pathways, (D) KEGG pathways, and (E) UniProt keywords. All the GO terms are defined by an FDR and an observed gene count. The GO term with the lowest FDR is always presented as a red dot. The details regarding the GO term can be found in Supplementary Table 8. The dotted line at  $-\log_{10}FDR = 2$  in each graph corresponds to an FDR of 0.01. (F) Venn diagram of the distribution of GO terms for the cellular component category. The Venn diagram was constructed based on the common proteins identified for each term. The percentages were calculated relative to the total number of proteins in the input.

### 4.3. Effect of HDACi treatment on CD8<sup>+</sup> T cell function

#### 4.3.1. Characterization of CD8<sup>+</sup> T cells

To better understand the impact of increased acetylation on CD8<sup>+</sup> T cells, several functional analyses were performed. First, the distribution of CD8<sup>+</sup> T cell subpopulations in PBMCs from healthy young and old



**Figure 17. CD8<sup>+</sup> T cell subpopulation distribution.** PBMC from all donors were stained for the subpopulation discrimination before proceeding with the magnetic sort of CD8<sup>+</sup> T cells. N = 16. \*\*\* = p value < 0.001, \*\*\*\* = p value < 0.0001.

blood donors was determined using multicolored flow cytometry (Figure 17). The subpopulations were defined as: naïve (CD45RA<sup>+</sup> CCR7<sup>+</sup>), CM (CD45RA<sup>-</sup> CCR7<sup>+</sup>), EM (CD45RA<sup>-</sup> CCR7<sup>-</sup>) and TEMRA (CD45RA<sup>+</sup> CCR7<sup>-</sup>).

In some young donors, naïve CD8<sup>+</sup> T cells reach up to 75% of the whole CD8<sup>+</sup> population, while it does not exceed 40% in older individuals. The decrease in the naïve subpopulation with aging is reflected by the increase in TEMRA cells. In older donors, the number of TEMRA cells can reach 70%, whereas the maximum limit for younger donors is around 30%. Moreover, CM and EM CD8<sup>+</sup> T cells show a marginal increase in older donors.

#### 4.3.2. Surface expression of activation markers and proliferation capacity

To confirm that the cells were activated post-culture and to ascertain the effect of HDACi treatment on the activation capacity of the cells, CD8<sup>+</sup> T cells were activated and treated as before, and after 2 days, the surface expression of activation markers was analyzed with flow cytometric methods. The activation markers investigated were CD69 – early activation marker, CD25 – IL-2 receptor alpha chain, and CD71 – transferrin receptor. The CD69 surface expression seemed to be very heterogenous for both age groups in both conditions (Figure 18.A). Overall, there appeared to be no difference between any of the groups. On an individual level, some donors showed different CD69 surface expressions between the untreated and HDACi-treated cells. Both CD25 and CD71 exhibited great variations between the age groups as well as when comparing the treated cells with the untreated ones. Compared to the young donors, activated and untreated CD8<sup>+</sup> T cells from the old donors showed an increase in both CD25 and CD71. In addition, CD25 showed a statistically significant difference between the HDACi-treated cells from young donors compared to older ones. The proliferation of the cells was analyzed with CFSE, after 5 days in culture (Figure 18.B). Activated cells from both age groups divided on average 4.5 times in 5 days. Cells from both

age groups have a severely reduced proliferation rate after receiving HDACi treatment, with just 1 division on average in 5 days.

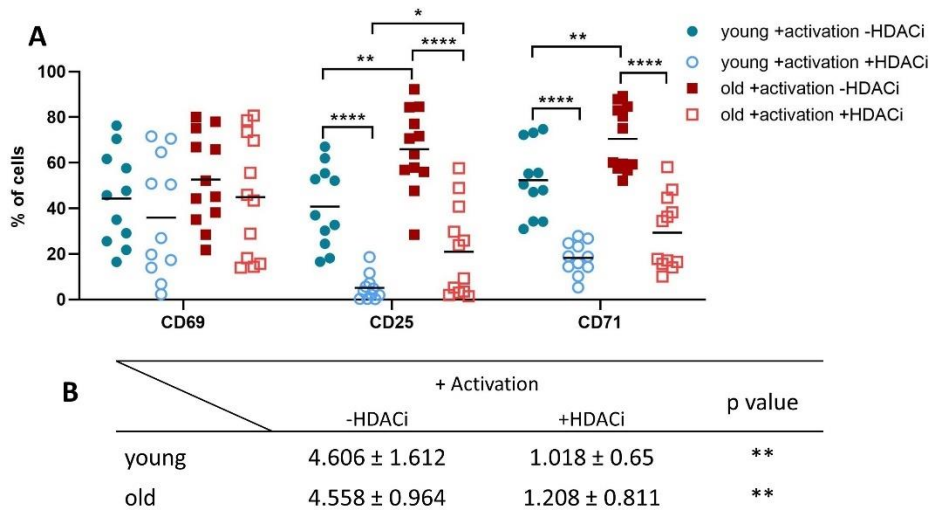


**Figure 18. Activation markers and proliferation indexes. (A).** The surface expression of activation markers was determined on CD8<sup>+</sup> T cells after 48h. Graph represents the percentage of the live CD3<sup>+</sup> CD8<sup>+</sup> T cells that express the indicated surface markers for each donor. *N* young = 11, *N* old = 12. **(B).** Proliferation indexes after 5 days in culture. Each proliferation index represents the average number of divisions the CD8<sup>+</sup> T cells went through.

#### 4.3.3. Cytokine secretion patterns during aging

The CD8<sup>+</sup> T cells were activated, treated or not with HDACi and cultured for 2 days, the supernatant was then collected and tested for the abundance of secreted soluble proteins. The soluble proteins tested for were IL-2, IL-3, IL-4, IL-5, IL-6, IL-10, GM-CSF, TNF- $\alpha$ , IFN- $\gamma$ , and granzymes A and B (Figure 19). Granzymes A and B are the only proteins that were in the ng/ml range, the rest were in the pg/ml range.

A substantial difference was observed between young and old activated, HDACi-untreated CD8<sup>+</sup> T cells for almost all the proteins analyzed. Granzyme A, for which the difference between young and old activated CD8<sup>+</sup> T cells was not considerable, was the only exception. After HDACi treatment, both age groups produced significantly less soluble proteins, and the most affected proteins were IFN- $\gamma$ , GM-CSF, granzyme B, IL-6, IL-5, and IL-10. The HDACi treatment reduced the secretion of all proteins measured for both age groups, but the secretion patterns of older donors remained very high even post-treatment.

Activated, untreated CD8<sup>+</sup> T cells from older donors secreted on average twice the quantity of younger CD8<sup>+</sup> T cells. Following HDACi treatment, younger donors had severely impaired secretion machinery, and the cytokine levels were therefore below the detection range. Activated CD8<sup>+</sup> T cells from older donors produced similar amounts of IFN- $\gamma$  after HDACi treatment as CD8<sup>+</sup> T cells from young donors prior to the treatment.

Young activated and untreated CD8<sup>+</sup> T cells secreted almost no IL-10 and IL-4, and following HDACi treatment, this low secretion was completely blocked. For IL-5 and IL-10, both age groups ceased secretion after HDACi treatment. For the mentioned cytokines, the old activated and untreated cells showed a

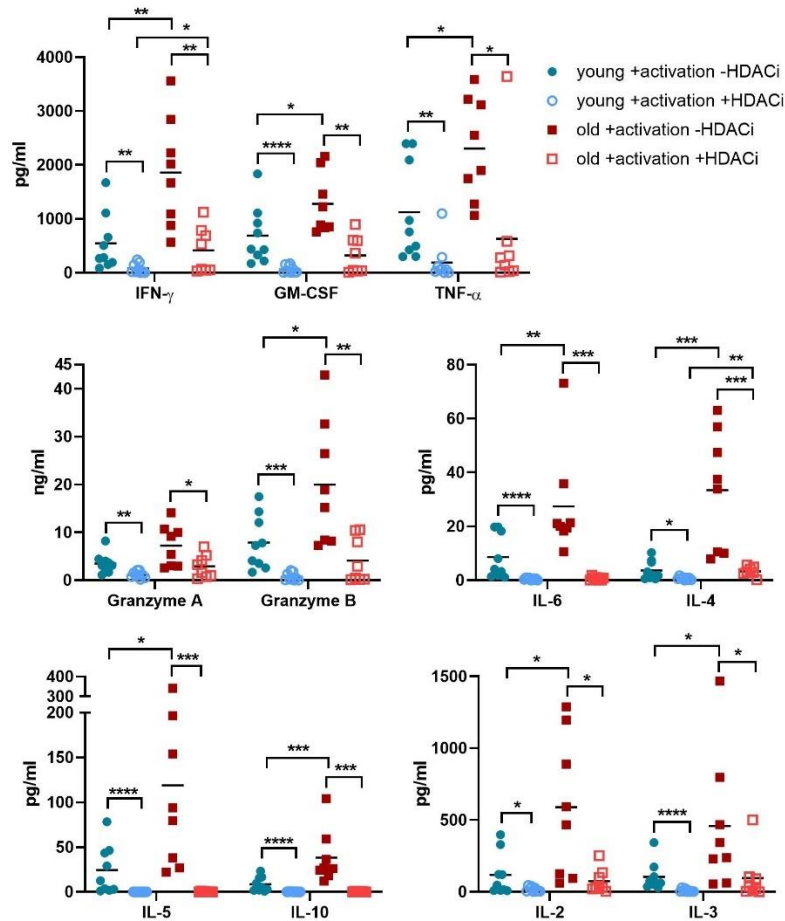


**Figure 19. Secretion phenotype.** Amounts of several cytokines and enzymes were determined in the supernatant of CD8<sup>+</sup> T cells, which were treated as indicated and kept in culture for 48h. Cytokines are grouped here according to the range of secretion. Results are presented as ng/ml and pg/ml. N young = 9, N old = 8. \* = p value <0.05, \*\* = p value < 0.01.

that HDACi treatment completely blocks the secretion of these cytokines.

One possible cause of the low secretion of T cells after HDACi treatment is that the cells cannot secrete the cytokines despite being able to produce them. To investigate this possibility, the transcript expression data of these secreted proteins were also collected (Figure 20). The fold change of the transcript expression is presented as  $\Delta\Delta Cq$  values, between the activated HDACi-treated and activated HDACi-untreated preparations.

For granzyme A, one young outlier has a  $\Delta\Delta Cq$  value of 2, but the rest of the donors present a homogeneous decreased expression. Granzyme B shows a similar pattern to granzyme A for both age groups, while TNF- $\alpha$  shows a minimal level of up-regulation relative to the housekeepers for the CD8<sup>+</sup> T cells from older donors after HDACi treatment. This contradicts the flow cytometric data, whereby the

heterogenous secretion. With the exception of granzyme A, this group displayed a great range, with very few donors having comparable secretions for each protein tested. As for IL-2, the amount secreted may not be enough to have a significant biological effect. And while activated, untreated CD8<sup>+</sup> T cells from old donors showed a heterogeneous secretion up to 1500pg/ml, the secretion of IL-2 is heterogenous for this group. IL-6 and IL-4 were produced in the lowest amounts from all the cytokines tested; however, older donor CD8<sup>+</sup> T cells that were activated but not treated with HDACi produced a much more significant amount than younger ones under similar stimulation. Furthermore, it can be observed

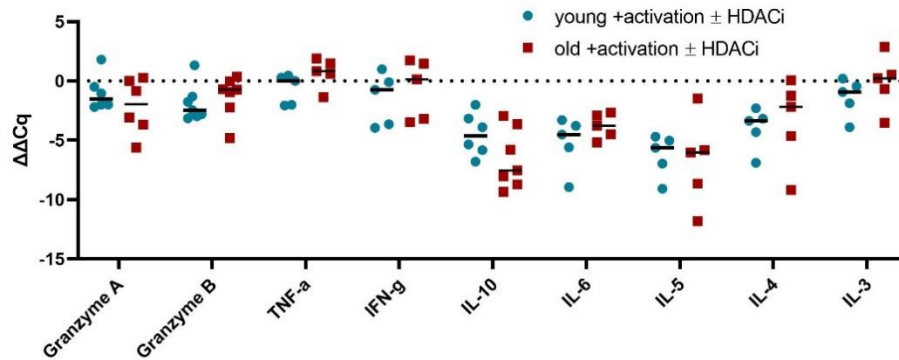


Figure 20. **Fold change of the gene expression of secreted cytokines.**  $\Delta\Delta Cq$  values are presented from the transcript expression qPCR analysis of selected enzymes and cytokines. The housekeeper genes were *SDHA* and *TBP*.  $N = 6$ .

other cytokines tested present a very heterogeneous fold change in the transcript expression and considerable down-regulation for most donors, which seems to align with the flow cytometric data, although the magnitude of the decrease after the HDACi treatment was much higher for the cytometric data.

post-treatment secretion of TNF- $\alpha$  decreased by half. IL-3 and IFN- $\gamma$  present similar patterns, with most donors showing no change in expression and two donors in each age group showing a fourfold decrease. All

#### 4.3.4. Apoptosis rates for the selected age groups

The apoptosis rate was verified with an Annexin kit after 2, 5 and 10 days in culture. In both age groups, the overall percentages of live cells after 2 days in culture was around 80% for untreated and 50% for treated CD8<sup>+</sup> T cells (Figure 21). At this time point, the percentages of apoptotic cells ranged from 20 to 40%, and dead cells represented only a small proportion of the total population. After 5 days in culture, the percentages of living and apoptotic CD8<sup>+</sup> T cells were almost at equilibrium, with a slight increase in the proportion of dead cells. However, after 10 days in culture, there were similar numbers of living, apoptotic, and dead cells. Overall, the decreasing trend in living cells was more pronounced than the increase in apoptotic and dead cells.

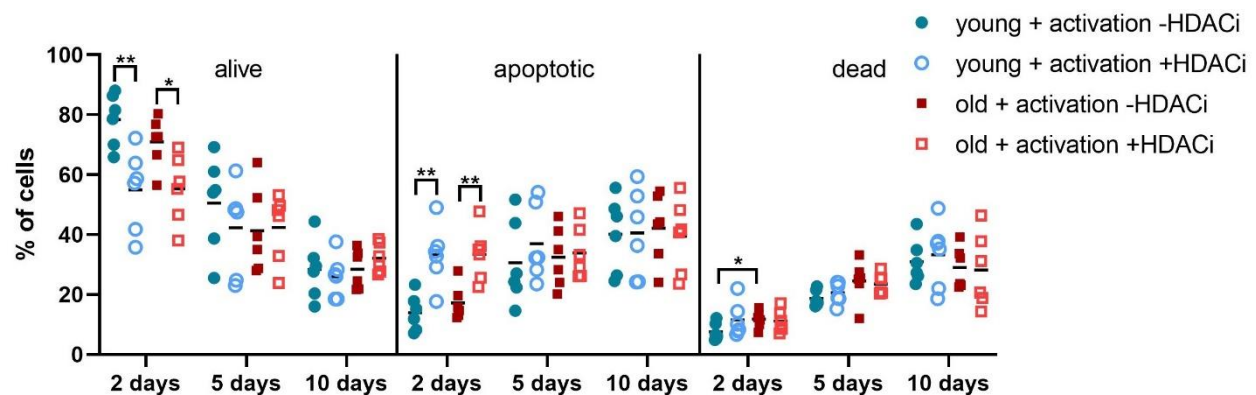
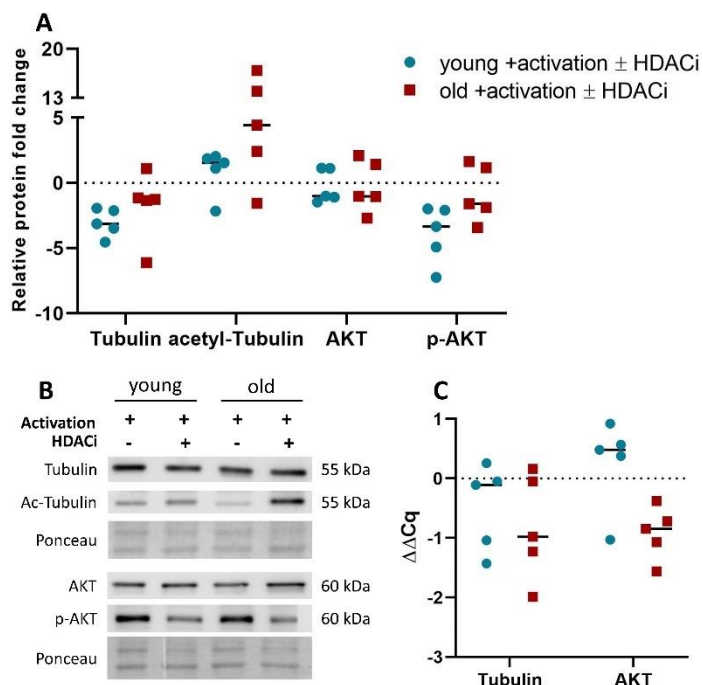


Figure 21. **Apoptosis assay.** The percentages of the cells that were alive (double negative), apoptotic (Annexin positive), and dead (double positive for Annexin and PI) are shown for all three time points.  $N = 6$ ; \* =  $p$  value < 0.05, \*\* =  $p$  value < 0.01.

After 2 days, the percentages of apoptotic cells increased following HDACi treatment for both age groups. The young activated CD8<sup>+</sup> T cells had a slightly higher percentage of living cells than the older group on day 2, and after HDACi treatment, both age groups had similar percentages. After 5 days in culture, both groups exhibited an increase in heterogeneity. Overall, both age groups showed a very similar yet heterogeneous rate of apoptosis following activation only as well as activation and HDACi treatment. After 5 and 10 days, there was no significant difference between the groups.

#### 4.3.5. Signaling transduction after HDACi treatment

To have a more detailed understanding of the cellular mechanisms occurring during HDACi treatment of activated CD8<sup>+</sup> T cells, the relative protein expression of tubulin and AKT was then tested by WB, and the fold change in transcript expression was assessed by qPCR (Figure 22) after 48h of culture. The protein expression of acetylated tubulin (acetyl tubulin) and phosphorylated AKT (p-AKT) was also analyzed. Both the protein and transcript expressions were calculated relative to the activated, untreated CD8<sup>+</sup> T cells. The expression of the modified proteins was first normalized to that of the unmodified structure.



**Figure 22. Expression of tubulin and AKT.** (A). CD8<sup>+</sup> T cells were cultured for 48h with the indicated stimulation. The relative protein expression was analyzed with WB and normalized to total protein staining with Ponceau S. For the modified proteins, an additional normalization to the unmodified protein was done. N = 5. (B). Representative blots for each protein. Two different membranes are shown. (C). The fold change in the transcript expression of tubulin and AKT was analyzed with qPCR. Two housekeepers were used: SDHA and TBP. N = 5.

Protein expression for both tubulin and AKT was not significantly different between the two age groups. While AKT showed a fairly unmodified protein expression, tubulin decreased slightly in both groups, with the young donors exhibiting a more clearly reduced expression.

Acetyl tubulin increased after HDACi treatment in both groups, although one outlier per group exhibited a decreased expression. The difference between young and old was not statistically significant; however, the increase in expression among old donors ranged from fourfold to 19-fold, whereas it hovered around threefold for young donors. The pattern of expression is similar to the 2DE data (Table 6), where the protein expression decreased in younger donors, although these data were

significant. Expression of p-AKT was reduced after HDACi treatment, and the decrease appeared to be more drastic in young donors. The transcript expression of both tubulin and AKT was highly heterogeneous, and no clear differences were found between young and old donors.

#### 4.4. Absolute quantification of transcript expression in activated CD8<sup>+</sup> T cells without HDACi treatment

##### 4.4.1. Functional comparison of the total CD8<sup>+</sup> T cells and CD8<sup>+</sup> CD45RA<sup>-</sup> memory T cells

Total RNA from healthy blood donors was collected for the total CD8<sup>+</sup> T cells and the CD8<sup>+</sup> CD45RA<sup>-</sup> memory T cells (Table 7); each group consisted of four women and four men. The total CD8<sup>+</sup> T cells and CD8<sup>+</sup> CD45RA<sup>-</sup> memory T cells were magnetically sorted, activated, and cultured for 48 h, without HDACi treatment. One donor from the CD8<sup>+</sup> CD45RA<sup>-</sup> memory T cells was excluded from the analysis for technical reasons (Supplementary table 11).

*Table 7. Donor information for all the preparations for RNA sequencing. Young (Y) and old donors (O) are grouped based on the CD8<sup>+</sup> T cell populations. For each donor, the age, sex, body mass index (BMI), cytomegalovirus (CMV) infection status and, when necessary, the ratio between CM and EM are presented. The mean and standard deviation are calculated when possible.*

	Donor	Age	Sex	BMI	CMV status	Ratio of EM/CM	
Total CD8 <sup>+</sup> T cells	Y11	29	M	30.42	-		
	Y12	27	M	27.70	-		
	Y13	27	M	26.56	-		
	Y14	23	F	19.53	+		
	Y15	27	F	33.41	-		
	Y16	24	M	34.54	+		
	Y17	25	F	22.60	+		
	Y18	23	F	19.84	-		
	Mean	25.63 ± 2.19		26.82 ± 5.81			
	O11	61	M	27.77	+		
O12	62	F	25.99	+			
O13	65	F	27.01	+			
O14	61	M	31.83	+			
O15	64	M	27.76	+			
O16	68	M	27.77	-			
O17	65	F	43.60	-			
O18	66	F	26.35	-			
Mean	64 ± 2.5		29.76 ± 5.87				
CD8 <sup>+</sup> CD45RA <sup>-</sup> memory T cells	Y22	28	F	17.56	+	3.06	
	Y23	27	F	33.41	-	3.59	
	Y24	24	M	20.30	-	4.61	
	Y25	30	M	25.25	-	5.56	
	Y26	25	F	22.60	+	2.26	
	Y27	25	M	20.91	-	1.90	
	Y28	23	F	20.91	-	2.55	
	Mean	26 ± 2.44		22.99 ± 4.77		3.36 ± 1.32	

O21	64	M	27.76	+	12.70
O22	60	F	22.55	-	2.32
O23	63	M	27.40	+	1.73
O24	68	M	27.77	-	1.95
O25	64	M	33.24	-	1.33
O26	66	F	26.35	-	4.55
O27	62	F	34.48	+	4.56
O28	64	F	26.22	+	1.42
Mean	63.88 ± 2.41		28.22 ± 3.87		3.82 ± 3.81

Information such as sex, body mass index (BMI), and cytomegalovirus (CMV) infection status was collected from each donor. For the CD8<sup>+</sup> CD45RA<sup>-</sup> memory T cells, the ratio of EM to CM CD8<sup>+</sup> T cells was investigated after the magnetic sort. The young groups had similar average ages but different average BMIs. The average BMI for the young total CD8<sup>+</sup> T cells was at the lower limit for overweight, while that of the young CD8<sup>+</sup> CD45RA<sup>-</sup> memory T cells was within normal weight limits. The old groups were of similar average ages and BMIs, which were beyond the overweight limit<sup>199</sup>.

For each preparation of the total CD8<sup>+</sup> T cells, the T cell subpopulations were also analyzed prior to the magnetic sort. The average proportion of the CD8<sup>+</sup> CD45RA<sup>-</sup> memory T cells is higher for the older donors, as expected (Figure 23.A). The post-sort EM/CM ratios for the preparations used for the CD8<sup>+</sup> CD45RA<sup>-</sup> memory T cells are similar for both age groups (Figure 23. B), although the old group presents one extreme outlier. This indicates that the preparations for the CD8<sup>+</sup> CD45RA<sup>-</sup> memory T cells are similar in cell composition.

After 48 h of culture, the surface expression of activation markers CD25, CD69, and CD71 was measured (Figure 24.A). The expression of CD69 was very heterogeneous for the young groups, and while the old

groups showed a stable CD69 expression, there was no significant difference between the age groups or the cell types. In contrast, CD25 expression increased for the CD8<sup>+</sup> CD45RA<sup>-</sup> memory T cells compared to the total CD8<sup>+</sup> T cells on average. The young CD8<sup>+</sup> CD45RA<sup>-</sup> memory T cells had more heterogeneous and reduced expression of CD25 compared to the old.

While CD71 exhibited a similar expression pattern to CD25, it had an increased heterogeneity in the old donors and

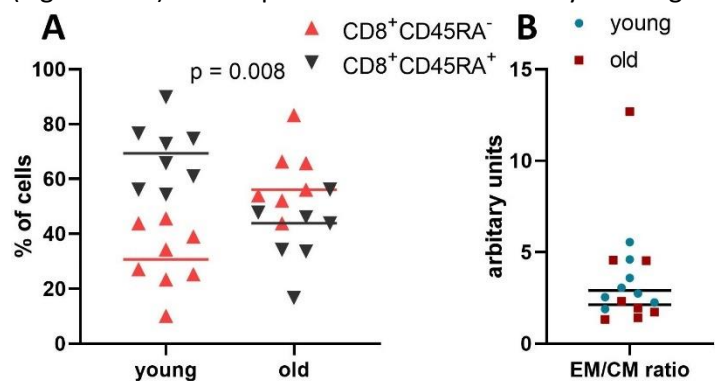


**Figure 23. Composition of the RNA sequencing preparations.** (A). Pre-sort distribution of the CD8<sup>+</sup> CD45RA<sup>-</sup> memory T cells (EM + CM) within the total CD8<sup>+</sup> T cell preparations. N = 8. (B). Post-sort ratios of CM and EM in the CD8<sup>+</sup> CD45RA<sup>-</sup> memory T cells after the sort. The ratio was calculated with the percentage of EM and CM cells from the total number of living cells after the memory sort. N = 8.

showed no statistical significance. The CD8<sup>+</sup> CD45RA<sup>-</sup> memory T cells expressed marginally more CD71 than the total CD8<sup>+</sup> T cells.

Additionally, the secretion patterns of the cells were analyzed by measuring the soluble proteins in the supernatant after 48 h in culture. The soluble proteins measured were IFN- $\gamma$ , TNF- $\alpha$ , GM-CSF, IL-10, IL-6, IL-5, IL-4, IL-3, IL-2, and granzymes A and B (Figure 24. B – F).

Significant differences between the young and old donors were found for the total CD8<sup>+</sup> T cells, except for TNF- $\alpha$ , IL-6, and both granzymes. There were several outliers in the old group for this cell population, yet no correlation with the EM/CM ratio was observed. These findings correspond to previous results on the secretion without HDACi treatment (Figure 19). Compared to the total CD8<sup>+</sup> T cells, the secretion pattern for the CD8<sup>+</sup> CD45RA<sup>-</sup> memory T cells had a more heterogeneous distribution; even so, it mirrored the pattern of the total CD8<sup>+</sup> T cells. Secreted IFN- $\gamma$ , TNF- $\alpha$ , and granzyme A were comparable between young

and old donors for the CD8<sup>+</sup> CD45RA<sup>-</sup> memory T cells, whereas IL-10, IL-6, and IL-2 only showed a marginal increase for the old. Conversely, the CD8<sup>+</sup> CD45RA<sup>-</sup> memory T cells from old donors secreted more GM-CSF, granzyme B, IL-5, IL-4, and IL-3 than their young counterparts.

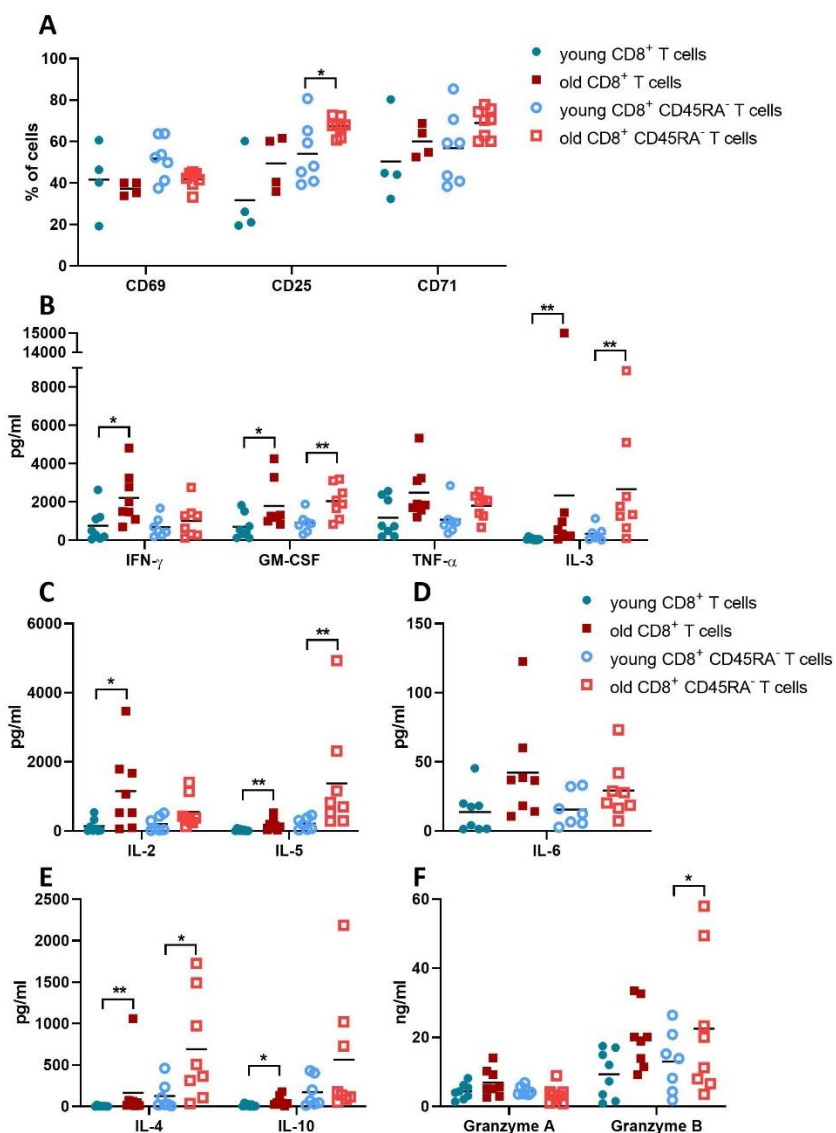


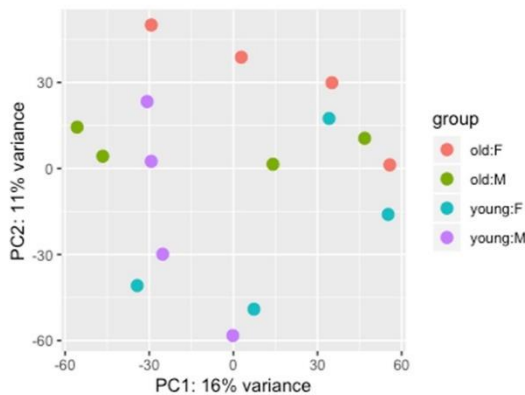
**Figure 24. Biological data for the RNA sequencing preparations. (A).** Activation markers for the RNA sequencing preparations. The surface expression of CD69, CD25 and CD71 was measured after 48 h.  $N$  total CD8<sup>+</sup> T cells = 4,  $N$  CD8<sup>+</sup> CD45RA<sup>-</sup> memory T cells = 8. \* =  $p$  value < 0.05, \*\* =  $p$  value < 0.01. **(B – F).** Soluble-protein secretion patterns for RNA sequencing preparations. Soluble proteins were measured in the supernatant after 48 h of culture. Secretion is presented as ng/ml or pg/ml.  $N=8$ ; \* =  $p$  value < 0.05, \*\* =  $p$  value < 0.01.

#### 4.4.2. Data overview and quality control

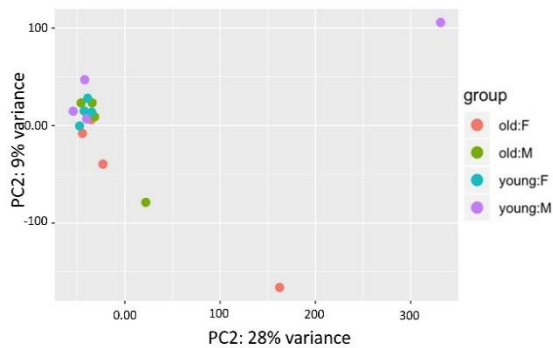
Several statistical tests were performed to verify the quality of the output, including PCA and the Pearson's correlation. Within the total CD8<sup>+</sup> T cells, the variance obtained for both components is 11% and 16%, respectively (Figure 25.A), and the individual preparations are not clustered based on age or sex. For this cell type, there was a strong positive correlation between the age groups identified with Pearson's correlation (data not shown).

From the CD8<sup>+</sup> CD45RA<sup>-</sup> memory T cells, one donor was responsible for most of the variance in the group in the PCA (Figure 25.B) and had the lowest positive correlation with the other preparations (data not shown). Upon further inspection, this donor expressed a large number of transcripts that were not found

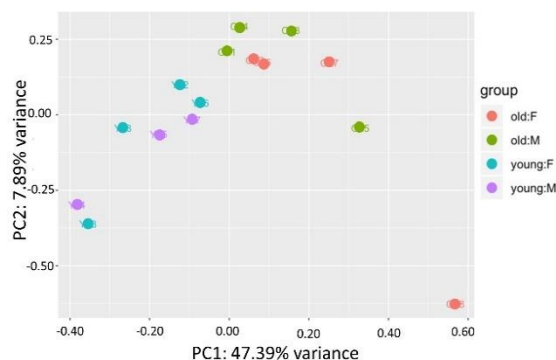
##### A Total CD8+ T cells



##### B CD8+ CD45RA- memory T cells with Y21



##### C CD8+ CD45RA- memory T cells without Y21



in other donors (571 transcripts). Therefore, the donor was excluded from further analysis (Supplementary Table 11).

The PCA for the rest of the preparations for the CD8<sup>+</sup> CD45RA<sup>-</sup> memory T cells shows a variance of 7.89% and 47.39%, respectively (Figure 25. C). While the groups do not cluster perfectly, there is a distinction between the age groups, with the young clustering more to the left and the old donors to the right. No sex-based distinction was found between the groups.

The total number of transcripts identified is close to 100,000 for each cell population; however, the number of transcripts with a biological significance is decidedly smaller. The magnitude of the  $\log_2(\text{FoldChange})$  value of the transcripts with an increased expression was then plotted against the adjusted  $p$  value (Figure 26.A). The

**Figure 25. PCA of the data variation in the RNA sequencing datasets. (A)** For the total CD8<sup>+</sup> T cells, the variance found was 16% and 11%, respectively. **(B)** For the CD8<sup>+</sup> CD45RA<sup>-</sup> memory T cells, the PCA returned a variance of 28% and 9%, respectively, which was caused by one donor only. This donor was excluded from further analysis. **(C)** One donor was excluded from the CD8<sup>+</sup> CD45RA<sup>-</sup> memory T cells. The variance in the PCA became 47.39 % and 7.89 %, respectively, and all donors participate in the variance. Red represents old female donors, green old male donors, blue young male donors, and purple young female donors.

extent of the  $\log_2(\text{FoldChange})$  is similar for both cell populations; however, for the total CD8<sup>+</sup> T cells, there were more transcripts with a significant  $p$  value than in the CD8<sup>+</sup> CD45RA<sup>-</sup> memory T cells.

The total number of *up-regulated* transcripts was similar for both age groups and both cell populations (Figure 26.B). For the total CD8<sup>+</sup> T cells, the difference between the age groups in terms of *up-regulated* transcripts was around 200 transcripts: 7,208 for the young and 7,002 for the old donors. This difference increased to around 500 in the CD8<sup>+</sup> CD45RA<sup>-</sup> memory T cells; the young had 7,795 *up-regulated* transcripts and the old donors had 7,290. The number of *up-regulated* transcripts that also were statistically significant was the highest in the young group of the total CD8<sup>+</sup> T cells and the lowest amongst the old group of the CD8<sup>+</sup> CD45RA<sup>-</sup> memory T cells. The number of *uniquely expressed* transcripts for the total CD8<sup>+</sup> T cells was almost identical between the young and old donors. Conversely, for the CD8<sup>+</sup> CD45RA<sup>-</sup> memory T cells, the old had a greater number of *uniquely expressed* transcripts than the young donors, which expresses a similar number of *unique transcripts* as both groups for the total CD8<sup>+</sup> T cells.

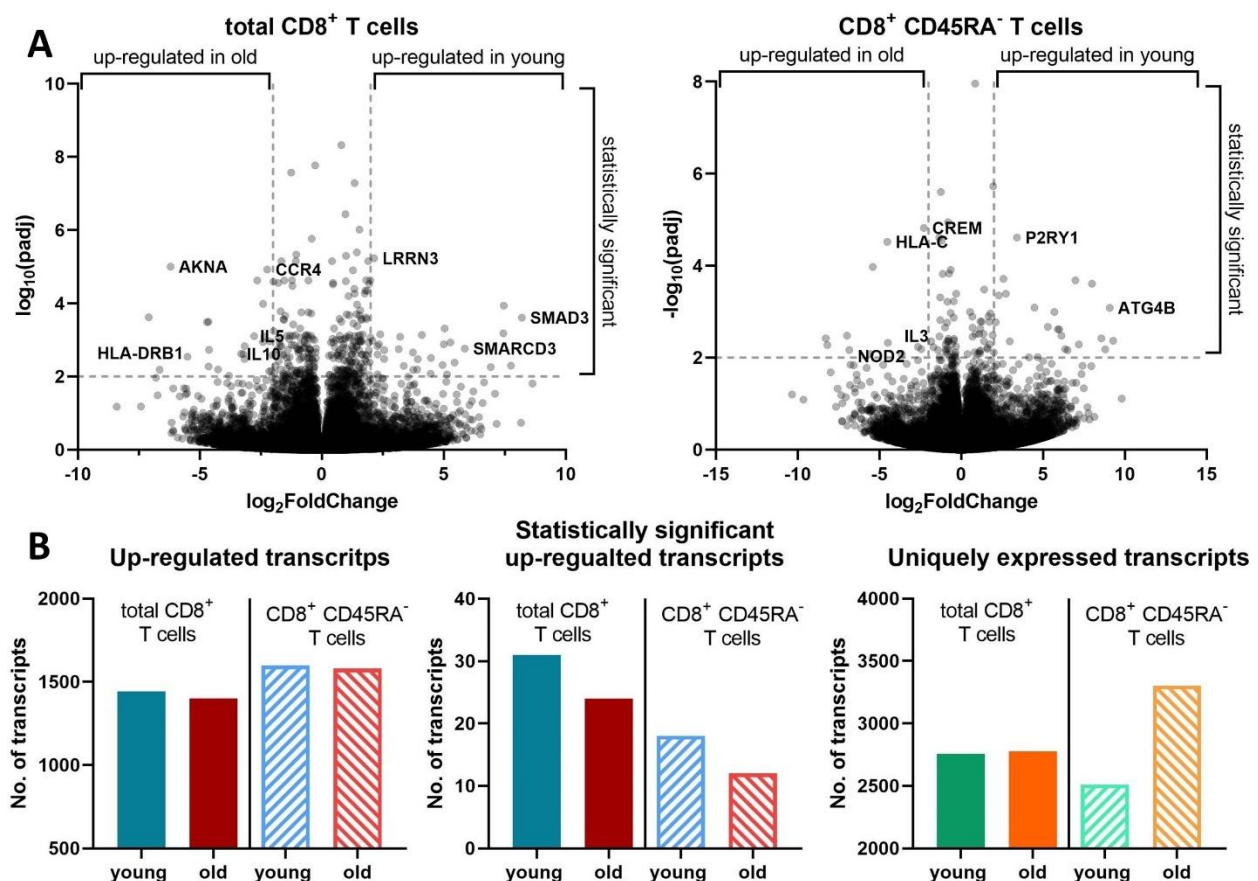


Figure 26. **Overview of the raw RNA sequencing data. (A).** Transcript distribution. All transcripts have XY coordinates which correspond to  $\log_2(\text{FoldChange})$  and  $-\log_{10}(\text{padj})$ . Selected transcripts with a very low adjusted  $p$  value are labeled.  $\text{padj}$  = adjusted  $p$  value. **(B).** Overview of the identified transcripts. Up-regulated transcripts have a  $\log_2(\text{FoldChange})$  value under  $-2$  or over  $+2$ . Statistical significance represents an adjusted  $p$  value  $< 0.01$ . The uniquely expressed transcripts are those that are only expressed in one of the age groups.

The overlap between the transcripts *up-regulated in young* and *up-regulated in old* of both cell types was calculated with Venny 2.1.0, as well as the overlap between the *uniquely expressed* transcripts (Figure 27). The overlap found between the cell populations was very similar across the age groups. Although the percentage of overlap was around 6% for each age group both for the *up-regulated* and the *uniquely*

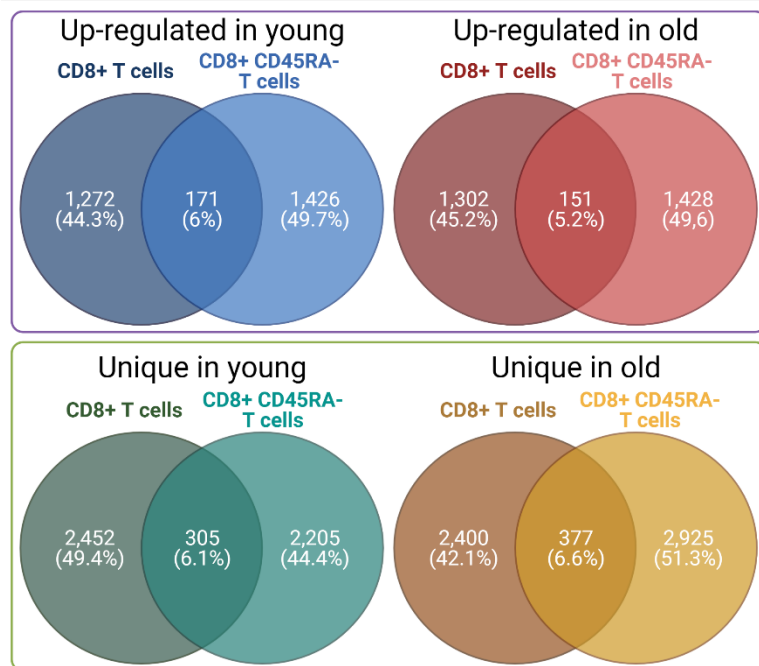


Figure 27. **Overlap among different lists of transcripts.** Percentages were calculated relative to the total number of transcripts within the input. Calculations were done with Venny 2.1.0 and the figure was created with BioRender.com.

expressed transcripts, it represented 171 and 151 transcripts for the transcripts *up-regulated in young* and *old*, respectively, and 305 and 377 transcripts for the *uniquely expressed in young* and *old*, respectively. That represents a double amount for each age group for the *uniquely expressed* transcripts. While the overlap in transcripts is not significantly different between the age groups, it is worth noting that the total CD8<sup>+</sup> T cells contain the CD8<sup>+</sup> CD45RA<sup>-</sup> memory T cells and that the old donors have significantly more memory T cells (Figure 23.A).

#### 4.4.3. Age-related GO term enrichment

The *up-regulated in old* and *up-regulated in young* lists were ranked according to the adjusted *p* value, prior to the GO term enrichment with the GOrilla online tool. The GO term anthology is divided into three categories: biological process, molecular function, and cellular component. The biological process category describes a larger action achieved by multiple molecules, while the molecular function category describes a function achieved at a molecular level by the transcript products. All GO terms identified with GOrilla have a *p* value under 0.05, however, the FDR is a more accurate statistical test, as it is a *p* value corrected for multiple testing.

The total number of transcripts deemed *biologically significant* was higher for the young group for each cell type, but the transcripts for the old groups exhibited more interactions, which was reflected in the statistical significance of the identified GO terms. For the older donors in the total CD8<sup>+</sup> T cells, the GO

term with the lowest FDR was “cytokine-mediated signaling pathways” (Figure 28). The transcripts annotated by this term include IL-5, IL-21, IL-10, IL-9, and IL-31. This supports the previous results that larger amounts of IL-5 and IL-10 are secreted by the CD8<sup>+</sup> T cells from older donors (Figure 24. B - F). The term “cytokine-mediated signaling pathways” appeared for the CD8<sup>+</sup> CD45RA<sup>-</sup> memory T cells of the old donors as well, albeit with a statistically non-significant FDR.

The biological processes identified for the transcripts *up-regulated in old* in the total CD8<sup>+</sup> T cells refer to immune-related functions such as “defense response,” “inflammatory response,” “positive regulation of

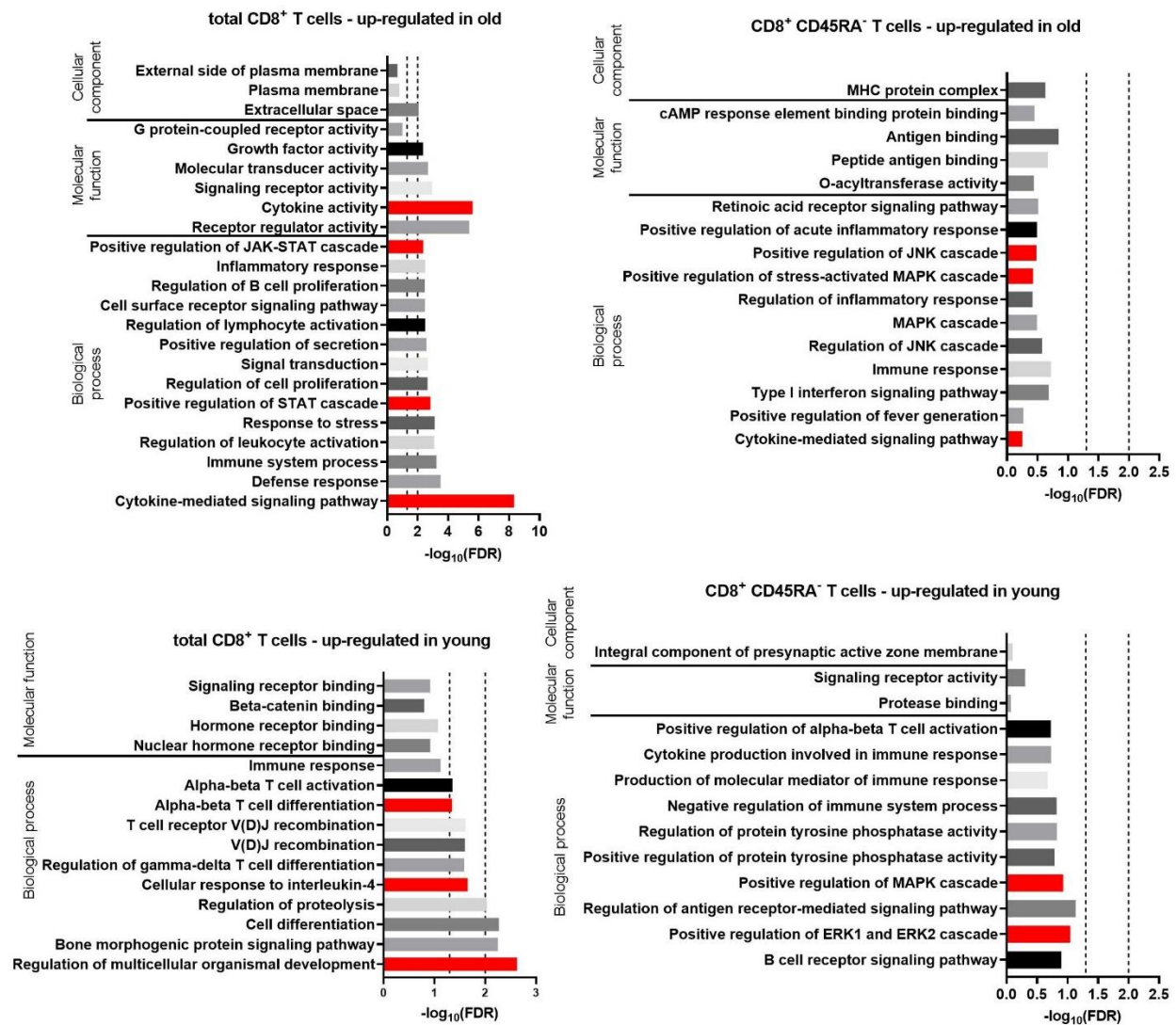


**Figure 28. GO terms for the transcripts with an increased expression for both cell populations retrieved with GOrilla.** The transcripts were divided into two subsets, increased in old and increased in young, and each list was then submitted for a separate GOrilla GO term enrichment. The resulting GO terms were classified as biological process, molecular function, or cellular component. The details regarding the GO terms can be found in Supplementary table 9. GOrilla calculates an FDR for each GO term. Two dotted lines are indicated in the diagrams: one at  $-\log_{10}(\text{FDR}) = 2$ , which corresponds to an FDR of 0.01, and one at  $-\log_{10}(\text{FDR}) = 1.3$ , which corresponds to an FDR of 0.05.

secretion,” and “regulation of lymphocyte activation” (Figure 28). This agrees with previous findings that CD8<sup>+</sup> T cell function is affected by aging. In addition, several GO terms related to the JAK-STAT pathway and other associated cellular pathways appear for the transcripts *up-regulated in old* in both cell populations. However, in contrast to the total CD8<sup>+</sup> T cells, none of these GO terms are statistically significant for the CD8<sup>+</sup> CD45RA<sup>-</sup> memory T cells.

The GO terms retrieved for the transcripts *up-regulated in young* for the total CD8<sup>+</sup> T cells describe biological processes associated with proliferation and differentiation. For the CD8<sup>+</sup> CD45RA<sup>-</sup> memory T cells, none of the GO terms are statistically significant, although they correlate with the terms retrieved for the total CD8<sup>+</sup> T cells (e.g., “alpha-beta T cell activation” for the total CD8<sup>+</sup> T cells and “positive regulation of alpha-beta T cell activation” for the CD8<sup>+</sup> CD45RA<sup>-</sup> memory T cells). Some terms linked to the JAK-STAT pathway<sup>200</sup>, such as “positive regulation of the mitogen-activated protein kinases (MAPK) cascade” and “positive regulation of the extracellular signal-regulated kinases 1 (ERK1) and ERK2 cascade” were identified as well, although different transcripts were annotated with these terms compared to the ones found in the old donors.

Although the GO terms for the old CD8<sup>+</sup> CD45RA<sup>-</sup> memory T cells are not statistically significant, some of them correspond to the terms identified for the old donors in the total CD8<sup>+</sup> T cells (e.g., “inflammatory response” for the total CD8<sup>+</sup> T cells and “regulation of the inflammatory response” for the CD8<sup>+</sup> CD45RA<sup>-</sup> memory T cells, or “response to stress” for the total CD8<sup>+</sup> T cells and “positive regulation of stress-activated MAPK cascade” for the CD8<sup>+</sup> CD45RA<sup>-</sup> memory T cells). Despite this apparent correlation, the transcripts annotated with these terms are dissimilar between the two cell populations (Figure 29).

The genes annotated for the 10 most statistically significant biological process GO terms for the old donors of both cell populations were compared in a binary heatmap. Transcripts common to both cell populations are HLA-C, HLA-DRB1, STAT2, nucleotide-binding oligomerization domain-containing protein 2 (NOD2), IL-5, neurofilament light (NEFL), and TNF receptor superfamily member 11 (TNFRSF11). The number of cytokine transcripts is higher for the old donors in the total CD8<sup>+</sup> T cells compared to the CD8<sup>+</sup> CD45RA<sup>-</sup> memory T cells, and there is partial overlap for the term “cytokine-mediated signaling pathway,” which describes both cell populations.

While IL-5 and HLA-DRB1 were annotated with a high number of the most significant GO terms for the total CD8<sup>+</sup> T cells, for the CD8<sup>+</sup> CD45RA<sup>-</sup> memory T cells both genes were annotated with only three GO terms. A similar pattern was visible for NOD3 and TNFRSF11A, however, these genes were more prevalent for the CD8<sup>+</sup> CD45RA<sup>-</sup> memory T cells.

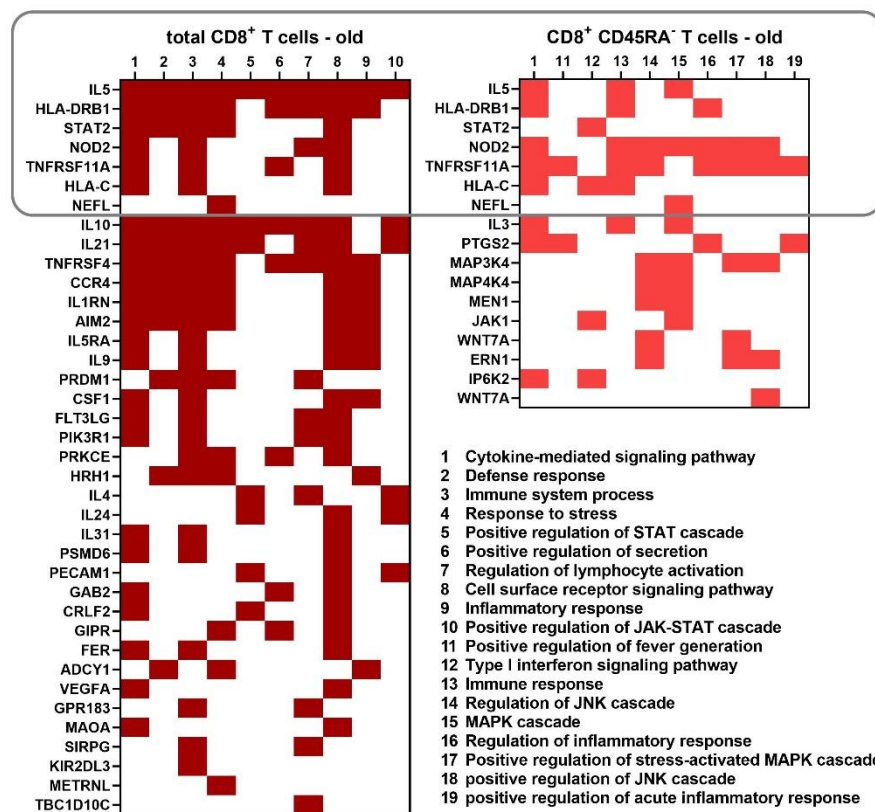


Figure 29. Comparison of the 10 most significant biological process GO terms identified for the old donors of both cell populations. A binary heatmap (color = yes, white = no) was established using the biological process GO terms with the lowest FDRs from both old groups. Transcripts present in both cell populations are highlighted with a border.

To have a broader view of which genes were the most annotated with the GO terms retrieved for each cell population, the output list of genes from GOrilla for all the biological process GO

terms was analyzed with a word cloud (Figure 30). Since all GO terms were considered, an easy visualization of the transcripts that participate in most of the shared functions was possible.

The old group of the total CD8<sup>+</sup> T cells has the most GO terms; therefore, the word cloud also has the most genes. IL-10 was the most frequently annotated gene with the identified GO terms for this group, the second most utilized genes were IL-21, IL-5 and HLA-DRB1. For the young group in the total CD8<sup>+</sup> T cells, the word cloud is considerably smaller and the most interconnected genes were lymphoid enhancer binding factor 1 (LEF1), noggin (NOG), and SMAD family member 3 (SMAD3).

While the word cloud for the old group of the CD8<sup>+</sup> CD45RA<sup>-</sup> memory T cells is smaller, there are a few common genes with the total CD8<sup>+</sup> T cells, such as TNF receptor superfamily member 11a (TNFRSF11a), IL-5, HLA-C and HLA-DRB1. The word cloud for the young group of the CD8<sup>+</sup> CD45RA<sup>-</sup> memory T cells is the smallest and shows that only a small number of the transcripts within this group participate in shared functions. The gene purinergic receptor P2Y1 (P2RY1) has the highest frequency for this group. No similarities were found between the word clouds of the young groups.



“interleukin-12-mediated signaling pathway” was identified with an FDR of 0.0718 and a  $p$  value of 0.000183, which is a component of the JAK-STAT signaling family<sup>200,201</sup>.

For the Molecular Function category, the terms “heterocyclic compound binding” and “nucleic acid binding” were retrieved for the transcripts *unique in old* from both cell populations. But while these terms had an FDR under 0.05 for the total CD8<sup>+</sup> T cells, those for the CD8<sup>+</sup> CD45RA<sup>-</sup> memory T cells had much lower FDRs. Interestingly, for these lists of genes the Cellular Component category had the lowest FDRs, the term “nuclear part” being present for all groups, except for the young total CD8<sup>+</sup> T cells, with an FDR lower than 0.01.

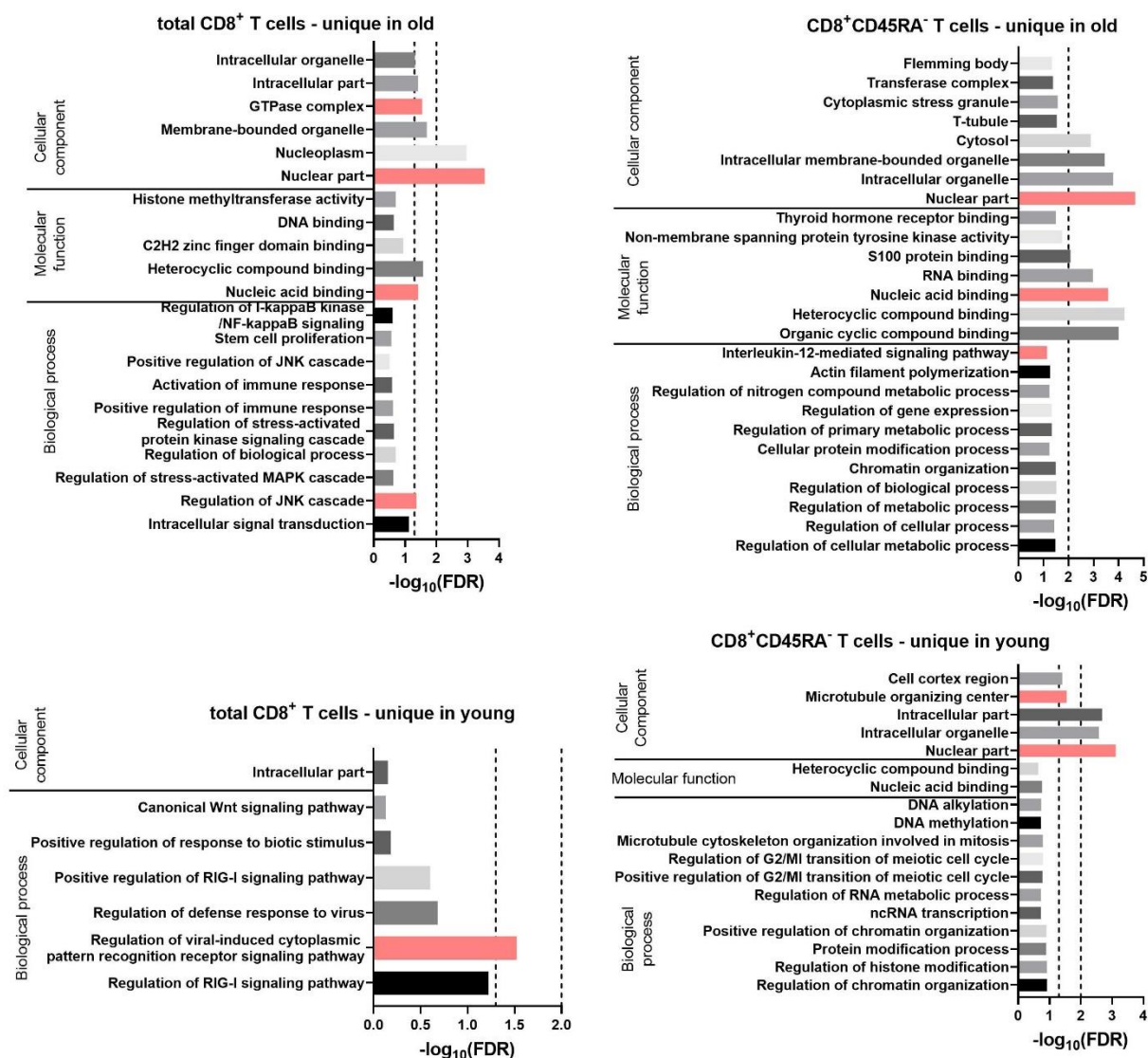


Figure 31. GO terms for uniquely expressed transcripts retrieved by GOrilla. All transcripts were ranked according to the normalized mean of the counts for all preparations. Resulting GO terms are classified as biological process, molecular function, or cellular component. The details regarding the GO terms can be found in Supplementary table 10. GOrilla calculates an FDR for each GO term. The two dotted lines, one at  $-\log_{10}(\text{FDR}) = 2$  and one at  $-\log_{10}(\text{FDR}) = 1.3$ , corresponds to FDRs of 0.01 and 0.05, respectively.



## 5. Discussion

The underlying goal of the current thesis is to study the effect of acetylation on the proteome of CD8<sup>+</sup> T cells, in the context of aging. Therefore, two age groups were defined as: young (<30 years old) and old (>60 years old). In each group, CD8<sup>+</sup> T cells from healthy human donors were sorted with microbeads. The donors were generally healthy; they had no known chronic infections and were over 18 years old, with a bodyweight over 50 kg. These cutoffs, including the age restriction, were imposed by the donation rules of the blood bank that provided the buffy coats<sup>174</sup>. The upper limit of the young group was 30 years old due to the aforementioned rules, namely the lower age limit and the body weight restriction on the possible number of donors, especially women. Besides these constraints, the upper age limit for the young group was chosen specifically due to the existing evidence that the second decade of life presents a similar T cell subpopulation pattern as the first<sup>202,203</sup>. In regards to the old group, the literature indicates that the T cell compartment is significantly altered after 60 years old<sup>204–206</sup>.

### 5.1. HDAC expression before and after inhibiting deacetylation

Acetylation influences the metabolism of immune cells; besides controlling cytoskeletal flexibility<sup>124,125</sup> and chromatin accessibility<sup>112</sup>, it is also strongly associated with T cell signaling pathways. For instance, the TCR signal strength determines the levels of Ac-CoA through an AKT-related process,<sup>98</sup> and acetyltransferases such as KAT6A play an important role in CD8<sup>+</sup> T cell memory formation<sup>207</sup> (Figure 33). In addition, deacetylases are involved in the maturation of CD8<sup>+</sup> T cells; HDAC3 knock-down mice have functionally defective naïve T cells<sup>131</sup>, HDAC4 controls the expression of transcription factor NF- $\kappa$ B,<sup>133,134</sup> and HDAC11 is a known negative regulator of immune functions<sup>136</sup>.

The gene and protein relative expression of HDAC3, HDAC4, and HDAC11 were analyzed for both activation only and activation with HDACi treatment. Although activation has an age-dependent effect on the gene expression of HDAC3 and HDAC4, their protein expression is essentially unchanged by either activation or treatment (Figures 10 and 12). Other studies have suggested that HDAC3 is involved in the maturation of CD4<sup>+</sup> T cells more than that of CD8<sup>+</sup> T cells,<sup>131,132</sup> and that HDAC4 is non-essential for the proper function of CD8<sup>+</sup> T cells,<sup>135</sup> although it is an important regulator of transcription factors.<sup>133,134</sup>

Only HDAC11 showed a significant age-dependent relative gene expression following HDACi treatment (Figure 12), which was not replicated at the protein level.

Considering the lack of a significant difference between the CD8<sup>+</sup> T cells from young and old donors for the relative gene and protein expression, the same HDACi treatment was applied to both age groups. With

the chosen concentrations, an increase in the intracellular acetylation levels of two-fold on average was observed for each age group (Figure 11).

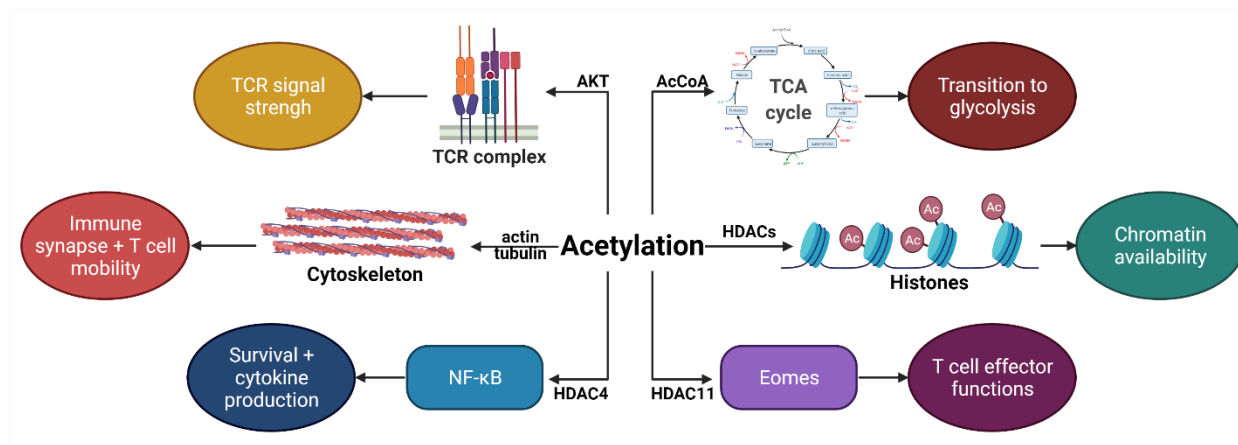


**Figure 33. Overview of the effect of acetylation on T cells.** T cell activation is affected by acetylation through Ac-CoA, which participates in the TCA cycle and thereby affects the transition of quiescent T cells to glycolysis when activated. Ac-CoA also influences AKT, which in turn affects the intensity of the TCR signal. The cytoskeleton participates in organizing the immune synapse when T cells encounter an APC; therefore, the acetylation of the cytoskeletal components reduces the mobility and activation of the T cells. Genomic transcription is regulated by the acetylation of histone proteins. HDAC4 regulates NF-κB and HDAC11 Eomes, which in turn regulate survival and effector functions, respectively. The figure was created with BioRender.com.

### 5.1. Identifying differently acetylated proteins based on 2DE expression profiles

Over the past decades, acetylation has been proven to affect numerous intracellular pathways by altering the chemistry of their components. The cytoskeleton<sup>123–126</sup>, GAPDH and the TCA cycle<sup>128–130</sup>, transcription factors<sup>95,106</sup>, chaperones<sup>117,121,122</sup>, and almost all proteins have their localization, function, or expression regulated by acetylation. To analyze how acetylation changes the proteome of CD8<sup>+</sup> T cells in the context of aging, 2D proteomic profiles were obtained using 2DE gels and DIGE dyes.

Through this method, a total of 1,500 spots were found to have changes in expression after HDACi treatment for each age group. It was observed that the number of spots with increased expression was much higher than that with decreased expression (Figure 13). On further evaluation, the young group had more of the former and the old group more of the latter. Analyzing only the spots with statistically significant expression, however, the young group presented more spots in both conditions. This can be attributed to greater biological diversity in the older group.

Spots were chosen for identification based on their RFs, and 31 proteins were identified in 22 spots (Table 6). Identifying multiple proteins in one spot is a documented pitfall of the identification method<sup>208</sup> that occurs when complex input materials such as cell lysates are used. It should also be emphasized that the

DIGE dyes have very high sensitivity. A final concentration of 10 pg/ml of each dye was used per 10  $\mu\text{g}$  of total protein (Figure 34). Using this method, even proteins with very low abundance can be visualized. Therefore, it was not feasible to identify all or even most of the differentiated proteins.

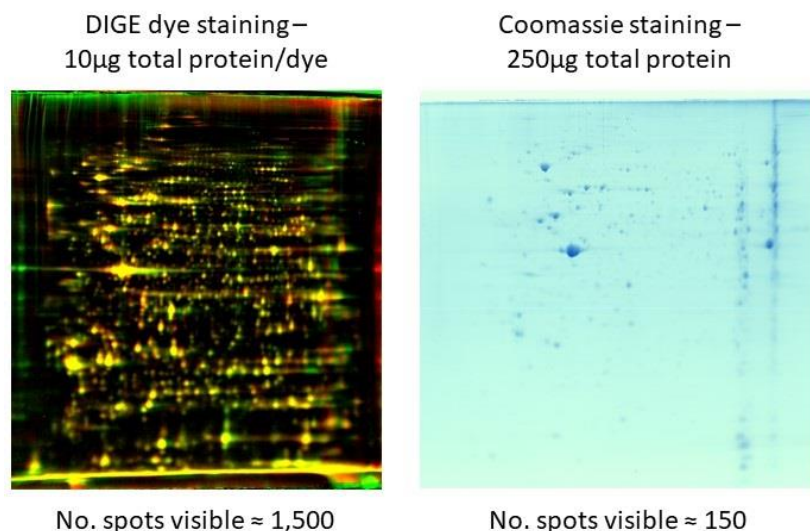


Figure 34. **The difference in sensitivity of the DIGE dyes and the Coomassie dye.** For the DIGE dyes 10  $\mu\text{g}$  of total protein were used for each dye, with a total of 30  $\mu\text{g}$  total protein per gel, whereas for the Coomassie dye 250  $\mu\text{g}$  total protein were necessary. Even so, the number of visible spots is 10-fold decreased for the Coomassie compared to the DIGE dyes.

14-3-3 proteins are an important component of the TCR signaling pathway; they bind to phosphorylated FoxO transcription factors and block the latter's activity, permitting the activation of T cells<sup>44,47</sup>. FoxO transcription factors are more active in quiescent naïve T cells; therefore, the need for 14-3-3 proteins was higher in the younger group than their older counterparts with a difference between the RFs of 1.62. The network formed between the proteins identified had a protein-protein interaction  $p$  value of  $10^{-13}$ , which indicates that these proteins were not a random group (Figure 15.A); instead, they interacted and performed shared functions. The connection between these proteins centered around the cytoskeleton, although additional clusters were formed by the HSPs and IF4A isoforms. The GO terms retrieved for the input proteins show that the interactions between these proteins were coordinated into cellular functions (Figure 16). Most of the GO terms relate to the immune system and describe the activation of T cells (e.g., "pathogenic Escherichia coli infection," "leukocyte activation involved in immune response") or other immune processes (e.g., "immune effector process," "cytokine signaling in immune system"). The "MHC class II antigen presentation" is one of the Reactome pathways identified, although the input was CD8<sup>+</sup> T cells which interact with the MHC class I antigen<sup>16</sup>. In addition, the cytoskeleton was a major presence within the network, and a large number of the proteins in the input were part of it (Figure 16.F).

A similar trend in regulation was found across both age groups (Table 6); the differences between the young and old groups were minute and mostly related to the statistical significance of the RF.

A highlight in the RF patterns was the 14-3-3  $\zeta/\delta$  protein, which had the highest RF out of all the identified proteins. This increase in expression was observed with WB as well, although not at the same magnitude (Figure 14). The

Interestingly, the UniProt keyword that describes the most proteins from the input and has the lowest FDR is “acetylation.” This can be considered an additional validation of the HDACi treatment. Four proteins were not annotated with this keyword, which suggests that they were not strongly influenced by the PTM or that they did not have many lysine residues capable of being acetylated, not that they were completely non-acetylated.

## 5.2. Age-dependent distribution of CD8<sup>+</sup> T cell subpopulations

The increase in the memory T cell subpopulations with aging is well documented.<sup>13–15,65,204–206</sup> This shift, however, is not a sign of disease, but rather the manifestation of a mature, more experienced adaptive immune system. For instance, athletes who train in the open air can accumulate more memory T cells by increasing their chances of encountering antigens<sup>209</sup>. Evidence also shows that both acute and chronic psychological stress<sup>210</sup>, such as caregiving for a child with autism spectrum disorder<sup>211</sup>, can produce this shift in T cell subpopulations. Nonetheless, a decrease in the naïve T cell population does contribute to lower efficiency in vaccines<sup>1</sup> and higher vulnerability to newly encountered pathogens<sup>2–6</sup>. Simultaneously, the increased accumulation of the memory T cell subpopulations leads to a chronic, sustained low level of inflammation<sup>78–80,83</sup> and hinders certain medical procedures such as transplants<sup>66,67</sup>.

The distribution of the T cell subpopulations (Figure 17) presented a clear pattern of increased naïve T cells in the young group and increased TEMRA cells in the old, although there was ample heterogeneity within each group. In the young group, for example, there were donors with naïve and TEMRA CD8<sup>+</sup> T cell counts comparable to those of older donors. These discrepancies within the young group can be attributed to lifestyle choices, such as physical exercise and nutrition<sup>209,212</sup>, stressful life events<sup>210,211</sup>, or simply a more experienced adaptive immune system.

## 5.1. Disruption of CD8<sup>+</sup> T cell functions and cellular signaling by inhibiting cellular deacetylation

The inhibitors in the HDACi cocktail used were TSA, NAM, and EX-527. TSA is considered a pan-inhibitor for Zn-dependent HDACs<sup>155</sup>, although evidence points to a possible interaction with SIRT6 as well<sup>213</sup>. NAM is the physiological inhibitor for sirtuins,<sup>168</sup> while EX-527 is specific to SIRT1<sup>162</sup>. The use of multiple inhibitors provided a broad spectrum of inhibition for deacetylation (Figure 11).

In a clinical setting, HDACis are used as anti-cancerous and anti-inflammatory agents<sup>7–10</sup>. TSA and EX-527 are being clinically tested for relapsed or refractory hematologic malignancies<sup>159</sup> and endometrial receptivity,<sup>167</sup> respectively. Since NAM is a physiologically occurring by-product of vitamin B3, it is also a dietary supplement primarily used to prevent pellagra, the cellular deficiency of vitamin B3<sup>173</sup>.

TSA has been shown to reduce proliferation in esophageal squamous<sup>156</sup> and pancreatic cancer<sup>158</sup> cell lines as well as induce apoptosis in human dermal lymphatic endothelial cells<sup>157</sup>. The anti-inflammatory properties of EX-527 are based on the reduction in mTOR activation<sup>165</sup> and thus T cell activation in general<sup>214</sup>. Meanwhile, NAM acts as an adjuvant for the anti-inflammatory activity of resveratrol on macrophages<sup>165</sup>.

Anti-CD3 and anti-CD28 mAbs<sup>24,25</sup> were used to activate *in vitro* the CD8<sup>+</sup> T cells by creating an mAb sandwich in the culture dish (Figure 6). Additionally, the aforementioned HDACi cocktail was used to analyze the effect of acetylation on the activation of CD8<sup>+</sup> T cells. The acetylation profiles (Figure 11) reveal that the levels of intracellular acetylation increase approximately two-fold after HDACi treatment for both age groups. To determine the effect of HDACi on CD8<sup>+</sup> T cell functions, the surface-marker expression, secretion patterns, and proliferation and apoptosis rates were evaluated.

The surface expression of activation markers CD69, CD25, and CD71, was evaluated after 2 days, as suggested in the literature<sup>27</sup>, using flow cytometric mAb (Figure 18.A). While CD69 exhibited a heterogeneous expression regardless of age group or treatment, activated CD8<sup>+</sup> T cells from older donors presented significantly greater expression of CD25 and CD71. This does not align with the literature findings, in which CD69 and CD71 have been found to decrease in CD8<sup>+</sup> T cells from older donors.<sup>215,216</sup> However, it was in accordance with the subpopulation distribution (Figure 17), because the older donors had a higher proportion of EM and CM T cells, which are more readily activated than naïve ones<sup>16</sup>. This increased expression of CD25 and CD71 would imply heightened secretion of IL-2<sup>32</sup> and proliferation<sup>36</sup>, respectively. Additionally, the increase in CD25 could result in a higher rate of proliferation, according to one study that compared sorted CD8<sup>+</sup>CD25<sup>+</sup> to CD8<sup>+</sup>CD25<sup>-</sup> T cells and found that the former produce more IL-2 and have a higher proliferation rate<sup>35</sup>.

Activated CD8<sup>+</sup> T cells from older donors presented an overall increase in secretion (Figure 19). All soluble proteins measured in the supernatant were significantly increased in the old group, including IL-2 and anti-inflammatory cytokines such as IL-4 and IL-10. This result aligns with the well-known phenomenon of inflammaging<sup>78-81</sup>, as all the pro-inflammatory factors were increased significantly for CD8<sup>+</sup> T cells from old donors. While granzyme A was not significantly increased, granzyme B was, which suggests that CD8<sup>+</sup> T cells from older donors exhibited an increased cytotoxic activity. The age-dependent increase of IL-2 has been observed in literature as well.<sup>80,81</sup> For IL-4 and IL-10, however, the information is mixed, showing either an increase or no change<sup>81,82</sup>.

The proliferation rates for the activated and untreated CD8<sup>+</sup> T cells presented virtually no differences between the age groups (Figure 18.B), although the CD71 expression was higher for CD8<sup>+</sup> T cells from

older donors. Other studies have observed an age-dependent reduction in the proliferation rate of naïve CD8<sup>+</sup> T cells in adult mice<sup>217,218</sup>. In humans, there is little evidence of older naïve CD8<sup>+</sup> T cells exhibiting reduced proliferation, and the differences seen in the total CD8<sup>+</sup> T cells can be explained by phenotype changes in the naïve CD8<sup>+</sup> T cells<sup>15,219</sup>. However, due to the toxicity of the reagents used<sup>176</sup>, the proliferation assay was performed within a time frame of 5 days, which might not have been sufficient for the detection of any significant differences.

After activation and increased proliferation, most activated CD8<sup>+</sup> T cells undergo apoptosis. It has been shown that in mouse models the apoptosis rate increases for older mice<sup>217,220</sup>. However, in the current study, apoptosis rates exhibited no distinction between young and old human donors (Figure 21). After 2 days in culture, there was a visible difference between the activated CD8<sup>+</sup> T cells and the activated and HDACi-treated cells. At the 5- and 10-day point, all groups presented strong heterogeneity, regardless of age or treatment.

HDACis have an overall reductive effect on the functions of CD8<sup>+</sup> T cells by interfering with activation, proliferation, and secretion without inducing severe apoptosis levels (Figure 35). After HDACi treatment, cell proliferation was arrested for both age groups at approximately equal rates (Figure 18.B). However, the CD8<sup>+</sup> T cells from the old donors nevertheless expressed more CD25 and CD71 (Figure 18.A) and secreted more soluble proteins in the supernatant (Figure 20) compared to those from younger donors. The old group only experienced a reduction in the secretion of IL-6, IL-5, IL-10, and IL-4 following HDACi treatment. The young group lost most of its secretion machinery, except TNF- $\alpha$  and IFN- $\gamma$ . The decrease in the secretion of inflammatory factors corresponds to the effect of HDACi described in the literature<sup>7-10</sup>. Conversely, the apoptotic effect of TSA on other cell types has been previously identified by other researchers<sup>157,158</sup>, although it did not have a clear-cut effect on activated CD8<sup>+</sup> (Figure 21).

The expression of tubulin and AKT was analyzed to discern the effects of aging on the intracellular environment and TCR signaling (Figure 22). While AKT expression was consistent in both age groups, tubulin decreased after HDACi treatment, and this decline was more intense for the younger donors. As tubulin participates in the proliferation and migration of CD8<sup>+</sup> T cells, this decrease mimicked the arrest of secretion and reduced activation of CD8<sup>+</sup> T cells in younger donors observed with other assays. In addition, acetyl-tubulin expression increased minimally within the young group, whereas the CD8<sup>+</sup> T cells from old donors experienced a slight decrease in tubulin and a strong increase in acetyl-tubulin.

Because HDACi treatment reduced the activation in both age groups and because p-AKT is required for T cell activation<sup>45</sup>, p-AKT expression was reduced as well. Nevertheless, it presented a similar pattern as tubulin. The young group had lowered expression of p-AKT, while the older group mostly experienced no

change in this regard. A high throughput study revealed several transcripts that are involved in T cell differentiation,<sup>221</sup> and their relative transcript expression was analyzed. However, with the exception of CNR2, none showed an age-related change, and the CNR2 expression was not strong enough to be considered biologically significant (data not shown).

### Untreated

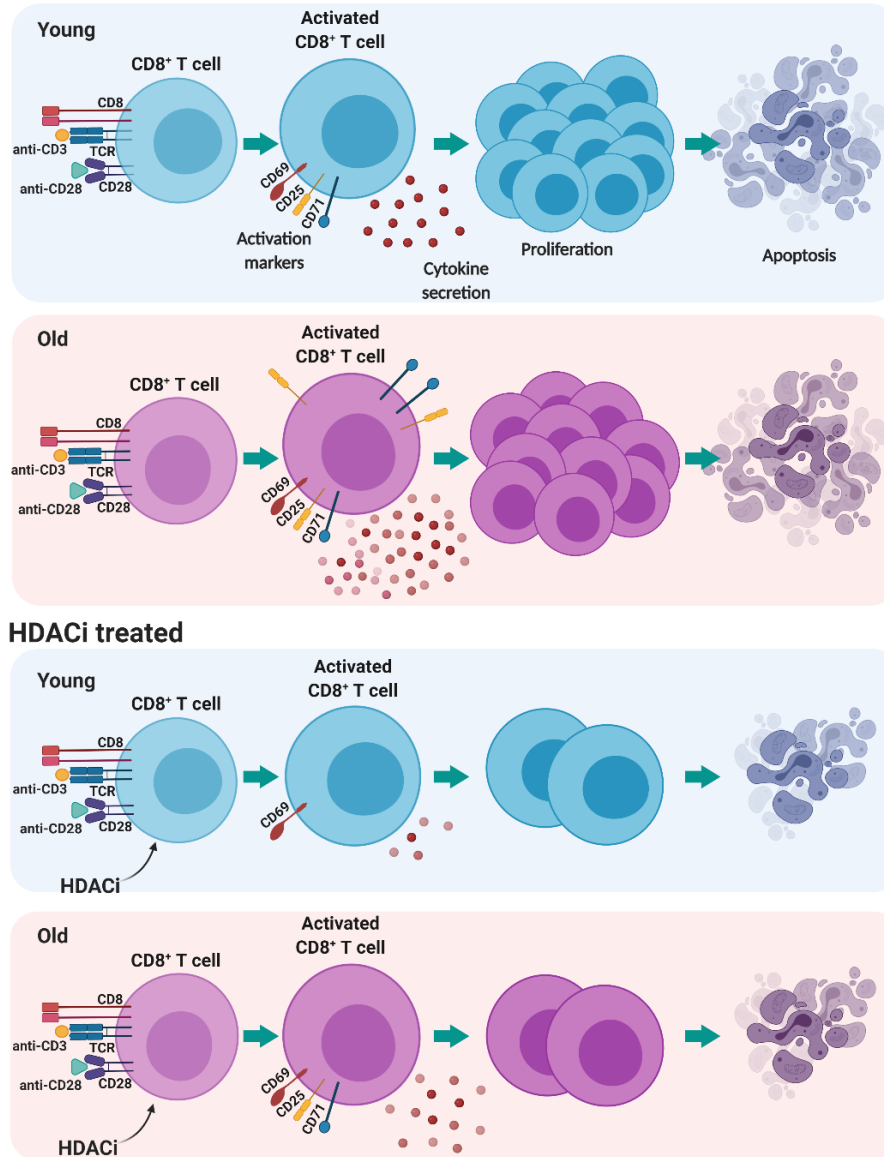


**Figure 35. Age-dependent response of CD8<sup>+</sup> T cells to HDACi treatment.** CD8<sup>+</sup> T cells were activated in vitro with anti-CD3 and anti-CD28 mAb. The surface expression of activation markers, presence of soluble proteins in the supernatant, proliferation capacity, and apoptosis rate were then analyzed. CD8<sup>+</sup> T cells from older donors (purple) showed greater surface expression of CD25 and CD71 as well as a stronger secretion than the CD8<sup>+</sup> T cells from younger donors (blue). When receiving HDACi treatment, CD8<sup>+</sup> T cells from young donors experienced massively reduced surface expression of activation markers and a compromised secretion, while CD8<sup>+</sup> T cells from old donors retained some expression of activation markers and low secretion. CD69 surface expression, proliferation, and apoptosis were equally affected for CD8<sup>+</sup> T cells from both young and old donors. The figure was created with BioRender.com.

## 5.2. Transcriptional differences between young and old donors without HDACi

To analyze the age-related transcriptional modifications, a total of eight preparations were made for the total CD8<sup>+</sup> T cells and the CD8<sup>+</sup> CD45RA<sup>-</sup> memory T cells. The balance between the donor groups was maintained to the greatest possible feasibility. However, the only group with a BMI within the average range was the young CD8<sup>+</sup> CD45RA<sup>-</sup> memory T cells group. Even so, the younger donors were on average

below the overweight limit<sup>199</sup> compared to their older counterparts (Table 7). The other parameters considered were either equally distributed, such as sex, or within the pre-established limits, such as age. The distribution of the CD8<sup>+</sup> CD45RA<sup>-</sup> memory T cells within the preparations for the total CD8<sup>+</sup> T cells was analyzed and a significant increase was found for the preparations for the older donors (Figure 23.A), in accordance to the information from literature<sup>13–15,65,204–206</sup>. The post-sort ratios of the CM and EM CD8<sup>+</sup> T cells were measured as well for the preparations for the CD8<sup>+</sup> CD45RA<sup>-</sup> memory T cells and revealed a balance between the age groups, despite one outlier for the older donors (Figure 23.B). Considering these results, the hypothesis was that the old preparations for the total CD8<sup>+</sup> T cells would resemble the old preparations for the CD8<sup>+</sup> CD45RA<sup>-</sup> memory T cells and that the preparations for the CD8<sup>+</sup> CD45RA<sup>-</sup> memory T cells of both age groups would be more homogeneous because the cell composition was similar.

Before the high throughput transcript analysis, the functionality of the cells used was investigated by measuring the surface expression of activation markers (Figure 24.A) and the quantity of soluble proteins secreted in the supernatant (Figure 24.B – F) after 48 h of culture. For the CD8<sup>+</sup> CD45RA<sup>-</sup> memory T cells, there were similar discrepancies between the young and old donors as with the total CD8<sup>+</sup> T cells. The older groups had stronger functioning secretion machinery and higher surface expression of CD25 and CD71. Although there were some outliers within the group, the secretion levels of GM-CSF, IL-3, and IL-5 were markedly increased in the older group, which did not correlate with the post-sort EM/CM ratios. TNF- $\alpha$  and granzyme A are the only soluble factors that showed no visible difference between the young and old donors of the CD8<sup>+</sup> CD45RA<sup>-</sup> memory T cells. The literature provides evidence of maturation differences in memory T cells in older individuals, which primarily results from a diminished naïve T cell pool<sup>15,219</sup>; however, little information has been provided for the functionality of these cells compared to memory CD8<sup>+</sup> T cells of younger individuals.

One significant difference between the cell populations examined was the number of transcripts found to be *up-regulated* and *uniquely expressed*. Although the number of transcripts with an increased expression was similar for both cell types, the statistical significance was higher for the total CD8<sup>+</sup> T cells groups, and there were more *uniquely expressed* transcripts within the CD8<sup>+</sup> CD45RA<sup>-</sup> memory T cells (Figures 26.A and B). Moreover, the overlap in transcripts between the same-aged groups in different populations was less than 6% in every instance (Figure 27). This points to the fact that the CD8<sup>+</sup> CD45RA<sup>-</sup> memory T cells was more diverse than the total CD8<sup>+</sup> T cells, although the total CD8<sup>+</sup> T cells was composed of naïve, EM, CM, and TEMRA cells. In the current RNA sequencing analysis, the total CD8<sup>+</sup> T cells appeared to be more homogenous as a group than the CD8<sup>+</sup> CD45RA<sup>-</sup> memory T cells.

The functional profile of each list of genes was acquired through GO term enrichment with GOrilla, which used the minimal hypergeometric test to assess the probability that the transcripts annotated with a certain GO term within the input were a random collection. With this approach, GOrilla found significantly enriched GO terms at the top of a ranked list. The final terms obtained describe a function or process in which multiple transcripts from the dataset participate<sup>222</sup>.

The cytokine activity and the JAK-STAT pathways were identified for the transcripts *up-regulated in old* for the total CD8<sup>+</sup> T cells (Figure 28), although the younger group presented a few terms associated with it as well (e.g., “cytokine production involved in the immune response,” “positive regulation of MAPK cascade”). The JAK-STAT pathway is a well-established part of the signal transduction of multiple cytokines, including IL-5<sup>223,224</sup> and other soluble factors<sup>225,226</sup>. There is evidence that defective signaling within the pathway leads to chronic inflammation<sup>226,227</sup> or even premature aging of stem cells<sup>228</sup>. In addition, JAK inhibitors, such as JAK1/2 inhibitor ruxolitinib, alleviate premature aging effects for individuals with Hutchinson–Gilford progeria syndrome<sup>229</sup>. The evidence of increased cytokine production in older individuals<sup>78–81</sup> has been previously discussed. Therefore, a strong correlation can be established between the increased functionality found earlier by measuring the soluble proteins in the supernatant of the cells and the presence of the JAK-STAT pathway in the GO terms for the older group of the total CD8<sup>+</sup> T cells.

For both the total CD8<sup>+</sup> T cells and the CD8<sup>+</sup> CD45RA<sup>-</sup> memory T cells, IL-5 and HLA-DRB1 appeared frequently in the most significant biological process GO terms (Figure 29). Both genes together with IL-10, IL-21 and TNFRSF11A were among the most annotated genes with the identified GO terms for the transcripts *up-regulated in old* for the total CD8<sup>+</sup> T cells (Figure 30). Moreover, IL-5 greatly increased in the supernatant of the older group for both cell types (Figure 24.B – F). HLA-DRB1 is an allele of the HLA-DR gene, and the HLA-DR<sup>+</sup> CD8<sup>+</sup> T cells have regulatory properties<sup>230,231</sup>. This subpopulation increases with aging, alongside other memory phenotypes<sup>232</sup>. Thus, this subpopulation may be increased in the current donor group as well.

The number of *uniquely expressed* transcripts was the highest among the old group in the CD8<sup>+</sup> CD45RA<sup>-</sup> memory T cells (Figure 26.B) and therefore GOrilla returned a higher number of GO terms for the gene lists for this cell population. While no GO terms were identified from the JAK-STAT pathway, several relating to it were returned for the transcripts *uniquely expressed in old* for both cell populations. For the total CD8<sup>+</sup> T cells the term “regulation of JNK cascade” and other terms related to the MAPK cascade were identified with FDRs under 0.05. Multiple kinases from the MAPK pathway were shown to activate the JAK-STAT pathway, including ERK<sup>233</sup> and JNK<sup>200</sup>. It was shown that the ERK<sub>1/2</sub> proteins in particular

phosphorylate STAT1 and STAT3 when the MAPK pathway is inhibited<sup>233</sup>. Furthermore, both signaling pathways are activated by the same ligands<sup>234</sup> (Figure 36).

For the transcripts *uniquely expressed in old* of the CD8<sup>+</sup> CD45RA<sup>-</sup> memory T cells, the term “interleukine-12-mediated signaling pathway” was identified. IL-12 signaling is closely tied to the JAK-STAT pathway<sup>200</sup>,

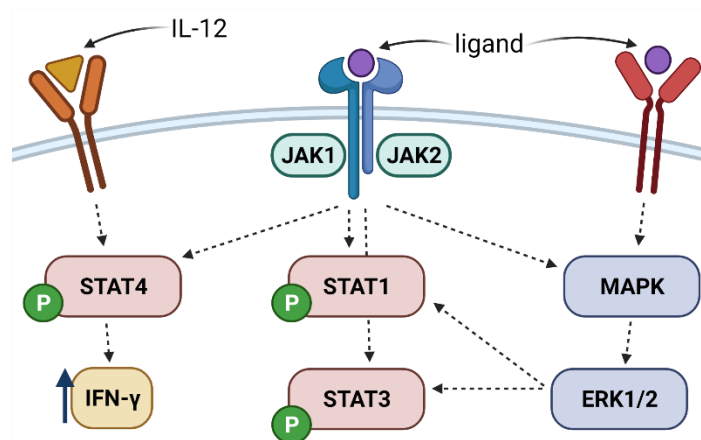


**Figure 36. Overview of the interconnected relationship between the JAK-STAT and MAPK cascades.** IL-12 and other cytokines act as ligands for both pathways, IL-12 phosphorylates STAT4, which increases the production of IFN- $\gamma$ . Similar ligands activate both pathways. Several proteins from the MAPK cascade activate the STAT proteins and the JAK-STAT signaling can activate the MAPK cascade as well. The figure was created with BioRender.com.

in T cells it activates the STAT4 protein, which triggers IFN- $\gamma$ <sup>201,235</sup>. Furthermore, for this subpopulation, JAK2 was one of the most frequently annotated genes (Figure 32).

Ultimately, the JAK-STAT pathway was present both in the *up-regulated* transcripts and in the *uniquely expressed* in CD8<sup>+</sup> T cells from older donors for both cell populations.

Other studies have found this pathway to be defective in older individuals<sup>227,236,237</sup>, however, most of these studies performed on memory T cells were rarely comparing memory CD8<sup>+</sup> T cells from young and old donors.

Additionally, when analyzing the most annotated genes for the *uniquely expressed* transcripts, several deacetylases were identified for the *uniquely expressed in young* list of genes for the CD8<sup>+</sup> CD45RA<sup>-</sup> memory T cells (Figure 32). While there is ample evidence in the literature that SIRT1, 3, and 6 are heavily involved in aging.<sup>138,139,144,145,147</sup>, SIRT3, 6 and 7 were identified in this list of genes. For the *uniquely expressed in old* list of genes for the CD8<sup>+</sup> CD45RA<sup>-</sup> memory T cells, KAT6B was frequently annotated with the identified GO terms. This acetyltransferase is crucial in CD8<sup>+</sup> T cell memory formation<sup>207</sup> and has been linked to the aging of the hematopoietic stem cells<sup>238</sup>.

### 6. Conclusions and future perspectives

Knowing the distribution of the different CD8<sup>+</sup> T cells subpopulations can serve as a helpful tool for assessing the severity of certain infections or the efficacy of treatments. For instance, the infection stage of tuberculosis can be determined by the predominance of CD45RA<sup>+</sup> or CCR7<sup>+</sup> CD8<sup>+</sup> T cells,<sup>239</sup> and the different distribution of CD8<sup>+</sup> T cells in older individuals can serve as a predictor of infection severity of the coronavirus<sup>240</sup>. The methodology required to ascertain the CD8<sup>+</sup> T cell subpopulations is becoming increasingly accessible to medical professionals; therefore, it is clinically relevant to understand whether there is a link between the accumulation of specific CD8<sup>+</sup> T cell subpopulations and physiological deficiencies or particular ailments.

Currently, HDACi are used as anti-inflammatory agents and in anti-cancer therapy. Due to inflammaging<sup>78-80</sup> and higher incidences of cancer<sup>241,242</sup> in older individuals, it is imperative to investigate the efficiency of these treatments across a wide age spectrum.

The current study found that the anti-inflammatory properties of HDACi are not as efficient in CD8<sup>+</sup> T cells from older individuals as they are for the young. The older donors had higher activation and secretion than their younger counterparts and HDACi treatment reduced these aspects partially for the old and completely for the young. This can be attributed to the increased number of CD8<sup>+</sup> memory T cells that accumulate with aging. When comparing the function of CD8<sup>+</sup> CD45RA<sup>-</sup> memory T cells from young and old donors, however, the older group retained a higher function.

The findings presented show that the intracellular mechanism of CD8<sup>+</sup> T cells is affected by aging, albeit minimally, which nevertheless contributes to broader effects at higher levels. The effect of the HDACi treatment on cellular signal transduction can be observed in the protein expression of acetyl-tubulin and p-AKT. Although these modified proteins were not altered significantly in the current study, it suggests a wider effect. The RNA sequencing data provides insight into this issue since a correlation was found between the increased functionality of CD8<sup>+</sup> CD45RA<sup>-</sup> memory T cells from old donors and the presence of the JAK-STAT pathway in the GO terms identified for this group. In addition, the pathways related to the JAK-STAT cascade were identified for the transcripts *uniquely expressed in old*, both for the total CD8<sup>+</sup> T cells and for the CD8<sup>+</sup> CD45RA<sup>-</sup> memory T cells, which emphasizes the importance of these signaling cascades.

An overarching goal of the current study was to identify proteins that were differentially expressed between the CD8<sup>+</sup> T cells of young and old individuals. This goal proved to be more challenging than anticipated, partially due to technical difficulties and also because identifying differentially expressed

proteins while avoiding the most abundant proteins in a cell requires more specialized approaches such as fractionation. Thus, the findings here confirmed previous knowledge that the cytoskeleton and chaperone proteins are primarily affected by acetylation<sup>124–126</sup>. However, differences in specific protein expressions have not been previously shown. These modified protein expressions were closely tied to the differences in activation and functioning that CD8<sup>+</sup> T cells experience with aging.

Ultimately, the age of the patient plays an important role in the efficiency of HDACi treatment, due to the intracellular modifications imposed by aging upon the cells. Admittedly, the current study represents an *in vitro* examination of CD8<sup>+</sup> T cell functions. Further analysis of the correlations between the age of the patient and the efficacy of HDACi treatment is therefore required.

Furthermore, while the effect of aging on the JAK-STAT pathway was explored<sup>226–228</sup>, it was done on a wide scale and not specific to CD8<sup>+</sup> T cell subpopulations. The current findings highlight this pathway as an important factor in understanding how to better attend to older individuals in the clinical setting.

## 7. Bibliography

1. Sallusto, F., Lanzavecchia, A., Araki, K. & Ahmed, R. From Vaccine to Memory and Back. *Immunity* **33**, 451–463 (2010).
2. Briceño, O. *et al.* Reduced naïve CD8(+) T-cell priming efficacy in elderly adults. *Aging Cell* **15**, 14–21 (2016).
3. Rane, S., Hogan, T., Seddon, B. & Yates, A. J. Age is not just a number: Naive T cells increase their ability to persist in the circulation over time. *PLoS Biol.* **16**, 1–20 (2018).
4. Egorov, E. S. *et al.* The changing landscape of naive T cell receptor repertoire With human aging. *Front. Immunol.* **9**, 1618 (2018).
5. Yoshikawa, T. T. Epidemiology and Unique Aspects of Aging and Infectious Diseases. *Clin. Infect. Dis.* **30**, 931–933 (2000).
6. Dhama, K. *et al.* Geriatric Population During the COVID-19 Pandemic: Problems, Considerations, Exigencies, and Beyond. *Front. Public Heal.* **8**, 1–8 (2020).
7. Adcock, I. M. HDAC inhibitors as anti-inflammatory agents. *Br. J. Pharmacol.* **150**, 829–831 (2007).
8. José-Enériz, E. S., Gimenez-Camino, N., Agirre, X. & Prosper, F. HDAC inhibitors in acute myeloid leukemia. *Cancers* vol. 11 (2019).
9. Uchida, H., Maruyama, T., Nagashima, T., Asada, H. & Yoshimura, Y. Histone Deacetylase Inhibitors Induce Differentiation of Human Endometrial Adenocarcinoma Cells through Up-Regulation of Glycodelin. *Endocrinology* **146**, 5365–5373 (2005).
10. Kelly, W. K., O'Connor, O. A. & Marks, P. A. Histone deacetylase inhibitors: from target to clinical trials. *Expert Opin. Investig. Drugs* **11**, 1695–1713 (2002).
11. López-Otín, C., Blasco, M. A., Partridge, L., Serrano, M. & Kroemer, G. The Hallmarks of Aging. *Cell* **153**, 1194–1217 (2013).
12. Lutz, W., Sanderson, W. & Scherbov, S. The coming acceleration of global population ageing. *Nature* **451**, 716–719 (2008).
13. Martínez de Toda, I., Mate, I., Vida, C., Cruces, J. & De la Fuente, M. Immune function parameters as markers of biological age and predictors of longevity. *Aging (Albany, NY)*. **8**, 3110–3119 (2016).
14. Matteucci, E., Ghimentì, M., Di Beo, S. & Giampietro, O. Altered Proportions of Naïve, Central Memory and Terminally Differentiated Central Memory Subsets among CD4 + and CD8 + T Cells Expressing CD26 in Patients with Type 1 Diabetes. *J Clin Immunol* **31**, 977–984 (2011).
15. Quinn, K. M. *et al.* Age-Related Decline in Primary CD8+ T Cell Responses Is Associated with the Development of Senescence in Virtual Memory CD8+ T Cells. *Cell Rep.* **23**, 3512–3524 (2018).
16. Abbas, A. K., Lichtman, A. H. & Pillai, S. *Basic Immunology: functions and disorders of the Immune System.* (2016).
17. Chondrogianni, N. *et al.* Protein damage, repair and proteolysis. *Mol. Aspects Med.* **35**, 1–71 (2014).
18. Kim, C., Fang, F., Weyand, C. M. & Goronzy, J. J. The life cycle of a T cell after vaccination – where does immune ageing strike? *Clin. Exp. Immunol.* **187**, 71–81 (2016).
19. Bretscher, P. & Cohn, M. A Theory of Self-Nonself Discrimination. *Cell* **169**, 1042–1049 (1970).
20. Linsley, P. S. *et al.* Human B7-1 (CD80) and B7-2 (CD86) bind with similar avidities but distinct kinetics to CD28 and CTLA-4 receptors [published erratum appears in *Immunity* 1995 Feb;2(2):following 203]. *Immunity* **1**, 793–801 (1994).
21. Whitmire, J. K. & Ahmed, R. Costimulation in antiviral immunity: Differential requirements for CD4+ and CD8+ T cell responses. *Curr. Opin. Immunol.* **12**, 448–455 (2000).
22. Berard, M. & Tough, D. F. Qualitative differences between naive and memory T cells. *Immunology* **106**, 127–138 (2002).
23. Cho, B. K., Wang, C., Sugawa, S., Eisen, H. N. & Chen, J. Functional differences between memory and naive CD8 T cells. *Proc. Natl. Acad. Sci. U. S. A.* **96**, 2976–2981 (1999).
24. Li, Y. & Kurlander, R. J. Comparison of anti-CD3 and anti-CD28-coated beads with soluble anti-CD3 for expanding human T cells: Differing impact on CD8 T cell phenotype and responsiveness to restimulation. *J. Transl. Med.* **8**, (2010).
25. Jiao, J. *et al.* Comparison of two commonly used methods for stimulating T cells. *Biotechnol. Lett.* **41**, 1361–1371 (2019).

26. Testi, R., Phillips, J. H. & Lanier, L. L. T cell activation via Leu-23. *J. Immunol.* **143**, 1123–1128 (1989).
27. Biselli, R., Matricardi, P. M., D'Amelio, R. D. & Fattorossi, A. Multiparametric Flow Cytometric Analysis of the Kinetics of Surface Molecule Expression after Polyclonal Activation of Human Peripheral Blood T Lymphocytes. *Scand. J. Immunol.* **35**, 439–447 (1992).
28. Sancho, D. *et al.* CD69 downregulates autoimmune reactivity through active transforming growth factor- $\beta$  production in collagen-induced arthritis. *J. Clin. Invest.* **112**, 872–882 (2003).
29. Vega-Ramos, J. *et al.* CD69 limits early inflammatory diseases associated with immune response to *Listeria monocytogenes* infection. *Immunol. Cell Biol.* **88**, 707–715 (2010).
30. Radulovic, K. *et al.* CD69 Regulates Type I IFN-Induced Tolerogenic Signals to Mucosal CD4 T Cells That Attenuate Their Colitogenic Potential. *J. Immunol.* **188**, 2001–2013 (2012).
31. Martín, P. *et al.* CD69 Association with Jak3/Stat5 Proteins Regulates Th17 Cell Differentiation. *Mol. Cell. Biol.* **30**, 4877–4889 (2010).
32. Malek, T. R. The Biology of Interleukin-2. *Annu. Rev. Immunol.* **26**, 453–479 (2008).
33. Lourenço, E. V. & La Cava, A. Natural regulatory T cells in autoimmunity. *Autoimmunity* **44**, 33–42 (2011).
34. Churlaud, G. *et al.* Human and mouse CD8 + CD25 + FOXP3 + regulatory T cells at steady state and during interleukin-2 therapy. *Front. Immunol.* **6**, 171 (2015).
35. Herndler-Brandstetter, D. *et al.* CD25-Expressing CD8 + T Cells Are Potent Memory Cells in Old Age. *J. Immunol.* **175**, 1566–1574 (2005).
36. Kawabata, H. Transferrin and transferrin receptors update. *Free Radic. Biol. Med.* **133**, 46–54 (2019).
37. González, A. & Hall, M. N. Nutrient sensing and TOR signaling in yeast and mammals. *EMBO J.* **36**, 397–408 (2017).
38. Vadlakonda, L., Dash, A., Pasupuleti, M., Kumar, K. A. & Reddanna, P. The paradox of Akt-mTOR interactions. *Front. Oncol.* **3**, 1–9 (2013).
39. Maciolek, J. A., Alex Pasternak, J. & Wilson, H. L. Metabolism of activated T lymphocytes. *Curr. Opin. Immunol.* **27**, 60–74 (2014).
40. O'Sullivan, D. *et al.* Memory CD8 + T cells use cell intrinsic lipolysis to support the metabolic programming necessary for development. *Immunity* **41**, 75–88 (2014).
41. Shestov, A. A. *et al.* Quantitative determinants of aerobic glycolysis identify flux through the enzyme GAPDH as a limiting step. *Elife* **3**, 1–18 (2014).
42. Abdel-Haleem, A. M. *et al.* The emerging facets of non-cancerous Warburg effect. *Front. Endocrinol. (Lausanne)*. **8**, 1–7 (2017).
43. Quinn, K. M., Palchadhuri, R., Palmer, C. S., L, N. & Gruta, L. The clock is ticking: the impact of ageing on T cell metabolism. *Clin. Transl. Immunol.* **8**, 1–18 (2019).
44. Navarro, M. N. & Cantrell, D. A. Serine-threonine kinases in TCR signaling. *Nat Immunol* **15**, 808–814 (2014).
45. Menk, A. V *et al.* Early TCR Signaling Induces Rapid Aerobic Glycolysis Enabling Distinct Acute T Cell Effector Functions. *Cell Rep.* **22**, (2018).
46. Jones, N. *et al.* Akt and STAT5 mediate naïve human CD4+ T-cell early metabolic response to TCR stimulation. *Nat. Commun.* **10**, 1- (2019).
47. Saravia, J., Raynor, J. L., Chapman, N. M., Lim, S. A. & Chi, H. Signaling networks in immunometabolism. *Cell Research* vol. 30 328–342 (2020).
48. Mosmann, T. R., Li, L. & Sad, S. Functions of CD8 T-cell subsets secreting different cytokine patterns. *Semin. Immunol.* **9**, 87–92 (1997).
49. Croft, M., Carter, L., Swain, S. L. & Dutton, R. W. Generation of Polarized Antigen-specific CD8 Effector Populations: Reciprocal Action of Interleukin (IL)-4 and IL-12 in Promoting Type 2 versus Type 1 Cytokine Profiles. *J. Exp. Med* **180**, 1715–1728 (1994).
50. Austin, L. M., Ozawa, M., Kikuchi, T., Walters, I. B. & Krueger, J. G. The majority of epidermal T cells in psoriasis vulgaris lesions can produce type 1 cytokines, interferon- $\gamma$ , interleukin-2, and tumor necrosis factor- $\alpha$ , defining TC1 (cytotoxic T lymphocyte) and TH1 effector populations: A type 1 differentiation bias is al. *J. Invest. Dermatol.* **113**, 752–759 (1999).
51. Iezzi, G. *et al.* Type 2 Cytotoxic T Lymphocytes Modulate the Activity of Dendritic Cells Toward Type 2 Immune Responses. *J Immunol* **177**, 2131–2137 (2006).
52. Hilvering, B. *et al.* Synergistic activation of pro-inflammatory type-2 CD8+ T lymphocytes by lipid mediators in severe eosinophilic asthma. *Mucosal Immunol.* **11**, 1408–1419 (2018).

53. Hinks, T. S. C., Hoyle, R. D. & Gelfand, E. W. CD8 + Tc2 cells: underappreciated contributors to severe asthma. *Eur Respir Rev* **28**, 190092 (2019).
54. Cho, B. A. *et al.* Characterization of effector memory CD8+ T cells in the synovial fluid of rheumatoid arthritis. *J. Clin. Immunol.* **32**, 709–720 (2012).
55. Ye, Z. *et al.* Type 1 CD8 + T Cells are Superior to Type 2 CD8 + T Cells in Tumor Immunotherapy due to Their Efficient Cytotoxicity, Prolonged Survival and Type 1 Immune Modulation. *Cellular & Molecular Immunology* vol. 4 (2007).
56. Tang, Y. *et al.* Antigen-specific effector CD8 T cells regulate allergic responses via IFN- $\gamma$  and dendritic cell function. *J. Allergy Clin. Immunol.* **129**, 1611-1620.e4 (2012).
57. Fox, A., Harland, K. L., Kedzierska, K. & Kelso, A. Exposure of human CD8+ T cells to type-2 cytokines impairs division and differentiation and induces limited polarization. *Front. Immunol.* **9**, 1141 (2018).
58. Swain, S. L. T-Cell Subsets: Who does the polarizing? *Curr. Biol.* **5**, 849–851 (1995).
59. Sallusto, F., Lenig, D., Foester, R., Lipp, M. & Lanzavecchia, A. Two subsets of memory T lymphocytes with distinct homing potentials and effector functions. *Nature* **401**, 708–712 (1999).
60. Thomas, M. L. The leukocyte common antigen family. *Annu. Rev. Immunol* **7**, 339–369 (1989).
61. Adamthwaite, D. & Cooley, M. A. CD8+ T-cell subsets defined by expression of CD45 isoforms differ in their capacity to produce IL-2, IFN- $\gamma$  and TNF- $\beta$ . *Immunology* **81**, 253–260 (1994).
62. Sallusto, F., Geginat, J. & Lanzavecchia, A. Central Memory and Effector Memory T cells subsets: Function, Generation, and Maintenance. *Annu. Rev. Immunol* **22**, 745–763 (2004).
63. Hayflick, L. The limited in vitro lifetime of human diploid cell strains. *Exp. Cell Res.* **37**, 614–636 (1965).
64. McHugh, D. & Gil, J. Senescence and aging: Causes, consequences, and therapeutic avenues. *J. Cell Biol.* **217**, 65–77 (2018).
65. Verma, K. *et al.* Human CD8+ CD57-T EMRA cells: Too young to be called 'old'. *PLoS One* **12**, 1–14 (2017).
66. Jacquemont, L. *et al.* Terminally differentiated effector memory CD8+T cells identify kidney transplant recipients at high risk of graft failure. *J. Am. Soc. Nephrol.* **31**, 876–891 (2020).
67. Betjes Id, M. G. H. & Litjens, N. H. R. High numbers of differentiated CD28null CD8+ T cells are associated with a lowered risk for late rejection and graft loss after kidney transplantation. *PLoS One* 1–11 (2020) doi:10.1371/journal.pone.0228096.
68. Nagai, K. *et al.* Depletion of SIRT6 causes cellular senescence, DNA damage, and telomere dysfunction in human chondrocytes. *Osteoarthr. Cartil.* **23**, 1412–1420 (2015).
69. Anwar, T., Khosla, S. & Ramakrishna, G. Increased expression of SIRT2 is a novel marker of cellular senescence and is dependent on wild type p53 status. *Cell Cycle* **15**, 1883–1897 (2016).
70. Chen, J. *et al.* Sirt6 overexpression suppresses senescence and apoptosis of nucleus pulposus cells by inducing autophagy in a model of intervertebral disc degeneration. *Cell Death Dis.* **9**, (2018).
71. Ota, H. *et al.* Sirt1 modulates premature senescence-like phenotype in human endothelial cells. *J. Mol. Cell. Cardiol.* **43**, 571–579 (2007).
72. Hayakawa, T. *et al.* SIRT1 suppresses the senescence-associated secretory phenotype through epigenetic gene regulation. *PLoS One* **10**, 1–16 (2015).
73. Aw, D. & Palmer, D. B. The origin and implication of thymic involution. *Aging Dis.* **2**, 436–443 (2011).
74. George, A. J. T. & Ritter, M. A. Thymic involution with ageing: Obsolescence or good housekeeping? *Immunol. Today* **17**, 267–272 (1996).
75. Dovey, O. M., Foster, C. T. & Cowley, S. M. Histone deacetylase 1 (HDAC1), but not HDAC2, controls embryonic stem cell differentiation. *Proc. Natl. Acad. Sci. U. S. A.* **107**, 8242–8247 (2010).
76. Jamaladdin, S. *et al.* Histone deacetylase (HDAC) 1 and 2 are essential for accurate cell division and the pluripotency of embryonic stem cells. *Proc. Natl. Acad. Sci. U. S. A.* **111**, 9840–9845 (2014).
77. Shin, M. S. *et al.* Dissecting alterations in human CD8+ T cells with aging by high-dimensional single cell mass cytometry. *Clin Immunol.* **200**, (2019).
78. Ferrucci, L. *et al.* The origins of age-related proinflammatory state. *Blood* **105**, 2294–2299 (2005).
79. Giovannini, S. *et al.* Interleukin-6, C-reactive protein, and tumor necrosis factor-alpha as predictors of mortality in frail, community-living elderly individuals. *J. Am. Geriatr. Soc.* **59**, 1679–1685 (2011).
80. Zanni, F. *et al.* Marked increase with age of type 1 cytokines within memory and effector/cytotoxic CD8+ T cells in humans: A contribution to understand the relationship between inflammation and immunosenescence. *Exp. Gerontol.* **38**, 981–987 (2003).

81. Palmeri, M. *et al.* Cytokine serum profile in a group of Sicilian nonagenarians. *J. Immunoass. Immunochem.* **33**, 82–90 (2012).
82. Pes, G. M. *et al.* Association between longevity and cytokine gene polymorphisms. A study in Sardinian centenarians. *Aging Clin. Exp. Res.* **16**, 244–248 (2004).
83. Callender, L. A. *et al.* Human CD8 + EMRA T cells display a senescence-associated secretory phenotype regulated by p38 MAPK. *Aging Cell* **17**, 1–9 (2018).
84. Uy, R. & Wold, F. Posttranslational Covalent Modification of Proteins. *Science (80-. )*. **198**, 890–896 (1977).
85. Ardito, F., Giuliani, M., Perrone, D., Troiano, G. & Muzio, L. Lo. The crucial role of protein phosphorylation in cell signaling and its use as targeted therapy (Review). *Int. J. Mol. Med.* **40**, 271–280 (2017).
86. Szyk, A. *et al.* Molecular basis for age-dependent microtubule acetylation by tubulin acetyltransferase. *Cell* **157**, 1405–1415 (2014).
87. Chung, H. S., Wang, S.-B., Venkatraman, V., Murray, C. I. & Van Eyk, J. E. Cysteine Oxidative Post-translational Modifications: Emerging Regulation in the Cardiovascular System. *Circ Res.* **112**, 382–392 (2013).
88. Walsh, C. T. *Posttranslational Modification of Proteins. Expanding Nature's Inventory.* (2006). doi:<https://doi.org/10.1002/anie.200585363>.
89. Harper, J. W. & Bennett, E. J. Proteome complexity and the forces that drive proteome imbalance. *Nature* **537**, 328–338 (2016).
90. Khoury, G. A., Baliban, R. C. & Floudas, C. A. Proteome-wide post-translational modification statistics: frequency analysis and curation of the swiss-prot database. *Sci. Rep.* **1**, (2011).
91. Verdin, E. & Ott, M. 50 years of protein acetylation: from gene regulation to epigenetics, metabolism and beyond. *Nat. Rev. Mol. Cell Biol.* **16**, 258–264 (2015).
92. Phillips, D. M. P. The presence of acetyl groups in histones. *Biochem. J* **87**, 258–263 (1963).
93. Allfrey, V. G., Faulkner, R. & Mirsky, A. E. Acetylation and methylation of histones and their possible role in the regulation of RNA synthesis. *Proc. Natl. Acad. Sci. USA* **51**, 786–794 (1964).
94. Inoue, A. & Fujimoto, D. Enzymatic deacetylation of Histone. *Biochem. Biophys. Res. Commun.* **36**, 146–150 (1969).
95. Ali, I., Conrad, R. J., Verdin, E. & Ott, M. Lysine Acetylation Goes Global: From Epigenetics to Metabolism and Therapeutics. *Chem Rev* **118**, 1216–1252 (2018).
96. Spange, S., Wagner, T., Heinzel, T. & Krämer, O. H. Acetylation of non-histone proteins modulates cellular signalling at multiple levels. *Int. J. Biochem. Cell Biol.* **41**, 185–198 (2009).
97. James, A. M. *et al.* Non-enzymatic N-acetylation of Lysine Residues by AcetylCoA Often Occurs via a Proximal S-acetylated Thiol Intermediate Sensitive to Glyoxalase II. *Cell Rep.* **18**, 2105–2112 (2017).
98. Hawse, W. F., Cattley, R. T. & Wendell, S. G. Regulates Acetyl-CoA Metabolism via AKT Cutting Edge: TCR Signal Strength. *J Immunol* **203**, 2771–2775 (2019).
99. Lee, K. K. & Workman, J. L. Histone acetyltransferase complexes: One size doesn't fit all. *Nat. Rev. Mol. Cell Biol.* **8**, 284–295 (2007).
100. Seto, E. & Yoshida, M. Erasers of Histone Acetylation: The Histone Deacetylase Enzymes. *Cold Spring Harb Perspect Biol* **6**, (2014).
101. Jiang, H. *et al.* SIRT6 regulates TNF $\alpha$  secretion via hydrolysis of long chain fatty acyl lysine. *Nature* **496**, 110–113 (2013).
102. Haigis, M. C. *et al.* SIRT4 Inhibits Glutamate Dehydrogenase and Opposes the Effects of Calorie Restriction in Pancreatic  $\beta$  Cells. *Cell* **126**, 941–954 (2006).
103. Du, J. *et al.* SIRT5 is an NAD-dependent protein lysine demalonylase and desuccinylase. *Science (80-. )*. **334**, 806–809 (2011).
104. Kane, A. E. & Sinclair, D. A. Epigenetic changes during aging and their reprogramming potential. *Crit Rev Biochem Mol Biol* **54**, 61–83 (2019).
105. Tuscher, J. J. & Day, J. J. Multigenerational epigenetic inheritance: One step forward, two generations back. *Neurobiology of Disease* vol. 132 104591 (2019).
106. Pagiatakis, C., Musolino, E., Gornati, R., Bernardini, G. & Papait, R. Epigenetics of aging and disease: a brief overview. *Aging Clin. Exp. Res.* (2019) doi:10.1007/s40520-019-01430-0.
107. Daskalaki, M. G., Tsatsanis, C. & Kampranis, S. C. Histone methylation and acetylation in macrophages as a mechanism for regulation of inflammatory responses. *J. Cell. Physiol.* **233**, 6495–6507 (2018).
108. Shoji, M. *et al.* Production of the Alzheimer amyloid b protein by normal proteolytic processing. *Science (80-*

- . ). **258**, 126–129 (1992).
109. Baba, M. *et al.* Aggregation of a-Synuclein in Lewy Bodies of Sporadic Parkinson's Disease and Dementia with Lewy Bodies. *American J. of Pathology* **152**, 879–884 (1998).
  110. Martinez-Naharro, A., Hawkins, P. N. & Fontana, M. Cardiac amyloidosis. *Clin. Med. (Northfield. Ill)*. **18**, s30–s35 (2018).
  111. El Kennani, S., Crespo, M., Govin, J. & Pflieger, D. Proteomic analysis of histone variants and their PTMs: Strategies and pitfalls. *Proteomes* **6**, 1–16 (2018).
  112. Görisch, S. M., Wachsmuth, M., Tóth, K. F., Lichter, P. & Rippe, K. Histone acetylation increases chromatin accessibility. *J. Cell Sci.* **118**, 5825–5834 (2005).
  113. Strahl, B. D. & Allis, C. D. The language of covalent histone modifications. *Nature* **403**, 41–45 (2000).
  114. Kurdistani, S. K., Tavazoie, S. & Grunstein, M. Mapping global histone acetylation patterns to gene expression. *Cell* **117**, 721–733 (2004).
  115. Yao, Y.-L., Yang, W.-M. & Seto, E. Regulation of Transcription Factor YY1 by Acetylation and Deacetylation. *Mol. Cell. Biol.* **21**, 5979–5991 (2001).
  116. Kernochan, L. E. *et al.* The role of histone acetylation in SMN gene expression. *Hum. Mol. Genet.* **14**, 1171–1182 (2005).
  117. Sterner, R., Vidali, G. & Allfrey, V. G. Studies of acetylation and deacetylation in high mobility group proteins. *J. Biol. Chem.* **254**, 11577–11583 (1979).
  118. L'hernault, S. W. & Rosenbaum, J. L. Chlamydomonas a-Tubulin Is Posttranslationally in the Flagella during Flagellar Assembly Modified. *J. Cell Biol.* **97**, 258–263 (1983).
  119. LeDizet, M. & Piperno, G. Identification of an acetylation site of Chlamydomonas alpha-tubulin. *Proc. Natl. Acad. Sci. U. S. A.* **84**, 5720–5724 (1987).
  120. Costantini, C., Hee, M. K., Cabell JONAS, M. & Puglielli, L. A reversible form of lysine acetylation in the ER and Golgi lumen controls the molecular stabilization of BACE1. *Biochem. J* **407**, 383–395 (2007).
  121. Pehar, M. & Puglielli, L. Lysine acetylation in the lumen of the ER: a novel and essential function under the control of the UPR. *Biochim. Biophys. Acta* **1833**, 686–697 (2013).
  122. Farrugia, M. A. & Puglielli, L. Nε-lysine acetylation in the endoplasmic reticulum - a novel cellular mechanism that regulates proteostasis and autophagy. *Journal of Cell Science* vol. 131 (2018).
  123. Serrador, J. M. *et al.* HDAC6 Deacetylase Activity Links the Tubulin Cytoskeleton with Immune Synapse Organization. *Immunity* **20**, 417–428 (2004).
  124. Matsuyama, A. *et al.* In vivo destabilization of dynamic microtubules by HDAC6-mediated deacetylation. *EMBO J.* **21**, 6820–6831 (2002).
  125. A, M., Fung, T. S., Kettenbach, A. N., Chakrabarti, R. & Higgs, H. N. A complex containing lysine-acetylated actin inhibits the formin INF2. *Nat. Cell Biol.* **21**, 592–602 (2019).
  126. Zhang, X. *et al.* HDAC6 modulates cell mobility by altering the acetylation level of cortactin. *Mol Cell.* **27**, 197–213 (2007).
  127. Choudhary, C. *et al.* Lysine acetylation targets protein complexes and co-regulates major cellular functions. *Science (80-. )*. **325**, 834–840 (2009).
  128. Li, T. *et al.* Glyceraldehyde-3-phosphate Dehydrogenase is activated by Lysine 254 Acetylation in response to Glucose signal. *J. Biol. Chem.* **289**, 3775–3785 (2014).
  129. Ventura, M. *et al.* Nuclear translocation of glyceraldehyde-3-phosphate dehydrogenase is regulated by acetylation. *Int. J. Biochem. Cell Biol.* **42**, 1672–1680 (2010).
  130. Zhao, S. *et al.* Regulation of Cellular Metabolism by Protein Lysine Acetylation. *Science (80-. )*. **327**, 1000–1004 (2010).
  131. Hsu, F.-C. *et al.* HDAC3 is required for T cell maturation. *J Immunol* **195**, 1578–1590 (2015).
  132. Phillips, R. L. *et al.* HDAC3 restrains CD8-lineage genes to maintain a bi-potential state in CD4 + CD8 + thymocytes for CD4-lineage commitment. *Elife* **8**, e43821 (2019).
  133. Wang, A. H. & Yang, X.-J. Histone Deacetylase 4 Possesses Intrinsic Nuclear Import and Export Signals. *Mol. Cell. Biol.* **21**, 5992–6005 (2001).
  134. Shao, L. & Hou, C. miR-138 activates NF-κB signaling and PGRN to promote rheumatoid arthritis via regulating HDAC4. *Biochem. Biophys. Res. Commun.* **519**, 166–171 (2019).
  135. Liu, Q. *et al.* HDAC4 is expressed on multiple T cell lineages but dispensable for their development and function. *Oncotarget* **8**, 17562–17572 (2017).

136. Yanginlar, C. & Logie, C. HDAC11 is a regulator of diverse immune functions. *Biochim. Biophys. Acta - Gene Regul. Mech.* **1861**, 54–59 (2018).
137. Woods, D. M. *et al.* T cells lacking HDAC11 have increased effector functions and mediate enhanced alloreactivity in a murine model. *Blood* **130**, 146–155 (2017).
138. Wang, R.-H. *et al.* Hepatic Sirt1 deficiency in mice impairs mTorc2/Akt signaling and results in hyperglycemia, oxidative damage, and insulin resistance. *J. Clin. Invest.* **121**, 4477–4490 (2011).
139. Bai, B., Vanhoutte, P. M. & Wang, Y. Loss-of-SIRT1 function during vascular ageing: Hyperphosphorylation mediated by cyclin-dependent kinase 5. *Trends Cardiovasc. Med.* **24**, 81–84 (2014).
140. Gong, H. *et al.* Age-dependent tissue expression patterns of Sirt1 in senescence-accelerated mice. *Mol. Med. Rep.* **10**, 3296–3302 (2014).
141. Herranz, D. *et al.* Sirt1 improves healthy ageing and protects from metabolic syndrome-associated cancer. *Nat. Commun.* **1**, 1- (2010).
142. Matsuzaki, T. *et al.* Disruption of Sirt1 in chondrocytes causes accelerated progression of osteoarthritis under mechanical stress and during ageing in mice. *Ann. Rheum. Dis.* **73**, 1397–1404 (2014).
143. Ramis, M. R., Esteban, S., Miralles, A., Tan, D. X. & Reiter, R. J. Caloric restriction, resveratrol and melatonin: Role of SIRT1 and implications for aging and related-diseases. *Mechanisms of Ageing and Development* vols 146–148 28–41 (2015).
144. Albani, D. *et al.* Modulation of human longevity by SIRT3 single nucleotide polymorphisms in the prospective study ‘Treviso Longeva (TRELONG)’. *Age (Omaha)*. **36**, 469–478 (2014).
145. Denu, R. A. SIRT3 Enhances Mesenchymal Stem Cell Longevity and Differentiation. *Oxid. Med. Cell. Longev.* **ID 5841716**, (2017).
146. Liu, J. *et al.* SIRT3 protects hepatocytes from oxidative injury by enhancing ROS scavenging and mitochondrial integrity. *Cell Death Dis.* **8**, e3158 (2017).
147. Banks, A. S. *et al.* SirT1 gain-of-function increases energy efficiency and prevents diabetes in mice. *Cell Metab.* **8**, 333–341 (2008).
148. Tian, X. *et al.* SIRT6 Is Responsible for More Efficient DNA Double-Strand Break Repair in Long-Lived Species. *Cell* **177**, 622–638 (2019).
149. Kanfi, Y. *et al.* The sirtuin SIRT6 regulates lifespan in male mice. *Nature* **483**, 218–221 (2012).
150. Mostoslavsky, R. *et al.* Genomic instability and aging-like phenotype in the absence of mammalian SIRT6. *Cell* **124**, 315–329 (2006).
151. Min, L. *et al.* Liver cancer initiation is controlled by AP-1 through SIRT6-dependent inhibition of survivin. *Nat. Cell Biol.* **14**, 1203–1211 (2012).
152. Wang, R. *et al.* Interplay among BRCA1, SIRT1 and Survivin during BRCA1-associated tumorigenesis. *Mol Cell.* **32**, 11–20 (2008).
153. Hayashi, A. *et al.* Type-specific roles of histone deacetylase (HDAC) overexpression in ovarian carcinoma: HDAC1 enhances cell proliferation and HDAC3 stimulates cell migration with downregulation of E-cadherin. *Int. J. Cancer* **127**, 1332–1346 (2010).
154. Poyet, C. *et al.* Expression of histone deacetylases 1, 2 and 3 in urothelial bladder cancer. *BMC Clin. Pathol.* **14**, 1–9 (2014).
155. Trichostatin A | C17H22N2O3 - PubChem. <https://pubchem.ncbi.nlm.nih.gov/compound/Trichostatin-A>.
156. Ma, J. *et al.* Trichostatin A, a histone deacetylase inhibitor, suppresses proliferation and promotes apoptosis of esophageal squamous cell lines. *Mol. Med. Rep.* **11**, 4525–4531 (2015).
157. Hrgovic, I. *et al.* The histone deacetylase inhibitor trichostatin a decreases lymphangiogenesis by inducing apoptosis and cell cycle arrest via p21-dependent pathways. *BMC Cancer* **16**, 1–16 (2016).
158. Piacentini, P. *et al.* Trichostatin A enhances the response of chemotherapeutic agents in inhibiting pancreatic cancer cell proliferation. *Virchows Arch* **448**, 797–804 (2006).
159. Search of: Trichostatin A - List Results - ClinicalTrials.gov. <https://clinicaltrials.gov/ct2/results?term=Trichostatin+A>.
160. Sourlingas, T. G., Kypreou, K. P. & Sekeri-Pataryas, K. E. The effect of the histone deacetylase inhibitor, trichostatin A, on total histone synthesis, H10 synthesis and histone H4 acetylation in peripheral blood lymphocytes increases as a function of increasing age: A model study. *Exp. Gerontol.* **37**, 341–348 (2002).
161. Fejes Tóth, K. *et al.* Trichostatin A-induced histone acetylation causes decondensation of interphase chromatin. *J. Cell Sci.* **117**, 4277–4287 (2004).

162. 6-Chloro-2,3,4,9-tetrahydro-1H-carbazole-1-carboxamide | C13H13ClN2O - PubChem. <https://pubchem.ncbi.nlm.nih.gov/compound/5113032#section=Drug-and-Medication-Information>.
163. Gertz, M. *et al.* Ex-527 inhibits Sirtuins by exploiting their unique NAD<sup>+</sup>-dependent deacetylation mechanism. *PNAS* **110**, E277-2-E2781 (2013).
164. Kim, B. S., Lee, C.-H., Chang, G.-E., Cheong, E. & Shin, I. A potent and selective small molecule inhibitor of sirtuin 1 promotes differentiation of pluripotent P19 cells into functional neurons OPEN. *Nat. Publ. Gr.* **6**, 1–12 (2016).
165. Huang, J. *et al.* The SIRT1 inhibitor EX-527 suppresses mTOR activation and alleviates acute lung injury in mice with endotoxiemia. *Innate Immun.* **23**, 678–686 (2017).
166. Kundu, A. *et al.* Protective effect of EX-527 against high-fat diet-induced diabetic nephropathy in Zucker rats. *Toxicol. Appl. Pharmacol.* **390**, 114899 (2020).
167. Search of: EX-527 - List Results - ClinicalTrials.gov. <https://clinicaltrials.gov/ct2/results?cond=&term=EX-527&cntry=&state=&city=&dist=>.
168. Braidy, N. *et al.* Role of Nicotinamide Adenine Dinucleotide and Related Precursors as Therapeutic Targets for Age-Related Degenerative Diseases: Rationale, Biochemistry, Pharmacokinetics, and Outcomes. *Antioxid. Redox Signal.* **30**, 251–294 (2019).
169. Imai, S.-I. & Guarente, L. It takes two to tango: NAD<sup>+</sup> and sirtuins in aging/longevity control. *Aging Mech. Disease* **2**, (2016).
170. Hwang, E. S. & Song, S. B. Nicotinamide is an inhibitor of SIRT1 in vitro, but can be a stimulator in cells. *Cell. Mol. Life Sci.* **74**, 3347–3362 (2017).
171. Camacho-Pereira, J. *et al.* CD38 dictates age-related NAD decline and mitochondrial dysfunction through a SIRT3-dependent mechanism. *Cell Metab.* **23**, 1127–1139 (2016).
172. Johnson, S. & Imai, S.-I. NAD<sup>+</sup> biosynthesis, aging, and disease. *F1000Research* **7** (F1000 F, 1–10 (2018).
173. Hegyi, J., Schwartz, R. A. & Hegyi, V. Pellagra : Dermatitis, dementia, and diarrhea. *Int. J. Dermatol.* **43**, 1–5 (2004).
174. Blutspende. <https://www.medizin.uni-halle.de/blutspende>.
175. Maecker, H. T., McCoy, J. P. & Nussenblatt, R. Standardizing immunophenotyping for the Human Immunology Project. *Nat. Rev. Immunol.* **12**, 191–200 (2012).
176. Quah, B. J. C. & Parish, C. R. New and improved methods for measuring lymphocyte proliferation in vitro and in vivo using CFSE-like fluorescent dyes. *J. Immunol. Methods* **379**, 1–14 (2012).
177. Bradford, M. M. A rapid and sensitive method for the quantification of microgram quantities of protein utilizing the principle of protein-dye binding. *Anal. Biochem.* **72**, 248–254 (1976).
178. Westermeier, R. & Scheibe, B. Difference Gel Electrophoresis Based on Lys/Cys Tagging BT - 2D PAGE: Sample Preparation and Fractionation. in (ed. Posch, A.) 73–85 (Humana Press, 2008). doi:10.1007/978-1-60327-064-9\_7.
179. Pappin, D. J. C., Hojrup, P. & Bleasby, A. J. Rapid identification of proteins by peptide-mass fingerprinting. *Curr. Biol.* **3**, 327–332 (1993).
180. Perkins, D., Pappin, D., Creasy, D. & Cottrell, J. Probability-based protein identification by searching sequence databases using mass spectrometry data. *Electrophoresis* **20**, 3551–3567 (1999).
181. Primer designing tool. <https://www.ncbi.nlm.nih.gov/tools/primer-blast/>.
182. RefSeq: NCBI Reference Sequence Database. <https://www.ncbi.nlm.nih.gov/refseq/>.
183. Pfaffl, M. W. Relative quantification. *Real-time PCR* 63–82 (2004) doi:10.1186/1756-6614-3-5.
184. Palmisano, I. *et al.* Amino acid starvation induces reactivation of silenced transgenes and latent HIV-1 provirus via down-regulation of histone deacetylase 4 (HDAC4). *Proc. Natl. Acad. Sci.* **109**, E2284–E2293 (2012).
185. Gao, L., Cueto, M. A., Asselbergs, F. & Atadja, P. Cloning and functional characterization of HDAC11, a novel member of the human histone deacetylase family. *J. Biol. Chem.* **277**, 25748–55 (2002).
186. Morissette, M. C., Parent, J. & Milot, J. Perforin, granzyme B, and FasL expression by peripheral blood T lymphocytes in emphysema. *Respir. Res.* **8**, (2007).
187. Hochegger, K. *et al.* Expression of granzyme A in human polymorphonuclear neutrophils. *Immunology* **121**, 166–173 (2007).
188. Vigano, P. *et al.* Interleukin-10 is produced by human uterine natural killer cells but does not affect their production of interferon-gamma. *Mol. Hum. Reprod.* **7**, 971–977 (2001).

189. R: The R Project for Statistical Computing. <https://www.r-project.org/>.
190. Sonesson, C., Love, M. I. & Robinson, M. D. Differential analyses for RNA-seq: transcript-level estimates improve gene-level inferences. *F1000Research* **4**, (2016).
191. Love, M. I., Huber, W. & Anders, S. Moderated estimation of fold change and dispersion for RNA-seq data with DESeq2. *Genome Biol.* **15**, 1–21 (2014).
192. von Mering, C. *et al.* STRING: Known and predicted protein-protein associations, integrated and transferred across organisms. *Nucleic Acids Res.* **33**, 433–437 (2005).
193. Szklarczyk, D. *et al.* STRING v11: Protein-protein association networks with increased coverage, supporting functional discovery in genome-wide experimental datasets. *Nucleic Acids Res.* **47**, D607–D613 (2019).
194. Eden, E., Navon, R., Steinfeld, I., Lipson, D. & Yakhini, Z. GOrilla: a tool for discovery and visualization of enriched GO terms in ranked gene lists. *BMC Bioinformatics* **10**, (2009).
195. Oliveros, J. C. Venny. An interactive tool for comparing lists with Venn's diagrams. <https://bioinfogp.cnb.csic.es/tools/venny/index.ht>.
196. Feinerer, I., Hornik, K. & Meyer, D. Text mining infrastructure in R. *J. Stat. Software, Artic.* **25**, 1–54 (2008).
197. Bouchet-Valat, M. Snowball Stemmers Based on the C 'libstemmer' UTF-8 Library [R package SnowballC version 0.7.0]. (2020).
198. CRAN - Package wordcloud. <https://cran.r-project.org/web/packages/wordcloud/index.html>.
199. Caballero, B. Humans against Obesity: Who Will Win? *Adv. Nutr.* **10**, S4–S9 (2019).
200. Seif, F. *et al.* The role of JAK-STAT signaling pathway and its regulators in the fate of T helper cells. *Cell Commun. Signal.* **115**, 1–13 (2017).
201. Finley, S. D., Gupta, D., Cheng, N. & Klinke, D. J. I. Inferring relevant control mechanisms for Interleukin-12 signaling in naïve CD4+ T cells. *Immunol. Cell Biol.* **89**, 100–110 (2011).
202. Thome, J. J. C. *et al.* Spatial map of human T cell compartmentalization and maintenance over decades of life. *Cell* **159**, 814–828 (2014).
203. Saule, P. *et al.* Accumulation of memory T cells from childhood to old age: Central and effector memory cells in CD4+ versus effector memory and terminally differentiated memory cells in CD8+ compartment. *Mech. Ageing Dev.* **127**, 274–281 (2006).
204. Li, M. *et al.* Age related human T cell subset evolution and senescence. *Immun. Ageing* **16**, 24 (2019).
205. Fagnoni, F. F. *et al.* Shortage of circulating naïve CD8 T cells provides new insights on immunodeficiency in aging. *Blood* **95**, 2860–2868 (2000).
206. Griffiths, S. J. *et al.* Age-Associated Increase of Low-Avidity Cytomegalovirus-Specific CD8+ T cells that Re-Express CD45RA. *J Immunol* **190**, 5363–5372 (2013).
207. Newman, D. M. *et al.* Acetylation of the Cd8 Locus by KAT6A Determines Memory T Cell Diversity. *Cell Rep.* **16**, 3311–3321 (2016).
208. Lim, H. *et al.* Identification of 2D-gel proteins: A comparison of MALDI/TOF peptide mass mapping to  $\mu$  LC-ESI tandem mass spectrometry. *J. Am. Soc. Mass Spectrom.* **14**, 957–970 (2003).
209. Teixeira, A. M. *et al.* Changes in naïve and memory T-cells in elite swimmers during a winter training season. *Brain, Behav. Immun. J.* 186–193 (2014) doi:10.1016/j.bbi.2014.01.002.
210. Segerstrom, S. C. & Miller, G. E. *Psychological Stress and the Human Immune System: A Meta-Analytic Study of 30 Years of Inquiry. Psychol Bull* vol. 130 (2004).
211. Prather, A. A. *et al.* Associations between chronic caregiving stress and T cell markers implicated in immunosenescence HHS Public Access. *Brain Behav Immun* **73**, 546–549 (2018).
212. de Frel, D. L. *et al.* The Impact of Obesity and Lifestyle on the Immune System and Susceptibility to Infections Such as COVID-19. *Frontiers in Nutrition* vol. 7 597600 (2020).
213. You, W. & Steegborn, C. Structural Basis of Sirtuin 6 Inhibition by the Hydroxamate Trichostatin A: Implications for Protein Deacetylase Drug Development. *J. Med. Chem.* **61**, 10922–1928 (2018).
214. Chi, H. Regulation and function of mTOR signalling in T cell fate decisions. *Nat. Rev. Immunol.* **12**, 325–338 (2012).
215. Lio, D. *et al.* In vitro T cell activation in elderly individuals: failure in CD69 and CD71 expression. *Mech. Ageing Dev.* **89**, 51–58 (1996).
216. Serra, J. A. *et al.* *Early T Cell Activation in Elderly Humans. Age and Ageing* vol. 25 <https://academic.oup.com/ageing/article/25/6/470/14350> (1996).
217. Smithey, M. J., Renkema, K. R., Rudd, B. D. & Nikolich-Zugich, J. Increased apoptosis, curtailed expansion and

- incomplete differentiation of CD8+ T-cells combine to decrease clearance of L. monocytogenes in old mice. *Eur J Immunol.* **41**, 1352–1364 (2011).
218. Ahmed, M. *et al.* Clonal Expansions and Loss of Receptor Diversity in the Naive CD8 T Cell Repertoire of Aged Mice. *J. Immunol.* **182**, 784–792 (2009).
219. Hussain, T. & Quinn, K. M. Similar but different: virtual memory CD8 T cells as a memory-like cell population. *Immunol. Cell Biol.* **97**, 675–684 (2019).
220. Zhang, Y. *et al.* Apoptosis and reduced influenza A virus specific CD8+ T cells in aging mice. *Cell Death Differ.* **9**, 651–660 (2002).
221. Best, J. A. *et al.* Transcriptional insights into the CD8 + T cell response to infection and memory T cell formation. *Nat Immunol* **14**, 404–412 (2013).
222. Yon Rhee, S., Wood, V., Dolinski, K. & Draghici, S. Use and misuse of the gene ontology annotations. *Nat. Rev. Genet.* **9**, 509–515 (2008).
223. Adachi, T. & Alam, R. The mechanism of IL-5 signal transduction. *Am. J. Physiol.* **275**, (1998).
224. Takatsu, K. Interleukin-5 and IL-5 receptor in health and diseases. *Proc. Jpn. Acad., Ser. B* **87**, 463–485 (2011).
225. O`Shea, J. J. *et al.* The JAK-STAT pathways: impact on human disease and therapeutic intervention. *Annu Rev Med.* **66**, 311–328 (2015).
226. Xin, P. *et al.* The role of JAK/STAT signaling pathway and its inhibitors in diseases. *Int. Immunopharmacol.* **80**, 106210 (2020).
227. Shen-Orr, S. S. *et al.* Defective Signaling in the JAK-STAT Pathway Tracks with Chronic Inflammation and Cardiovascular Risk in Aging Humans. *Cell Syst.* **3**, 374-384.e4 (2016).
228. Lenhart, K. F., Capozzoli, B., Warrick, G. S. D. & DiNardo, S. Diminished Jak/STAT Signaling Causes Early-Onset Aging Defects in Stem Cell Cytokinesis. *Curr. Biol.* **29**, 256-267.e3 (2019).
229. Griveau, A., Wiel, C., Ziegler, D. V., Bergo, M. O. & Bernard, D. The JAK1/2 inhibitor ruxolitinib delays premature aging phenotypes. *Aging Cell* **19**, 1–6 (2020).
230. Arruvito, L. *et al.* Identification and Clinical Relevance of Naturally Occurring Human CD8 + HLA-DR + Regulatory T Cells. *J. Immunol.* **193**, 4469–4476 (2014).
231. Machicote, A., Belén, S., Baz, P., Billordo, L. A. & Fainboim, L. Human CD8+HLA-DR+Regulatory T Cells, similarly to classical CD4+Foxp3+cells, suppress immune responses via PD-1/PD-L1 axis. *Front. Immunol.* **9**, 1–13 (2018).
232. Yani, S. L. *et al.* CD8+HLADR+ regulatory T cells change with aging: They increase in number, but lose checkpoint inhibitory molecules and suppressive function. *Front. Immunol.* **9**, 1–12 (2018).
233. Malik, A., Pal, R. & Kumar Gupta, S. Interdependence of JAK-STAT and MAPK signaling pathways during EGF-mediated HTR-8/SVneo cell invasion. *PLoS One* **May 25**, 1–18 (2017).
234. Winston, L. A. & Hunter, T. Intracellular signalling: Putting JAKs on the kinase MAP. *Curr. Biol.* **6**, 668–671 (1996).
235. Bousoik, E. & Montazeri Aliabadi, H. “Do We Know Jack” About JAK? A Closer Look at JAK/STAT Signaling Pathway. *Front. Oncol.* **8**, 1–20 (2018).
236. Goronzy, J. J., Li, G., Yu, M. & Weyand, C. M. Signaling pathways in aged T cells - a reflection of T cell differentiation, cell senescence and host environment. *Semin. Immunol.* **24**, 365–372 (2012).
237. Xu, M., Tchkonja, T. & Kirkland, J. L. Perspective: targeting the JAK/STAT pathway to fight age-related dysfunction. *Pharmacol Res.* **111**, 152–154 (2016).
238. Khokhar, E. S. *et al.* Aging-associated decrease in the histone acetyltransferase KAT6B is linked to altered hematopoietic stem cell differentiation. *Exp. Hematol.* **82**, 43–52 (2020).
239. Pollock, K. M. *et al.* T-cell immunophenotyping distinguishes active from latent tuberculosis. *J. Infect. Dis.* **208**, 952–968 (2013).
240. Jiang, M. *et al.* T cell subset counts in peripheral blood can be used as discriminatory biomarkers for diagnosis and severity prediction of COVID-19. *J. Infect. Dis.* **222**, 198–202 (2020).
241. DeSantis, C. E. *et al.* Cancer statistics for adults aged 85 years and older, 2019. *CA A Cancer J Clin* **69**, 452–467 (2019).
242. White, M. C., Holman, D. M., Goodman, R. A. & Richardson, L. C. Cancer Risk among Older Adults: Time for Cancer Prevention to Go Silver. *Gerontologist* **59**, S1–S6 (2019).

## 8. Theses

1. Increased acetylation levels were observed in both age groups after HDACi treatment, however the expression of HDACs was not disturbed by the treatment, neither at a protein level or an mRNA level.
2. The expression profiles of the CD8<sup>+</sup> T cells showed a general increase in expression; however, the most abundant proteins had a decreased expression.
3. The proteome is affected by the HDACi-mediated increase in acetylation in an organized manner. The proteins identified to be differently expressed after HDACi treatment were part of a network which was involved in the structure of the cytoskeleton and included cellular chaperones, proteins involved in secretion and proliferation after activation.
4. HDACi treatment disrupts the functioning of CD8<sup>+</sup> T cells in an age-dependent manner. Cells from young donors ceased their secretion and expression of surface markers, while cells from old donors maintained the secretion of pro-inflammatory factors and the surface expression of activation markers. The apoptosis and proliferation rates of both age groups were not affected by the HDACi treatment.
5. The transcriptome analysis revealed that the JAK-STAT pathway is more active in old donors, both in the total CD8<sup>+</sup> T cells and in the CD8<sup>+</sup> CD45RA<sup>-</sup> memory T cells.

## 9. Supplementary material

Table 8. Details regarding the GO terms returned by STRING for the MS identified protein.

GO term	Term description	Observed gene count	Background gene count	Strength	FDR
<b>Biological process</b>					
GO:0007010	cytoskeleton organization	13	953	0.91	1.49E-06
GO:0002252	immune effector process	12	927	0.89	8.84E-06
GO:0002366	leukocyte activation involved in immune response	10	616	0.98	1.71E-05
GO:0006996	organelle organization	19	3131	0.56	1.71E-05
GO:0043312	neutrophil degranulation	9	485	1.04	1.71E-05
GO:0045055	regulated exocytosis	10	691	0.93	1.71E-05
GO:0002253	activation of immune response	7	393	1.02	0.00016
GO:0038096	Fc-gamma receptor signaling pathway involved in phagocytosis	4	73	1.51	0.00031
GO:0019221	cytokine-mediated signaling pathway	8	655	0.86	0.00035
GO:0042267	natural killer cell mediated cytotoxicity	3	26	1.84	0.00047
GO:0030029	actin filament-based process	7	493	0.93	0.00048
GO:0051973	positive regulation of telomerase activity	3	36	1.69	0.00098
<b>Molecular Function</b>					
GO:0005200	Structural constituent of cytoskeleton	10	106	1.75	6.63E-13
GO:0000166	Nucleotide binding	21	2097	0.77	3.83E-11
GO:0003723	RNA binding	11	850	0.88	1.10E-06
GO:0005525	GTP binding	8	366	1.11	1.69E-06
GO:0005524	ATP binding	13	1462	0.72	2.82E-06
GO:0003924	GTPase activity	7	283	1.17	3.72E-06
GO:0031625	Ubiquitin protein ligase binding	7	311	1.13	6.21E-06
GO:0016787	Hydrolase activity	15	2448	0.56	2.13E-05
GO:0016887	ATPase activity	7	392	1.02	2.33E-05
GO:0003725	Double-stranded RNA binding	4	70	1.53	4.31E-05
GO:0030235	Nitric-oxide synthase regulator activity	2	6	2.3	0.0004
<b>Cellular Component</b>					
GO:0005829	cytosol	26	4958	0.49	2.68E-08
GO:0034774	secretory granule lumen	10	323	1.26	2.68E-08
GO:0043232	intracellular non-membrane-bounded organelle	23	4005	0.53	4.58E-08
GO:0005856	cytoskeleton	16	2068	0.66	9.04E-07
GO:0032991	protein-containing complex	22	4792	0.43	5.91E-06
GO:1990904	ribonucleoprotein complex	10	770	0.89	5.91E-06
<b>Reactome pathways</b>					
HSA-168256	Immune System	22	1925	0.83	1.49E-12
HSA-389977	Post-chaperonin tubulin folding pathway	5	20	2.17	1.00E-08
HSA-69275	G2/M Transition	8	189	1.4	1.65E-08

## Supplementary material

HSA-194315	Signaling by Rho GTPases	9	402	1.12	2.01E-07
HSA-1280215	Cytokine Signaling in Immune system	10	654	0.96	6.95E-07
HSA-5336415	Uptake and function of diphtheria toxin	3	6	2.47	2.74E-06
HSA-168249	Innate Immune System	11	1012	0.81	3.49E-06
HSA-449147	Signaling by Interleukins	8	439	1.03	3.78E-06
HSA-162582	Signal Transduction	16	2605	0.56	7.15E-06
HSA-2132295	MHC class II antigen presentation	5	119	1.4	1.05E-05
HSA-2565942	Regulation of PLK1 Activity at G2/M Transition	4	85	1.45	6.26E-05
HSA-9020591	Interleukin-12 signaling	3	47	1.58	0.00031
HSA-8953854	Metabolism of RNA	7	652	0.8	0.00035
HSA-1280218	Adaptive Immune System	7	733	0.75	0.0007
KEGG pathways					
hsa05130	Pathogenic Escherichia coli infection	9	53	2	5.09E-14
hsa04145	Phagosome	8	145	1.51	5.47E-09
hsa04540	Gap junction	6	87	1.61	2.61E-07
hsa04520	Adherens junction	4	71	1.52	0.00015
hsa04141	Protein processing in endoplasmic reticulum	4	161	1.17	0.0022
hsa04612	Antigen processing and presentation	3	66	1.43	0.0024
hsa00620	Pyruvate metabolism	2	39	1.48	0.0142
hsa04390	Hippo signaling pathway	3	152	1.07	0.0142
hsa04921	Oxytocin signaling pathway	3	149	1.08	0.0142
hsa05110	Vibrio cholerae infection	2	48	1.39	0.0156
hsa05164	Influenza A	3	168	1.02	0.0156
UniProt keywords					
KW-0007	Acetylation	29	3335	0.71	1.10E-16
KW-0547	Nucleotide-binding	20	1758	0.83	7.43E-12
KW-0488	Methylation	15	959	0.97	2.69E-10
KW-0558	Oxidation	6	30	2.07	5.08E-10
KW-0206	Cytoskeleton	15	1200	0.87	3.52E-09
KW-0963	Cytoplasm	26	4979	0.49	3.52E-09
KW-0225	Disease mutation	19	2968	0.58	3.20E-07
KW-0067	ATP-binding	13	1367	0.75	1.59E-06
KW-0342	GTP-binding	7	338	1.09	1.24E-05
KW-0832	Ubl conjugation	15	2381	0.57	1.86E-05
KW-0597	Phosphoprotein	26	8067	0.28	8.08E-05
KW-0702	S-nitrosylation	3	55	1.51	0.00076
KW-0143	Chaperone	4	196	1.08	0.0019
KW-0648	Protein biosynthesis	3	128	1.14	0.0069

Table 9. Details regarding the GO terms returned by GOrilla for the datasets for the total CD8<sup>+</sup> T cells.

GO term	Description	P-value	FDR
Biological Process			
GO:0019221	cytokine-mediated signaling pathway	6.91E-13	4.69E-09
GO:0006952	defense response	0.000000092	0.000312
GO:0002376	immune system process	0.000000514	0.000581
GO:0002694	regulation of leukocyte activation	0.000000846	0.00082
GO:0006950	response to stress	0.000000903	0.000766
GO:1904894	positive regulation of STAT cascade	0.00000212	0.00144
GO:0042127	regulation of cell proliferation	0.00000357	0.0022
GO:0007165	signal transduction	0.0000041	0.00214
GO:0051047	positive regulation of secretion	0.00000654	0.00261
GO:0051249	regulation of lymphocyte activation	0.00000848	0.0032
GO:0007166	cell surface receptor signaling pathway	0.00000962	0.00327
GO:0030888	regulation of B cell proliferation	0.0000102	0.00329
GO:0006954	inflammatory response	0.0000109	0.00321
GO:0046427	positive regulation of JAK-STAT cascade	0.0000188	0.00424
Molecular Function			
GO:0030545	receptor regulator activity	2.82E-09	0.00000413
GO:0005125	cytokine activity	3.36E-09	0.00000246
GO:0038023	signaling receptor activity	0.00000382	0.00112
GO:0060089	molecular transducer activity	0.00000849	0.00207
GO:0008083	growth factor activity	0.0000206	0.00431
GO:0004930	G protein-coupled receptor activity	0.000804	0.0981
Cellular Component			
GO:0005615	extracellular space	0.00000944	0.0085
GO:0005886	plasma membrane	0.000513	0.154
GO:0009897	external side of plasma membrane	0.000945	0.213
GO term	Description	P-value	FDR
Biological Process			
GO:0035556	Intracellular signal transduction	0.00000974	0.0752
GO:0046328	Regulation of JNK cascade	0.00001110	0.0427
GO:0032872	Regulation of stress-activated MAPK cascade	0.00009140	0.2350
GO:0050789	Regulation of biological process	0.00010200	0.1980
GO:0070302	Regulation of stress-activated protein kinase signaling cascade	0.00014500	0.2240
GO:0050778	Positive regulation of immune response	0.00018800	0.2420
GO:0002253	Activation of immune response	0.00026700	0.2580
GO:0046330	Positive regulation of JNK cascade	0.00036100	0.3100
GO:0072089	Stem cell proliferation	0.00042600	0.2740
GO:0043122	Regulation of I-kappaB kinase/NF-kappaB signaling	0.00047700	0.2460
Molecular function			
GO:0003676	Nucleic acid binding	3.98E-05	0.0382
GO:1901363	Heterocyclic compound binding	4.08E-05	0.0261

Up-regulated in old

Uniquely expressed in old

	GO:0070742	C2H2 zinc finger domain binding	2.37E-04	0.1140
	GO:0003677	DNA binding	5.94E-04	0.2280
	GO:0042054	Histone methyltransferase activity	7.19E-04	0.1970
	Cellular Component			
	GO:0044428	Nuclear part	2.68E-07	0.0003
	GO:0005654	Nucleoplasm	2.04E-06	0.0011
	GO:0043227	Membrane-bounded organelle	5.65E-05	0.0200
	GO:1905360	GTPase complex	1.86E-04	0.0283
	GO:0044424	Intracellular part	2.88E-04	0.0383
	GO:0043229	Intracellular organelle	4.06E-04	0.0480
	GO term	Description	P-value	FDR
	Biological Process			
Up-regulated in young	GO:2000026	regulation of multicellular organismal development	0.0000033	0.00237
	GO:0030509	Bone morphogenic protein signaling pathway	0.00000866	0.00561
	GO:0030154	cell differentiation	0.00000915	0.00538
	GO:0030162	regulation of proteolysis	0.0000187	0.00931
	GO:0045586	regulation of gamma-delta T cell differentiation	0.000136	0.0259
	GO:0033151	V(D)J recombination	0.000136	0.0251
	GO:0033153	T cell receptor V(D)J recombination	0.000136	0.0244
	GO:0046632	alpha-beta T cell differentiation	0.00039	0.0451
	GO:0046631	alpha-beta T cell activation	0.00039	0.0443
	GO:0006955	immune response	0.000899	0.0756
	Molecular Function			
	GO:0035257	nuclear hormone receptor binding	0.0000864	0.121
	GO:0051427	hormone receptor binding	0.000122	0.0852
	GO:0008013	beta-catenin binding	0.000341	0.159
	GO:0005102	signaling receptor binding	0.000346	0.121
	GO term	Description	P-value	FDR
	Biological process			
Uniquely expressed in young	GO:0039535	regulation of RIG-I signaling pathway	0.00000757	0.0598
		regulation of viral-induced cytoplasmic pattern		
	GO:0039531	recognition receptor signaling pathway	0.00000757	0.0299
	GO:0050688	regulation of defense response to virus	0.00007910	0.2080
	GO:1900246	positive regulation of RIG-I signaling pathway	0.00012700	0.2500
	GO:0002833	positive regulation of response to biotic stimulus	0.00041500	0.6550
	GO:0060070	canonical Wnt signaling pathway	0.00056200	0.7400
	Cellular Component			
	GO:0044424	intracellular part	0.000682	0.704

Table 10. Details regarding the GO terms returned by GOzilla for the datasets for the CD8<sup>+</sup> CD45RA<sup>-</sup> memory T cells.

GO term	Description	P-value	FDR
Biological Process			
GO:0019221	cytokine-mediated signaling pathway	0.0000838	0.559
GO:0031622	positive regulation of fever generation	0.000162	0.54
GO:0060337	type I interferon signaling pathway	0.000279	0.207
GO:0006955	immune response	0.000286	0.19
GO:0046328	regulation of JNK cascade	0.000477	0.265
GO:0000165	MAPK cascade	0.000625	0.321
GO:0050727	regulation of inflammatory response	0.000799	0.381
GO:0032874	positive regulation of stress-activated MAPK cascade	0.000839	0.373
GO:0046330	positive regulation of JNK cascade	0.000839	0.329
GO:0002675	positive regulation of acute inflammatory response	0.000867	0.321
GO:0048384	retinoic acid receptor signaling pathway	0.000878	0.308
Molecular Function			
GO:0008374	O-acyltransferase activity	0.000225	0.363
GO:0042605	peptide antigen binding	0.000264	0.213
GO:0003823	antigen binding	0.000264	0.142
GO:0008140	cAMP response element binding protein binding	0.000878	0.354
Cellular Component			
GO:0042611	MHC protein complex	0.000264	0.235
GO term	Description	P-value	FDR
Biological process			
GO:0031323	Regulation of cellular metabolic process	0.0000040	0.0333
GO:0050794	Regulation of cellular process	0.0000133	0.0366
GO:0019222	Regulation of metabolic process	0.0000156	0.0322
GO:0050789	Regulation of biological process	0.0000186	0.0306
GO:0006325	Chromatin organization	0.0000236	0.0324
GO:0006464	Cellular protein modification process	0.0000700	0.0577
GO:0080090	Regulation of primary metabolic process	0.0000787	0.0463
GO:0010468	Regulation of gene expression	0.0000926	0.0477
GO:0051171	Regulation of nitrogen compound metabolic process	0.0001190	0.0577
GO:0030041	Actin filament polymerization	0.0001230	0.0531
GO:0035722	Interleukin-12-mediated signaling pathway	0.0001830	0.0718
Molecular function			
GO:0097159	Organic cyclic compound binding	0.000000052	0.000100
GO:1901363	Heterocyclic compound binding	0.000000060	0.000058
GO:0003676	Nucleic acid binding	0.00000041	0.000260
GO:0003723	RNA binding	0.000002	0.001070
GO:0044548	S100 protein binding	0.000022	0.008360
GO:0004715	Non-membrane spanning protein tyrosine kinase activity	0.000056	0.017900
GO:0046966	Thyroid hormone receptor binding	0.000115	0.031200

		Cellular component	
	GO:0044428	Nuclear part	0.0000002 0.000022
	GO:0043229	Intracellular organelle	0.0000046 0.000165
	GO:0043231	Intracellular membrane-bounded organelle	0.0000168 0.000365
	GO:0005829	Cytosol	0.00000706 0.001280
	GO:0030315	T-tubule	0.000370 0.028700
	GO:0010494	Cytoplasmic stress granule	0.000371 0.026800
	GO:1990234	Transferase complex	0.000644 0.041100
	GO:0090543	Flemming body	0.000759 0.045800
GO term	Description	P-value	FDR
		Biological Process	
Up-regulated in young	GO:0050853	B cell receptor signaling pathway	0.0000195 0.126
	GO:0070374	positive regulation of ERK1 and ERK2 cascade regulation of antigen receptor-mediated signaling pathway	0.0000279 0.0903
	GO:0050854	positive regulation of MAPK cascade	0.0000343 0.0739
	GO:0043410	positive regulation of protein tyrosine phosphatase activity	0.0000909 0.118
	GO:1903615	regulation of protein tyrosine phosphatase activity	0.000253 0.164
	GO:1903613	regulation of protein tyrosine phosphatase activity	0.000253 0.149
	GO:0002683	negative regulation of immune system process production of molecular mediator of immune response	0.000303 0.151
	GO:0002440	cytokine production involved in immune response	0.000622 0.212
	GO:0002367	positive regulation of alpha-beta T cell activation	0.000806 0.186
	GO:0046635		0.000843 0.188
		Molecular Function	
	GO:0002020	protease binding	0.000582 0.85
	GO:0038023	signaling receptor activity	0.00068 0.496
		Cellular Component	
	GO:0099059	integral component of presynaptic active zone membrane	0.000901 0.801
GO term	Description	P-value	FDR
		Biological process	
Uniquely expressed in young	GO:1902275	Regulation of chromatin organization	0.0000779 0.120
	GO:0031056	Regulation of histone modification	0.0001100 0.121
	GO:0036211	Protein modification process	0.0002980 0.127
	GO:1905269	Positive regulation of chromatin organization	0.0003090 0.125
	GO:0098781	ncRNA transcription	0.0005700 0.190
	GO:0051252	Regulation of RNA metabolic process	0.0005900 0.189
	GO:0110032	Positive regulation of G2/M1 transition of meiotic cell cycle	0.0006280 0.167
	GO:0110030	Regulation of G2/M1 transition of meiotic cell cycle	0.0006280 0.161
	GO:1902850	Microtubule cytoskeleton organization involved in mitosis	0.0006630 0.164
	GO:0006306	DNA methylation	0.0009330 0.189
	GO:0006305	DNA alkylation	0.0009330 0.184

Molecular function				
GO:0003676	Nucleic acid binding		0.000096	0.17
GO:1901363	Heterocyclic compound binding		0.000253	0.23
Cellular component				
GO:0044428	Nuclear part		0.0000008	0.00077
GO:0043229	Intracellular organelle		0.0000080	0.00266
GO:0044424	Intracellular part		0.0000083	0.00207
GO:0005815	Microtubule organizing center		0.00028	0.02820
GO:0099738	Cell cortex region		0.00043	0.03930

**Table 11. Details regarding the GO terms returned by STRING for the transcripts uniquely expressed in donor Y21, which was removed from the further high throughput analysis of the CD8<sup>+</sup> CD45RA<sup>-</sup> memory T cells.**

GO term ID	Term description	Observed gene count	Background gene count	FDR
Biological Process				
GO:0006464	cellular protein modification process	115	2999	0.00037
GO:0043412	macromolecule modification	121	3197	0.00037
GO:0033043	regulation of organelle organization	55	1155	0.0011
GO:0044260	cellular macromolecule metabolic process	201	6413	0.0011
GO:0044267	cellular protein metabolic process	126	3603	0.0017
GO:0006807	nitrogen compound metabolic process	243	8349	0.0056
GO:0043161	proteasome-mediated ubiquitin-dependent protein catabolic process	19	257	0.009
GO:0010498	proteasomal protein catabolic process	20	284	0.0096
Cellular Component				
GO:0005737	cytoplasm	336	11238	3.33E-09
GO:0043229	intracellular organelle	355	12193	5.73E-09
GO:0043227	membrane-bounded organelle	328	11244	0.000000229
GO:0005815	microtubule organizing center	44	683	0.000000575
GO:0005813	centrosome	31	468	0.0000293
GO:0005654	nucleoplasm	124	3446	0.0000314
UniProt keyword				
KW-0025	Alternative splicing	376	10225	9.03E-36
KW-0597	Phosphoprotein	303	8067	2.82E-23
KW-0832	Ubl conjugation	101	2381	0.000000508
KW-0206	Cytoskeleton	51	1200	0.0022
KW-0254	Endocytosis	12	124	0.0023
KW-0343	GTPase activation	15	190	0.0024
KW-0007	Acetylation	109	3335	0.0057
KW-0727	SH2 domain	10	108	0.0091

## Declarations

1. I declare that I have not completed or initiated a doctorate procedure at any other university.
2. I declare that all information given is accurate and complete. The thesis has not been used previously at this or any other university in order to achieve an academic degree.
3. I declare under oath that this thesis is my own work entirely and has been written without any help from other people. I met all regulations of good scientific practice and I used only the sources mentioned and included all the citations correctly both in word and in content.

Georgiana Toma,

Halle (Saale), March 2021

## Acknowledgements

The work for this thesis has been funded by the DFG (Deutsche Forschungsgemeinschaft) through the ProMoAge graduate program (RTG 2155).

Firstly, I would like to thank my supervisor and the thesis committee members for their expert advice that has guided me throughout the project: Prof. Dr. Barbara Seliger, Prof. Dr. Marcus Glomb and an especially warm thank you to Prof. Dr. Regine Heller for her support.

I would like to express my sincere gratitude to the whole consortium of the ProMoAge graduate program, especially to Prof. Dr. Andreas Simm, Dr. Patrick Winterhalter, Anja Kirshner and Dr. Nancy Zimmermann.

I would like to thank the students within the consortium who have become valuable collaborators and friends, especially Ioana Lemnian, Dr. Veronika Piskovatska, Arina Urazova, and Dr. Tim Baldensperger.

I would also like to acknowledge my colleagues from the Institute of Medical Immunology for offering their help and valuable feedback on a daily basis: Dr. Dagmar Quandt, Dr. Chiara Massa, Dr. Jürgen Bukur, Dr. Michael Friedrich, Dr. Simon Jasinski-Bergner, Steffi Turzer, Anja Müller and Katharina Biehl. Additionally, I would also like to acknowledge the administrative staff of the Institute of Medical Immunology and I would like to express my humble gratitude to Nicole Ott for all of her help and support throughout the years.

Furthermore, I would like to single out and thank Dr. Jette Rahn for her technical guidance, active troubleshooting and advice, as well as Dr. Rudolph Lichtenfels for his encouragement and for his technical and theoretical guidance. Notably, I would also like to thank Dr. Marifili Lazaridou and Dr. Karthik Subbarayan for their unceasing support, without which I could not have completed this thesis in a timely manner.

Finally, I am immensely grateful to my friends and family for helping me overcome the inevitable strain of these past four and a half years. Without your encouragement and kindness, I truly would not have been able to complete this work.

